DEVELOPMENT OF PLA-CALCIUM PHOSPHATE COMPOSITES WITH HIGH COMPRESSIVE STRENGTH EMPLOYING A SILANE COUPLING AGENT (A-174)

by
Feyza Kevser Öner
B.S., Chemical Engineering, Boğaziçi University, 2016

Submitted to the Institute for Graduate Studies in
Science and Engineering in partial fulfillment of
the requirements for the degree of
Master of Science

Graduate Program in Chemical Engineering
Boğaziçi University
2019

DEVELOPMENT OF PLA-CALCIUM PHOSPHATE COMPOSITES WITH HIGH COMPRESSIVE STRENGTH EMPLOYING A SILANE COUPLING AGENT (A-174)

APPROVED BY:

Assoc. Prof. Sezen Soyer Uzun .....
(Thesis Supervisor)

Assoc. Prof. Burak Alakent .....

Assoc. Prof. Erdem Günay .....

DATE OF APPROVAL: 02.08.2019

ACKNOWLEDGEMENTS

Firstly, I would like to express my most sincere gratitude to my thesis supervisor, Assoc. Prof. Sezen Soyer Uzun for her guidance, contribution, trust in me and motivation during my thesis. I will always remember her support and politeness. It is privilege to work with her.

I would like to thank my thesis committee members, Assoc. Prof. Burak Alakent and Assoc. Prof. Erdem Günay for devoting their valuable time for my thesis defense and for their helpful recommendations. I am also grateful to Assoc. Prof. Alper Uzun and Samira Kurtoğlu for their permission and help in spectroscopy and diffraction measurements. Morever, I want to thank Assoc. Prof. Nilüfer Özyurt Zihnioğlu and Onur Öztürk for their support and help in compressive strength measurements.

I would particularly like to appreciate my dear friend Özlem Özbek for her encouragement and help. Her irreplaceable friendship is always very special for me. I would like to thank all friends whom I have shared good moments during years of Boğaziçi University, including Elif Esvap, Ayşegül Karakuş, Dilara Göreke, Begüm Yağcı, Selin Baç Bilgi, Müge Kasım, Özge Selçuk, Merve Yüce, Sezi Yiğit and Seymen İlke Kaykanat. I am happy for opportunity of having friendship and good times with them. I also thank to Kardelen Kaya for her friendship. I would like to thank to my friend Semanur Soykan for enjoyable moments and her support.

My dearest thank is for my beloved family for their endless loving, patience, prays and supporting. They always trust me on everything throughout in my whole life. I specially thanks to my brother Emin Öner for his help in my experiments and life and my mother her endless support.

Finally, financial support of this thesis provided by TÜBİTAK (Grant No: 117Z675) is acknowledged.

ABSTRACT

DEVELOPMENT OF PLA-CALCIUM PHOSPHATE COMPOSITES WITH HIGH COMPRESSIVE STRENGTH EMPLOYING A SILANE COUPLING AGENT (A-174)

Polymer-ceramic composites are being investigated in bone tissue engineering applications to obtain bone-like properties so that problems including the necessity of a second operation for metal implants are avoided. These composite materials, unfortunately, suffer from low mechanical performance compared to cortical bone and incompatible biodegradation due to low interaction between polymer and ceramic parts. In this study interaction between polymer (polylactic acid, PLA) and ceramic components (hydroxyapatite, HAP and beta-tricalcium phosphate, β-TCP) is enhanced by surface treatment of the ceramic parts using a silane coupling agent (Methacryloxypropyl trimethoxysilane, A-174). PLA-HAP and PLA-β-TCP composites were synthesized by solving casting method. The effect of ceramic surface treatment on structure, mechanical and degradation properties was investigated. Structural characterization employing FTIR, XPS, SEM and XRD was performed for raw materials and composites. It was concluded that surface treatment using silane A-174 can increase polymer dispersion on ceramic surface and improve polymer-ceramic interactions in both systems. The composite synthesized by 3% silane treated HAP and PLA in equal mass proportions (PLA50H50Si3) displayed a compressive strength value of 364 MPa, exhibiting a superior performance compared to other composites previously reported. It was observed that surface modification results in obtaining a more controlled degradation in PLA-β-TCP composites while it does not seem to influence the degradation in already stable PLA-HAP composite within the time frame the experiments were performed.

ÖZET

SİLAN BAĞLAYICI AJANI (A-174) UYGULANARAK YÜKSEK BASINÇ DAYANIMLI PLA-KALSİYUM FOSFAT KOMPOZİTLERİNİN GELİŞTİRİLMESİ

Kemik benzeri özellikler elde etmek böylece metal implantlar için ikinci bir işlem gerekliliği de dahil olmak üzere sorunları aşmak için kemik doku mühendisliği uygulamalarında polimer-seramik kompozitleri araştırılmaktadır. Bu kompozit malzemeler polimer ile seramik kısımlar arasındaki düşük etkileşimden dolayı kortikal kemikten daha düşük mekanik performans ve uyumsuz biyobozunurluğa sahiptir. Bu çalışmada, polimer (polilaktik asit, PLA) ve seramik bileşenler (hidroksiapatit, HAP ve beta-trikalsiyum fosfat, β-TCP) arasındaki etkileşim, seramik parçaların silan bağlayıcı ajanı (Metakriiloksipropil trimetoksisilan, A-174) kullanılan yüzey işlemi ile geliştirilmiştir. PLA-HAP ve PLA-β-TCP kompozitleri, döküm metodu çözülerek sentezlenmiştir. Seramik yüzey işlemenin yapı, mekanik ve bozunma özellikleri üzerine etkisi incelenmiştir. Hammaddeler ve kompozitler için yapısal karakterizasyon FTIR, XPS, SEM ve XRD kullanılarak yapılmıştır. Silan A-174 kullanılarak yapılan yüzey işleminin, seramik yüzeydeki polimer dağılımını artırabileceği ve her iki sistemde de polimer-seramik etkileşimlerini artırabileceği sonucuna varıldı. % 3 silan ile muamele edilmiş HAP ve PLA ile eşit kütle oranlarında (PLA50H50Si3) sentezlenen kompozit, daha önce bildirilen diğer kompozitlere kıyasla daha üstün bir performans sergileyen 364 MPa'lık bir basınç dayanımı değeri sergilemiştir. Yüzey modifikasyonunun, PLA-β-TCP kompozitlerinde daha kontrollü bir bozulma elde edilmesine yol açtığı, deneylerin yapıldığı zaman zarfında hali hazırda stabil PLA-HAP kompozitindeki bozulmayı etkilemediği görülmüştür.

TABLE OF CONTENTS

LIST OF FIGURES

LIST OF TABLES

LIST OF ACRONYMS/ABBREVIATIONS

FTIR	Fourier Transform Infrared Spectroscopy
HAP	Hydroxyapatite
HBSS	Hanks' Balanced Salt Solution
PLA	Poly-Lactic Acid
PLA50H50	Composite contains 50 wt.% of PLA and 50 wt.% of HAP
PLA40H60	Composite contains 40 wt.% of PLA and 60 wt.% of HAP
PLA50T50	Composite contains 50 wt.% of PLA and 50 wt.% of β-tri-calcium phosphate
PLA40T60	Composite contains 40 wt.% of PLA and 60 wt.% of β-tri-calcium phosphate
PLA50H50Si3	Composite contains 50 wt.% of PLA and 50 wt.% of 3 wt.% silane A-174 treated HAP
PLA40H60Si1	Composite contains 40 wt.% of PLA and 60 wt.% of 1 wt.% silane A-174 treated HAP
PLA50T50PASi3	Composite contains 50 wt.% of PLA and 50 wt.% of phosphoric acid and 3 wt.%silane A-174 treated β-tri-calcium phosphate
PLA40T60PASi1	Composite contains 40% of PLA and 60 wt.% of phosphoric acid and 1 wt.% silane A-174 treated β-tri-calcium phosphate
SBF	Simulated Body Fluid
SEM	Scanning Electron Microscopy
XPS	X-ray Photoelectron Spectroscopy
XRD	X-Ray Diffraction
β-TCP	β-tri-calcium phosphate

1. INTRODUCTION

Biomaterials are used to replace or supplement function of tissues of human body. Their usages originate from ancient civilizations. For example, artificial eyes and teeth were found in Egyptian mummies. Today biomaterials are used frequently in the form of implants (like bone plates, heart valves, dental implants) and medical devices (like artificial heart, biosensor) to restore function of traumatized and degenerated tissues [1]. Biomaterials can be classified according to their material types or applications. Metals, alloys, ceramics, polymers and composites are main types of materials [2].

Bone is an important part of human skeleton. Its functions can be summarized as supporting muscle and tissues, satisfying load bearing feature for skeleton system, protection of internal organs, providing movement, storing mineral and energy for body [3]. Bone is a natural composite and it has two major components; collagen protein and mineral hydroxyapatite [4]. Bone replacement and treating bone fractures are frequently studied because globally more than 2 million applications are needed because of diseases like tumor, accidents or trauma [5]. In these applications biocompatibility, biodegradability, bioactivity and chemical and mechanical similarity with bone matrix are important issues for consideration. Although different metal-type implants are used today for applications to hold bone fragments together like screws, plate; recent researches focus on composite materials with bio-absorbability feature, i.e. they don't need another surgery for removing from body [2].

Composite materials consist of two or more constituents or phases and generally a binding agent for uniform dispersion and/or increased binding interaction. Constituents are mechanically and physically separable. These constituents eliminate drawbacks of each other and achieve optimum and unique property for a given purpose. For example, ceramic biomaterials like hydroxyapatite (HA) are used in implants due to biocompatible and non-toxic properties. However, unfortunately they display low toughness. Polymers are another choice for implant applications; however they also have some drawbacks in terms of mechanical and load bearing

properties. For bone implant applications, widely used polymers are biocompatible polyethylene (PE), polyamide (PA), poly-lactic acid (PLA), and poly ε-caprolactone (PCL) [6], [7]. Ceramic part usually consists of hydroxyapatite (HA, Ca/P ratio is 1.67), tri-calcium phosphate (TCP, Ca/P ratio is 1.50) and BCP (mixture of TCP and HA) in these composites [2].

The aim of this work is to develop high performance polymer-calcium phosphate composites for bone tissue engineering applications that are capable to display controlled biodegradation rates. The binding interaction between PLA and ceramic phase was modified by employing coupling agent silane A-174 in the synthesis procedures. This thesis includes five chapters as following; Theoretical Background includes general information about biomaterials, bone tissue engineering, bone structure, biomaterials and literature survey on calcium phosphate bio-ceramics and polymer composites (Chapter 2). Used materials, production and characterization methods, compressive strength and biodegradation measurement methods are illustrated in Materials and Methods part (Chapter 3). In the Results and Discussion section XRD, FTIR, SEM and XPS analysis results, compressive strength of the composites and biodegradation experiments of the composites are given (Chapter 4). Significant results and suggestions for future studies are presented in the last chapter, Conclusion and Recommendations (Chapter 5).

2. THEORETICAL BACKGROUND

2.1. General Terms in Biomedical Area

2.1.1. Biomaterials

Biomaterials are synthetic and natural substances that are used as directly isolated materials and more general in devices to contact biological systems. Usage areas of biomaterials are cited as growing cells in culture, biotechnological application to produce biomolecules in equipment, investigational cell-silicon biochips [8]. However, they are applied generally in medical field therefore in literature they are also named as biomedical materials [2], [8]. Generally, they are classified their material types and usage areas [9].

Use of biomaterials starts from Egyptian mummy as artificial eyes and noses. Also, teeth from seashell in Mayan people in 600 a. d. and iron dental implant in Europe in 200 a. d. show that biomaterial have been operated for years. Another early application of biomaterials is metallic sutures that are seen in early Greek literature (130-200 a. d.). In early applications of biomaterials were generally obtained from natural materials like wood, glue and rubber and manufactured materials such as gold, iron, zinc and glass [2]. After Second World War studies on biomaterials developed. First hip replacement in 1891, studies about artificial kidney, contact lenses, stents, knee prostheses and vascular grafts are some examples of this development [8].

Early applications of biomaterials depend on removal of damaged tissues. Removal of tissues satisfies with transplants. Transplantations are mainly divided into three categories which are autograft, heterograft and homograft. Autografts are made from own tissue of patient, homografts are obtained from human source and heterografts are transplanted from both living and non-living other species. However, removal of tissue had some major limitations such as application in small parts only. With improvement in medicine area, removal of damaged tissue shifts to replacement of damaged tissue. Hence, implantation becomes alternative option for

tissue healing [8]. This development is shown in Figure 2.1 [8]. Implants are produced from man-made biomaterials. Availability, reproducibility and reliability are main advantages of implants with respect to transplants.

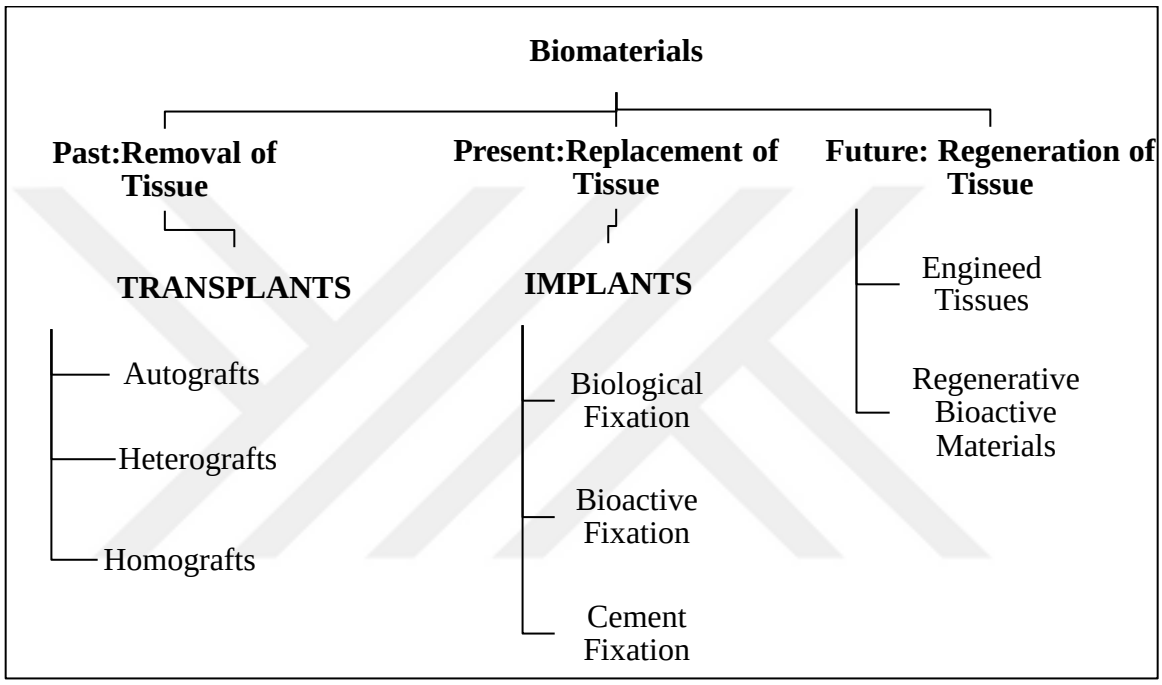

Figure 2.1. History and classification of biomaterials [8].

2.1.2. Biofunctionality

Biofunctionality is defined as the expected properties which device should perform as long as necessary. Expected properties from biomaterial are similar support (comparable to bone or tissue) in the early stages of healing, graded load transfer, tensile transmission, compressive transmission, load transmission, stress distribution, articulation, blood and other fluid flow and transmission of light features of tissue that is to be regenerated [8].

2.1.3. Biocompatibility

Biocompatibility is the acceptance of biomaterials by tissue that is to be regenerated mechanically, chemically, pharmacologically and morphologically. It refers to the long term ability of the biomaterial to maintain its function. Biocompatible materials and their degradation products must not show inflammatory response, extreme immunogenicity or cytotoxicity [2], [8].

2.1.4. Bioreactivity

Bioreactivity refers to the reactivity with tissue. Biomaterials are divided into two classes according to their bioreactivity, namely, bioactive and bioinert. This classification is made under the term of biocompatibility in some studies [10]. Bioinert means exhibition of minimum interaction between tissue and material. Titanium and steel-based materials in medicine are some examples of bioinert materials. Bioactive can be defined as the interaction of materials with the part they are placed into, like bone, tissue and etc. Implants based on synthetic hydroxyapatite and glass-ceramic apatite-wollastonite are examples of bioactive materials that are currently being used. In these implants bioactive materials forms the carbonate apatite crystal layer on implant by ion change with bone. This layer is chemically similar to bone and it interacts with bone proteins. Hence, by this interaction bone reconstruction starts [2], [11].

2.1.5. Bioresorption

Bioresorption refers to the removal ability of materials with cell activity and/or dissolution in biological environment. This process includes degradation of material, elimination of by-products and complete absorption in body. Tricalcium phosphate and poly-lactic– poly-glycolic acid copolymers are examples of bioresorbable implant materials [11], [12]. Although in some cases non-resorbable materials are used, it is not preferred generally due to need for active remove after treatment with another operation [13].

2.1.6. Biodegradation

Biodegradation is gradual fragmentation of material by specific biological and/or biochemical activity. Biodegradation and bioresorption are similar terms however their causes are different from each other. Bioresorption are affected from cell activity and/or dissolution in biological environment. Biodegradation is related with the action of living systems and physical-chemical factors, and cell behavior [2], [14], [15].

2.1.7. Biointegration

Biointegration defines the acceptance of material by tissue in process of healing with stable and low-grade interactions. With time diffusion of material or its products takes place in body. Absence of local or general adverse reaction, toxicity, carcinogenicity, allergenic situation and radioactivity are required from biomaterial. Biointegration includes all these terms and biocompatibility term [16], [17].

2.2. Bone Tissue Engineering

One of the usage areas of biomaterials is bone tissue engineering. Tissue engineering is an interdisciplinary field used clinical medicine, mechanical engineering, materials science, genetic and similar discipline in engineering and science to heal tissue and improve its function. Term of tissue engineering was officially started to be used in 1988 at National Science Foundation workshop. Although term of tissue engineering is new and after mid-1980s studies and reviews published show tremendous increase, replacing the tissue is back to study of Gasparo Tagliacozzi in 16^{th} century which describe nose replacement from constructing forearm flap [3], [18], [19].

Bone disease causes the limitation of bone functions and fracture of its structure. Every year millions of people need bone healing surgeries. For example, worldwide osteoporotic fractures in people after age of 50 is estimated 158 million and it is estimated to will be doubled

in 2040 [20]. Different reasons like trauma, tumor or bone related diseases and old age cause bone defects [21]. Today treat of bone damages are generally performed by autografts, allograft and xenogeneic [22]. Autograft means the shifting of bone from one site to another in same person, allografts from one individual to patient and xenogeneic from animal source to individual. They depend on transplant of bone and they have some disadvantages. Harvesting of bone is expensive and painful process with shortage of bone grafts. Also, they have risk of disease transmission, infection, hematoma, rejection by immune system and anatomical limitations [18], [21]. To exceed these problems studies for alternative synthetic bone grafts start to increase in last two decades [22], [23]. Target of these biomaterials is not only to fill bone defects but also satisfy mechanical and structural support [23]. Shortly, aim is regenerating of bone both *in vivo* and *in vitro* to replace defected bone.

Used biomaterials in treatment of bone defects should induce similar properties with bone to achieve healing of bone. Since bone has three-dimensional structure, these requirements are extensively satisfied by using porous three-dimensional scaffolds to obtain suitable environment for regeneration of bones [18], [19]. As well as three-dimensional structure, similarity of scaffold with natural bone in terms of chemical structure, mechanical, osteoconductive, and osteoinductive properties is essential to repair or regenerate bone. In order to choose appropriate materials and produce successful bone scaffolds, information about bone biology like bone structure, bone mechanics and tissue formation is fundamental [3], [19].

2.3. Natural Bone

Bone has important function in body to form framework of human body with its different physiological functions. In addition, bone satisfies load-bearing capacity for skeleton and protect internal organs. Moreover, bone includes biological elements for hematopoiesis, and it prevents entrance of dangerous materials such as lead into circulatory system. Calcium and phosphate ion storage in bone is crucial to continue homeostasis of key electrolytes. These properties and additionally its regenerative capacity make bone an ultimate smart material [3], [24]. Despite of the different functional features of bone, it also has different structural

properties. These complex properties mainly are related with simple microscopic hierarchical architecture of bones which has constituents of soft collagen protein and stiffer apatite minerals [3], [25].

Bone consists of calcified bone matrix, cells and bioactive factors. Their percentages change according to species, age, sex and type of bones. Mineral materials (65%), organic materials (25%) and water (10%) are ingredients of average human bone matrix. Main inorganic mineral part of bone matrix comes from hydroxyapatite with Ca/P ratio is between 1.3:1 and 1.9:1 and it involves some impurities. Size of hydroxyapatite is usually below hundred nanometers. Although some impurities cause poor crystallization, deficient calcium and carbonation of HA, presence of impurities has important role in bone growth and effect on bone metabolism [2], [23], [24]. Organic part of bone matrix is formed by proteins such as collagen. Up to now, 28 collagen types are observed for vertebrates and four collagen are named for bone including species which are I, III, V and XXIV collagen [23]. Elemental composition of bone mainly includes calcium and phosphorous as shown in Table 2.1 [26].

Table 2.1. Bone Composition Percentage of Adults [26]

Components	**Percentage in Bones (%)**
Calcium	34.8
Phosphorous	15.2
Carbonates	7.4
Sodium	0.9
Magnesium	0.72
Chlorine	0.13
Pyrophosphates	0.07
Potassium	0.03
Fluorine	0.03
Others	0.04

Functionality and mechanical properties and bone types are determined by ratio and place of these hydroxyapatite and collagens. For example, stiffness which is related with the functionality of bone is determined by collagen/mineral ratio. Over 80% of the mineral ratio of ear enables vibrating to permit sound transmitting. Similarly, 20% percent ratio of long bone enables to absorb energy and have light weight for mobility. Moreover, compressive strength and tensile stress are mineral phase and collagen-related properties, respectively [27]. Also, nanocomposite structure of bones, which are formed by positioning of tough and flexible collagen fibers are reinforced by hydroxyapatite crystals, is important for compressive strength and high fracture toughness [3], [25].

Bones in human and other mammal bodies are generally classified as two basic morphological types: cortical (compact) and trabecular (cancellous or spongy). Cortical bone has dense structure and it is found in outer shell around cancellous bone and in shaft of long bones. Its porosity is in the range between 5% and 10%. Trabecular bones have more porosity and lower density than cortical bones. However, biological activity of trabecular bones is higher than compact bone; this enables self-renewal property. Trabecular bones have web-like matrix which is formed by connecting three dimension of rod or plate like elements. They are found generally in epiphyses and metaphysis of long bones and they are also included in all regular and irregular shaped bones [2], [3], [28], [29].

Bones are exposed to 4 MPa stress approximately on daily basis. This stress changes and can be repetitive for different daily activities. With respect to differences in their compositions, bones show different mechanical properties. For example, collagens, like polymers, satisfy high toughness, and low modulus. Inorganic phase of hydroxyapatite gives stiffness to bones. Human bone shows good toughness because of its hierarchical structure that stops the cracks after propagation. Bearing of bones in different stress conditions changes according to humidity, rate and direction of load [2].

Understanding mechanical properties of human bone is crucial to design scaffold and to choose appropriate materials for scaffolds. Compressive features of cancellous bone and tensile properties of cortical bone are more important among other mechanical properties [2].

Compressive strength of cortical bone is given between 88 and 193 MPa in different sources according to applied direction [2], [26], [30]. Compressive strength of cancellous bone is reported to be between 3 and 12 MPa [30], [31]. Tensile strength value ranges of cortical and cancellous bones are stated as 50-174 MPa and 1-8 MPa, respectively [2], [26], [30], [32]. Another important mechanical parameter related to bone is Young's modulus. Its values change between 13 and 18.9 GPa for cortical bone and 0.4-0.5 for cancellous bone [2], [30].

Although bone is thought as lifeless structure, it is living tissue in body due to existence of blood and nerve vessels and different cells in it. Four types of cells which are found in bone are osteoblasts, bone lining cells, osteocytes, and osteoclasts. Except of osteoclast all cells are originated from mesenchymal stem cells. Osteoclasts come from hematopoietic stem cell. Osteoblasts are responsible for bone forming function and they don't have division ability. Bone lining cell prevents the interaction of osteoclast and bone matrix in undesired bone resorption situations. Osteocytes are important for bone survival and they satisfy transportation of materials by its long extension structures. Osteoclasts are liable for resorption [33].

Process of bone formation is named as osteogenesis or ossification. Osteogenesis (ossification) targets formation of skeleton in embryos, bone growth and bone remodeling and repair [34]. It includes series of biological events that includes different cell types and pathways to form new mineralized tissue [35]. Osteogenesis (ossification) starts with collagenous mesenchymal tissue change with bone. This change forms a primitive bone and then primitive bone remodeled to mature lamellar bone includes regular rings of collagens. This lamellar bone is reformed by osteoclasts and osteoblasts [36]. Osteogenesis (ossification) happens via two ways which are intramembranous osteogenesis (ossification) and endochondral osteogenesis (ossification). In intramembranous osteogenesis (ossification), bones are formed by differentiating from mesenchymal stems in embryo. This type is observed in many locations of the skeleton and in formation of flat bones of the cranium and facial bones. It occurs direct forming of mesenchymal precursor cells to osteoblasts during development of some skull and facial bones [34]. Endochondral osteogenesis (ossification) occurs with replacement of cartilage with natural bone. Chondrocytes are differentiated from mesenchymal cells in endochondral ossification. It occurs during skeleton formation of most mammalian except skull bones,

development of long bones and repairing of vertebrae and bone [34]. In addition to osteogenesis (ossification) angiogenesis is an important process for bone repair. Angiogenesis satisfies formation of new vessels from existing vessels and this is important for nutrients, oxygen and bone precursor cells to reach injured part [37].

2.4. Biomaterials for Bone Healing

In the first implant applications bioinert materials were used. However with second generation biomedical devices, demand starts to shift bioactive materials thanks to its ability to integrate with biological molecule, cells and regenerate tissues [22], [38] . Choice of biomaterial for bone expectation is osteoconductivity which refers providing framework to promote new bone formation, osteoinductivity which describes the capability to satisfy differentiation of progenitor cells to osteoblastic lineage, and osseointegration which relates with ability of forming bony tissue at bone-implant interface [22], [25]. Materials are mainly used in implants can be categorized as metals, ceramic and glasses, polymers and composites.

2.4.1. Metals

Metals and their alloys are first used implant materials. Their advantages are biocompatibility and desirable mechanical properties. Corrosion like wear debris and possible byproducts of degradation, release and accumulation of metal ions are problematic issues for metals and their alloy. Although it is tried to be decreased by titanium based implants, inflammation is still risk due to these problems [13], [30].

2.4.2. Ceramics and Glasses

Ceramics and glasses are inorganic materials that are used in implants due to their similar chemical composition to mineral phase of bone [22]. Both of them can be used as individually or together. Their stability in physiological environments is the most attractive property for bone healing applications [13]. Also heat and electricity insulation property of ceramics are another

important feature in manufacturing process [30]. They have three classes according to their surface reactivity. These groups are inert materials, soluble materials, and intermediate materials. Alumina and certain calcium phosphate ceramics like dense hydroxyapatite are examples of inert group. Tri-calcium phosphate is an example of biodegradable class ceramics with lower strength [13], [22]. Among ceramic classes, hydroxyapatite is the most preferable ceramic due to direct bond with bone. Porous surface scaffolds show the good properties for bone growth with prosthesis stability. However, cracks in prosthesis causes break, therefore strength of prosthesis another main concerns in this area in addition to biocompatibility and biodegradation [23], [30].

Hydroxyapatite is used commonly ceramic with 1.67 of Ca/P ratio. Bone regeneration application of it starts at mid-1980s [39]. It has good biocompatibility, osteoconductivity and bone-bonding (bioactivity) ability. It has also good compressive strength with low resistance to tension and shear load. However, when its bioactive processes are compared with bioactive materials, it has some disadvantages. For example, bioactive process takes a few minutes in silica-based glasses, it takes days in hydroxyapatite. In order to exceed this disadvantage silicon addition in hydroxyapatite is a common method. Silicon substituted hydroxyapatites have comparable biocompatibility and mechanical properties with developed bioactivity [23], [40].

β-TCP is another widely used calcium phosphate with 1.5 of Ca/P ratio good osteoconductivity, biocompatibility and biodegradability. Its good biodegradability compared with the hydroxyapatite enables faster degradation and replacement with newly bone tissue [23]. It also has good resorption rate therefore it is used to increase biocompatibility of bone scaffolds. It helps the proliferation of osteoblasts and bone marrow stromal cell [39].

Biphasic calcium phosphates are improved for desired property of both hydroxyapatite and β-TCP (or other tri-calcium phosphate). First mixture of hydroxyapatite and β-TCP is made in 1986. Effect of Ca/P ratio in absorption rate and mechanical properties is important. Changing this ratio with usage amount of hydroxyapatite and β-TCP in biphasic calcium phosphate enables the combining of biodegradation of β-TCP and stability of hydroxyapatite and attaining desired bioactivity, bio-resorbability, osteoinductive property and mechanical strength [39].

2.4.3. Polymers

Polymers are long repetitive chain molecules. These chains are formed by covalent bond and secondary bond; Van der walls and hydrogen bonds. They have different mechanical property ranges with easy forming shape. Their low cost is the most attractive feature to use them in many applications [2]. They are classified as natural and synthetic polymers according to their origins. Proteins, polysaccharides and chitosan are natural polymers that are used in bone tissue applications. Natural polymers show good biocompatibility and osteoconductive properties, however they have low mechanical stability. Aliphatic polymers like PLA and poly-glycolide are mostly used synthetic polymers in bone tissue engineering. Polymers also categorized two groups according to their degradability as non-resorbable and resorbable (biodegradable). Polyethylene and polypropylene are examples of non-resorbable polymer. Poly-glycolic acid, poly-lactic acid, polycarbonate and chitosan are resorbable (biodegradable) polymers. Although demand features from polymers can be adjusted with composition, type, molecular weight etc., both natural and synthetic polymers demonstrate common low mechanical property with respect to requirements of implant applications [2], [41], [42].

Poly-lactic acid is a type of cheap aliphatic polyester which shows thermoplastic and biodegradable behavior. It and its composites are non-harmful and non-toxic after degradation in body and degradation products can be eliminated with kidney. However, degradation product of lactic acid may cause the inflammatory response. It has good biocompatibility, biodegradability and process ability properties. Its mechanical property is high with respect to other bio-absorbable polymers but it is brittle after glass transition temperature; approximately 55 °C [43]. It is also produced with copolymer of another monomer. These properties enable it to be used in biomedical areas like tissue engineering, drug delivery and medical implants. Poly-lactic acid scaffolds show slow degradation. It starts after 4 weeks and total degradation continues 12 months [44]–[47].

2.4.4. Composites

Composites consist of two or more materials that are in different classes. Composites give ability to adjust desired properties of different materials. First bio-composite material was applied in orthopedic applications by plaster of Paris. Composites in orthopedic applications aim the mimic of real bone by addition of inorganic and organic phases. Organic phase is generally coming from polymer and inorganic part is from ceramics. Toughness and biodegradability of polymer phase and compressive strength, osteoconductivity and bioactivity of inorganic part can be combined with composite application. Hence materials with improved mechanical, bioactivity properties and good biodegradability can be developed. Composites also give opportunity to neutralize acidic degradation of polymers which cause inflammatory with alkalinity of inorganic part [22], [30].

Poly-lactic acid/ceramics composites are common composite application to satisfy requirement of bone tissue applications. Poly-lactic acid is used generally improve biodegradation. These composites are fabricated with different methods. These are electrospinning, gas foaming, freeze drying, solvent casting, particle leaching and thermally induced phase separation methods [48]. Among ceramics hydroxyapatite, β-TCP and biphasic tri-calcium phosphate are used frequently in poly-lactic composites. Poly-lactic acid/hydroxyapatite and poly-lactic acid/β-TCP composites are appropriate to use in non-load-bearing and high rate of degradation applications [43]. Chemical similarity with bone of both hydroxyapatite and B-TCP improves biocompatibility of poly-lactic acid. Also, osteoconductivity property of poly-lactic acid/hydroxyapatite shows improvement in composites [3]. Two composites are highly biomimetic, and they induce calcium phosphate formation, precipitation and deposition in simulated body fluid. However, main problem of these composites is low mechanical properties due to adhesion and dispersion problems between polymer and ceramics [49]. Mechanical properties of these composites are affected from different parameters like structure of polymer, production method, structure of polymer, particle size of ceramic and weight fraction of polymer and ceramic, surface modification of ceramics [6], [49]. Shortly, aim of poly-lactic acid/calcium phosphate is desired mechanical property and biodegradability in simulated body fluid which does not exceed bone regeneration capacity.

2.5. Studies on Production, Characterization, Mechanical Properties and Degradation of Hydroxyapatite and β-TCP-Poly-Lactic Acid Composites

In bone tissue engineering applications composites of hydroxyapatite, β-TCP and biphasic tri-calcium phosphate with polymer are used to mimic bone and to obtain successful implants. These composites are investigated by different characterization methods to understand interaction between polymer and ceramic. Also, compressive strength, tensile strength and bending strength of these composites are tried to be developed with changing of different parameters. Also, biodegradation studies are done to investigate the implants which are appropriate in bone regeneration. Desired properties are studied with changing polymer/ceramic ratio, polymer type, and hydroxyapatite particles. In addition to these, effect of surface modification of ceramics with different agents is commonly investigated on expected features of composites.

Two main desired features of composites may cause adverse effect on each other. For example, poly-L-lactic acid/hydroxyapatite composites are fully resorbable in human body. However, resorbability causes the low mechanical strength of implant. Russias *et al.* investigated the poly-L-lactic acid/hydroxyapatite composites by changing the hydroxyapatite particles as fine grained and coarser whisker. They used simple hot-pressing procedure for production of composites. They also changed hydroxyapatite content from 40 % to 100 %. Surface modification of produced composites was searched by scanning electron microscopy (SEM). Mechanical tests were performed after production, and after storage in Hank's Balanced Salt Solution (HBSS) that was used as simulated body fluid for 1, 10 and 20 days. They obtained composite with Young's Moduli of above 10 GPa, which is assumed lower limit for cortical bone, for composite containing 70- 85 wt.% of hydroxyapatite. Composites that includes 70-85 wt.% hydroxyapatite were found promising after Hank's Balanced Salt Solution (HBSS) degradation. All composites displayed approximately 8-17% reduction of elastic moduli after 20 days. This reduction was higher for composite which have higher ceramic contents and whisker shaped due to degradation of low amount of polymer [50].

Another study investigated the effect of polymer type (poly-L-lactic acid and its copolymer), hydroxyapatite content between 10 and 40%, surface modification of hydroxyapatite with 3-aminopropyltriethoxysilane (AMPTES) and 3-mercaptopropyltrimethoxysilane (MPTMS) and percent of silane coupling agents on mechanical and structure of composites. Mechanical improvements were measured by tensile test and microstructure effects were searched with SEM images. Composites were produced through solvent casting method for treated and untreated ceramic and polymer composites. It was found both silane treatment improved the dispersion of hydroxyapatite in polymer matrix. Tensile strength showed increase with increasing hydroxyapatite content both untreated and treated composite up to 30%. Reduction after 30% was attributed to possibility of agglomeration hydroxyapatite which causes the low adhesion between polymer and hydroxyapatite. Also, maximum mechanical improvement for composites containing 20% hydroxyapatite was observed in 1 wt.% 3-aminopropyltriethoxysilane (AMPTES) treated composites of hydroxyapatite-poly-L-lactic acid and 0.5 wt.% 3-mercaptopropyltrimethoxysilane (MPTMS) treated composites of hydroxyapatite-copolymer [51].

Zhou *et al.* cleared up the bonding mechanism of poly-D, L-lactic acid (PDLLA) and hydroxyapatite. Hydrogen bonding was investigated by SEM, differential scanning calorimetry (DSC), Fourier transform infrared spectroscopy (FTIR) and X-ray photoelectron spectroscopy (XPS). Composites were produced with weight ratios of polymer: ceramic as 1:1, 2:1, 3:1. It was found that uniform distribution of hydroxyapatite on polymer surface without agglomeration from SEM analysis. This was referred as interaction between two phases not only physically but also chemically thanks to the preventing agglomeration effect of chemical actions. SEM and glass transition temperature of nanocomposite showed evident of close interaction, i.e. chemical bond. Also, hydrogen bonding between C=O and P-O groups on surface of hydroxyapatite was indicated by FTIR and XPS results. Hydrogen bonding increase was observed with increasing amount of hydroxyapatite. Also, positive effect of composite on shape memory properties was proved by comparing the shape memory behavior of pure PDLLA and composites [52].

Another study researched on effect of production methods on hydroxyapatite/poly-L-lactic acid and β-TCP/ poly-L-lactic acid composites with SEM and tensile modulus measurements. Ceramic ratios of composites were kept 5% and 10% for each type. Three compared production methods were dry process before compression molding, solvent solution and melt extrusion. SEM images showed the solvent and melt extrusion methods exhibited the more homogenous dispersion than dry process. Also melt extrusion method was found to be the highest modulus. It was found that plasticization of molecules due to chloroform resulted in low modulus in solvent solution method. Also, study observed that a composite with 10% ceramic ratio has higher modulus value. Moreover, tensile modulus of hydroxyapatite including composites were found higher than β-TCP including composites [53].

Study on effect of hydroxyapatite percent (10, 20 and 30 %) on tensile properties of composite that were produced with melt extrusion and following injection moulding displayed increasing ceramic ratio evolved the tensile strength and hence decreased the tensile modulus. Also, it was found that increasing ceramic ratio caused the reduction of elongation at break percentage. SEM images showed the more agglomeration occurred in 30% hydroxyapatite [54].

Nejati *et al.* synthesized and analyzed the rod-shaped hydroxyapatite and then produced hydroxyapatite/poly-L-lactic acid composite scaffold with thermally induced phase separation method. Compressive strength of nanocomposite was found 14.9 MPa which is higher than micro composite. Biocompatibility and cell affinity of nanocomposites were found higher than micro composite by experiment on rats. FTIR result showed the new peak formation in composite at 1414 cm^{-1} which was referred to calcium and ionized form of carboxyl group bond. This peak was found with similar intensity in micro composite. This new peak was assumed to evidence for molecular interaction and chemical bonding between polymer and ceramics. XRD results of composites were compared with their raw materials and intensity decrease was observed. Scaffold porosity reduced with the addition of ceramic due to possible filling ability of ceramic. Produced composite was nominated as bone tissue application of cancellous bone [55].

High agglomeration of hydroxyapatite and low compatibility between poly-lactic acid and hydroxyapatite were tried to be exceeded by surface treatment of hydroxyapatite with 2% of 3-aminopropyltriethhoxysilane (APES) and 3-methacryloxypropyltrimethoxysilane (MPTS). Success of silane treatment was proved by FTIR and SEM analysis. It was found that thermal stability of composites enhanced with silane treatment. Hydroxyapatite content was changed from 10 % to 40 %. SEM images of composites indicated the interfacial adhesion was increased with both silane additions. Also, tensile modulus, tensile strength and elongation at break percent increased with silane treatment. Moreover, study applied ISO 10993-5:1999(E) standard with human osteoblast cultured cells for cytotoxicity of composites and it was found that there was no toxic effect to human osteoblast [56].

Another comprehensive study investigated the different silane promoters with different functionality of vinyl, methacryloxy, amine and diamine. After silane treatment XPS analysis was done for treated hydroxyapatite. Bonding of silane agents to hydroxyapatite surface was proved. In study two dissolution analyses were done in simulated body fluid and Gomori's tris-meleate buffer. It was found that coupling agents did not prevent tendency to dissolution. Dissolution started after 4 hour and they are same after 2 or 3 days for all coupling agents. Only aminosilane coating delayed the calcium and phosphate ions during first two days in Gomori's tris-meleate buffer [57].

Another comprehensive study investigated the nanofibrous poly-lactic acid and hydroxyapatite scaffolds morphologically, mechanically and thermally. Two concentrations of hydroxyapatite were worked as 5% and 20%. Electrospinning technique was used. Smooth surface of composites and decrease of pore mean dimeter of composites with respect to polymer were observed from SEM images. Increasing hydroxyapatite content affected the tensile strength positively, i.e. higher tensile strength. Also, ATR-FTIR, XRD, TEM and TGA proved the existence of hydroxyapatite on composite surface and homogenous distribution of it on polymer. Osteoblast culture was prepared to see proliferation of scaffolds. It was observed cell viability continued and proliferated for 21 days. It was concluded that nanofibrous hydroxyapatite/poly-lactic acid scaffold is good candidate for bone regeneration area because of both mechanical strength and proliferation ability [48].

Degradation of porous poly-lactic acid/hydroxyapatite composites was characterized by ATR-FTIR in another study. Composite was produced by solvent casting/salt-leaching method. Phosphate-buffered saline (PBS) solution was used for *in vitro* degradation measurements. Every seven-day measurement was done for 105 days. After drying FTIR of composite was studied and an analysis method was used to analyze FTIR result. First aim of this study is deciding using ability of this analysis method in degradation study. However, this study also gave information about degradation days of poly-lactic acid/hydroxyapatite composite. Degradation was followed by intensity ratio of FTIR band 1026 cm^{-1} which shows the P-O groups in hydroxyapatite with FTIR band of 1755 cm^{-1} which indicates the stretching vibration of C=O group. First degradation started in day 14 for composite. It was observed first 56 days degradation was slow and it fastened up to 84 days and then kept constant. After day 84, shape of ratio changed to negative pattern due to decrease in hydroxyapatite content [58].

A comprehensive study was searched for *in vitro* and *vivo* degradation of poly D,L- lactic acid/ nano-sized hydroxyapatite. Study used logical saline (SPS) and a simulated body fluid (SBF) for *in vitro* studies. Composites were produced by 50 wt. % of ceramic and polymer with extrusion method. Human mesenchymal stromal cells were used *in vivo* study as culture and implants were put in dogs. Measurement of degradation was done for 12 weak. It was observed that swelling of composites was higher than polymer. Dry weight of composites decreased 4% and 7% in different two fluid medium. This trend was similar to polymer weight loss percentage trend. Weight percentage after 12 hours and 12 months of polymer and composites did not show big difference. pH of only polymer particles kept constant however it decreased in both fluid after 12 weak immersion. *In vivo* study more degradation was found for only polymer case, differently [59].

Effect of surface modification on interfacial adhesion, swelling property, and mechanical properties of poly-lactic acid and hydroxyapatite composites was investigated in study of Zhang *et al.* Composites were produced by volume 20% of hydroxyapatite. Three surface modifications were applied by gamma-amino-propyltriethoxy silane, gamma-2,3-cyclopropoxy-propyll-trimethoxy silane and gamma-methypropenionyloxy-propyl-trimethoxy silane. Also, modification was done two solution medium DMF and ethanol-water for each

silane agents. FTIR analysis of silanated hydroxyapatites was done and new peak was found belongs to P-O-Si bond. It was observed silane treated composites reached swelling equilibrium 1 or 3 days later than pure hydroxyapatite including composite. SEM image showed the homogenous dispersion with silane treatment in composites. This indicated that silane affected to reach desired swelling property. Also, bending strength of composite was enhanced after all silane treatments. Maximum bending strength improvement was obtained in gamma-amino-propyltriethoxy silane including composites by 27.8%. Bending strength of gamma-methypropenionyloxy-propyl-trimethoxy silane including composites, produced in ethanol and water solution medium, was found similar to untreated counterparts. This was thought as partial hydrolysis of gamma-methypropenionyloxy-propyl-trimethoxy silane into free carboxyl acid group. It was thought that this group may be absorbed by hydroxyapatite surface and surface caused degradation of poly-lactic acid which leads reduction of strength [60].

Another study searched the degradation of β-TCP and poly-lactic acid composites. Composite was produced by water/oil/water emulsion technique. Achievement of composite production method was investigated with SEM, EDX and XRD analyses. Degradation study was done with accumulated weight loss. Released calcium ion was detected by atomic absorption spectrophotometer. It was observed that composite showed rapid degradation in first 10 days and then it decreased. After 40 days, degradation of composites was found 9% higher than poly-lactic acid microspheres [61].

Surface modification of β-TCP was investigated in a comprehensive study. Stearic acid was used for surface treatment. Modification success was determined by TEM, FTIR, TGA and XPS analyses. New peak was found in FTIR spectrum belongs to $CaHPO_4$ group. This proved the protonation reaction between PO_4^{-3} groups of ceramic with H^+ of stearic acid hydrolysis. Hence, surface treatment was achieved. Then, composites of modified and unmodified β-TCP and poly-lactic acid were produced with electrospinning method. Three different polymer/ceramic ratios were tried as 0, 10 and 20% of β-TCP contents. Tensile strength of pure poly-lactic acid decreased in all composites. However, surface treated composites showed higher tensile strength and Young's modulus [62].

In order to understand and interpret degradation mechanism, silane effect on mechanical test and characterization further four additional studies that includes different polymer or ceramic including composite systems were investigated. Eight different coupling agents were tried in study of Hassan *et al.* to choose potential candidates for phosphate glass. FTIR analysis results indicated covalent bond between phosphate glass and three agents; 3-aminopropyltriethoxysilane (APS), etidronic acid (EA) and hexa-methylene diisocyanate (HDI). P-O-Si band was detected in 1190 cm^{-1} wavenumber. XPS analysis was conducted for phosphate glass systems which include these three coupling agents separately. Changes in O 1s and N 1s spectra of these systems confirmed the FTIR results. Reaction schemes of six coupling agents with phosphate glass were visualized from results of FTIR and XPS analyses. Standard test condition of ISO 10993-13:20 were followed with phosphate buffered saline solution in degradation studies for poly-lactic acid and phosphate glasses composites. It was found that the degradation rate decreased with 3-aminopropyltriethoxysilane (APS), etidronic acid (EA) and hexa-methylene diisocyanate (HDI) coupling agents [63].

Another comprehensive study investigated the poly-(ε-caprolactone) (PCL) /silanated tri-calcium phosphate (TCP) scaffolds. TCP was treated with silane agent and FTIR and XPS analyses were conducted to see achievement of silanization. Composites were produced with screw extrusion method. Compressive strength of composite increased 2.3 times when silane treated TCP was used. Maximum compressive strength was obtained as 82.6 MPa for composites. Also, carbonated hydroxyapatite-gelatin coated was done for composites to increase the osteoconductivity [31].

Study of β-TCP and poly-caprolactone (PCL) composite aimed to produce strong bioresorbable composite including low amount of polymer with low process temperature. Low temperature was stated as important condition for future studies which allow incorporation of drug and molecules for help of healing process and of preventing inflection risk. Polymer ratio was kept 5% and 15%, separately. SEM, FTIR and XRD analyses were done to detect achievement of production method and interaction between polymer and ceramic was detected. Compressive strength of composite was found 140 MPa for highest composite. Degradation study in Tris buffer and bioactivity study were done with simulated body fluid (SBF). It was observed dissolution of composites is like dissolution of pure β-TCP in first days. After 2 weeks

composites lost their compressive strength approximately 15%. Uptake of Ca and P ions were flowed in SBF. After SBF immersion for 4 days, FTIR analysis was repeated and it was observed P-O bond of ceramic was changed. This was assumed as evident of bone-like apatite surface and showed bioactivity of composite [64].

In order to see effect of solvent during silanization and percent of 3-trimethoxysilyl propyl methacrylate on mechanical performance of hydroxyapatite and acrylic composites, acetone/water and methanol/water systems were tried for 1, 2 and 3% of silane agent separately. It was found that methanol/water system showed the higher compressive strength (max. 107.8 MPa) and bending strength (max. 62.3 MPa). Tensile strength was found similar for two solvent systems and different 1, 2 and 3% percentages of -trimethoxysilyl propyl methacrylate silane agents. From all result it was found that methanol/water system with 3% of -trimethoxysilyl propyl methacrylate was better than others [65].

2.6. Compressive Strength of Polymer-Ceramic Composites

Table 2.2 shows the summary of compressive strength values regarding calcium phosphate involving composites in the literature that were summarized in section 2.5. For comparison, it should be noted that maximum compressive strength values of cortical bone and cancellous bone are 193 MPa and 12 MPa, respectively [2], [26], [30], [32].

It is known that after degradation experiments compressive strength values of the composites decrease [64]. Therefore, targeting higher compressive strength values compared to natural bone would be a good strategy for bone tissue regeneration area.

Table 2.2. Compressive Strength Values of Composites from Literature.

Polymer Type	**Ceramic Type**	**Treatment**	**Compressive Strength**
Poly-lactic acid	Hydroxyapatite	No	14.9 MPa [55]
Poly-lactic acid	Hydroxyapatite	Hot Press	139 MPa [66]
Poly-D,L-lactic-co-glycolide	NC calcium phosphate	Hot Press	82 MPa [67]
-	Hydroxyapatite with acrylic solution	MPS (3%)	107.8 MPa [65]
Polyamide66	Hydroxyapatite	Carbon Fiber (10%)	212 MPa [68]
Poly-(ε-caprolactone)	Tricalcium phosphate	GPTMS (10%)	82.6 MPa [31]
Poly-caprolactone	β-TCP	High Pressure	140 MPa [64]
Poly-caprolactone	Hydroxyapatite	No	27 MPa [69]
Carboxy-methyl Cellulose	Hydroxyapatite	Functionalized Carbon Fiber (0.75%)	118 MPa [70]

3. MATERIALS AND METHODS

3.1. Materials

In this study, hydroxyapatite ($Ca_5(OH)(PO_4)_3$) (Sigma Aldrich, CAS number: 1211674-7) and β-tri-calcium phosphate (β-TCP) ($Ca_3(PO4)_2$) (Sigma Aldrich, CAS number: 7758-87-4) were used as the calcium phosphate ceramic part of composites. Composites were produced with poly-L-Lactic acid (PLA) powder ($H(C_3H_4O_2)nOCH_3$) (Sigma Aldrich, CAS number: 765112) and these ceramics for characterization studies. Due to high price of powder of PLA, pellet form of poly-lactic acid was used for mechanical and degradation studies. In order to determine similarity of two form PLA, FTIR and XRD analyses results of them were compared and using pellet form in mechanical and degradation studies was found acceptable. XRD and FTIR results of powder poly-lactic acid are shown in Figure 4.3 and Figure 4.18 of Chapter 4, respectively. XRD and FTIR results of pellet PLA were displayed in Figure A.1 and Figure A.2 of Appendix part, respectively. Chloroform (Merck, CAS number: 67-66-3) and ethanol (Merck, CAS number: 64-17-5) were used in experiments as solvent.

Surface of ceramic components was modified with 3-(Trimethoxysilyl) propyl methacrylate (Methacryloxypropyl trimethoxysilane) (Silane-A174) ($C_{10}H_{20}O_5Si$) (Sigma Aldrich, CAS number: 2530-85-0). Ortho-phosphoric acid (Merck, Lot number: K50214873 818) was used for surface modification of β-tri-calcium phosphate before silane treatment. Sulfuric acid was used (Merck, CAS number: 7664-93-9, wt. 98%) for pH arrangement during surface treatment of HAP.

Hanks' Balanced Salt Solution (HBSS) (Sigma Aldrich, CAS number: H6648) was used for degradation studies.

3.2. Manufacturing Methods

3.2.1. Compositional Parameters for Composites

Summary of the compositional design parameters used for composite synthesis in this study was exhibited in Table 3.1.

Table 3.1. Summary of Composites Contents in Study.

	Polymer Type and Percentage	**Ceramic Type and Percentage**	**Surface Treatment Type of Ceramic**
PLA50H50	PLA (50 wt.%)	HAP (50 wt.%)	No
PLA40H60	PLA (40 wt.%)	HAP (60 wt.%)	No
PLA50H50Si3	PLA (50 wt.%)	HAP (50 wt.%)	3 wt.% Silane-A174
PLA40H60Si1	PLA (40 wt.%)	HAP (60 wt.%)	1 wt.% Silane-A174
PLA50T50	PLA (50 wt.%)	β-TCP (50 wt.%)	No
PLA40T60	PLA (40 wt.%)	β-TCP (60 wt.%)	No
PLA50T50PASi3	PLA (50 wt.%)	β-TCP (50 wt.%)	Phosphoric acid and 3 wt.% Silane-A174
PLA40T60PASi1	PLA (40 wt.%)	β-TCP (60 wt.%)	Phosphoric acid and 1 wt.% Silane-A174

3.2.2. Surface Treatment of HAP

HAP surface modification was done in line with the literature [2], [57], [65]. HAP was mixed with volume percent 90% of ethanol solution as 2/1 ratio for ethanol (ml)/ HAP (g) for few minutes. pH of 3.5-4 was arranged with 0.1 N of sulfuric acid solution. Then three materials (HAP, ethanol solution and sulfuric acid) were mixed for 45 minutes in magnetic stirrer. Silane A-174 should be used under inert condition according to MSDS of it. Therefore, nitrogen balloon was set on the beaker while continuing the mix. Silane A-174 was added the beaker

with 1% or 3% (according to desired amount) weight percent of initial HAP amount. Mixture continued to be stirred under nitrogen atmosphere for one hour. After mixing, it was dried at room condition, 120 °C and 50 ℃ for 2 hours, one hour and until complete drying (between 12 and 24 hours), respectively [71].

3.2.3. Surface Treatment of β-TCP

In order to increase success of silane treatment, surface of β-TCP was protonated phosphoric acid firstly by regarding previous studies [31], [72], [73]. Volume percent of 1 % phosphoric acid solution in anhydrous ethanol was prepared. β-TCP was mixed with phosphoric acid solution with 1/10 of β-TCP (g)/solution (ml) ratio for one hour at room temperature. Then, it was dried 110 ºC for 6-12 hours [72].

For silanization, protonated β-TCP was blended with ethanol with the ratio of 1(g)/6 (ml) for 10 minutes in magnetic stirrer. Nitrogen balloon was installed in beaker mouth. Silane A-174 was added the beaker with 1% or 3% (according to desired amount) weight percent of initial protonated β-TCP amount. Then it was mixed for 3-6 hours at 110 ºC. It was dried at 110ºC until complete dry (between 4 and 24 hour).

3.2.4. Synthesis of HAP and PLA Composite

Pure PLA and chloroform were mixed for 50 minutes at room temperature. PLA/ chloroform ratio was kept range between 5 and 10 % [2]. In 50 minutes, all polymer dissolved in chloroform. Treated or untreated HAP was added this solution with polymer/ceramic ratio of 40/60 or 50/50. Mixture was blended for 12 hours at room temperature in magnetic stirrer for characterization samples. This blending time (12 hour) was reduced to approximately 4 hours for samples of mechanical test and degradation study to be able to pour the mold. After mixing, characterization and degradation samples were dried at room temperature for one night and 40 ℃ until complete drying (between 4 hours to overnight). Mechanical test samples were put jolting apparatus (conforms the EN 196-1 standard) for 3 minutes and shaker (GFL Shaking

Incubator 3032) for one night with 250 rpm at room temperature due to large depth of mechanical test mold. Then, they were dried similarly at 40 ℃ until complete drying.

3.2.5. Synthesis of β-TCP and PLA Composite

β-TCP and PLA composites were manufactured at room conditions, similar to a previous study in literature [64]. Treated or untreated β-TCP and 20-30 ml of chloroform were mixed for a few minutes at magnetic stirrer [2]. Necessary amount of PLA was added to this solution to satisfy desired polymer/ceramic ratio as 40/60 or 50/50 under high rate stirring. Mixture was agitated for one hour with moderate rate at magnetic stirrer. 15-25 ml of ethanol was added, and mouth of beaker was closed. Stirring was continued until desired consistency was achieved (takes 30 minutes to 2 hour). Characterization and degradation samples were dried at room temperature for one night and 50 ℃ for 48 hours. Mechanical test samples were put in a jolting apparatus (conforms the EN 196-1 standard) for 3 minutes and in shaker (GFL Shaking Incubator 3032) for overnight with 250 rpm and at room temperature. Then, they were dried at 50 ℃ for 48 hours.

3.3. Characterization Methods

3.3.1. X-Ray Diffraction (XRD) Analysis

XRD analysis (model: D/Max 2200-PC with Cu absorber, brand: Rigaku) was applied to see amorphous and crystalline phases of raw materials, treated ceramics and composites. Raw powder materials were directly purchased however they were also analyzed to ensure existence of their characteristic peaks and absence of impurities.

3.3.2. Scanning Electron Microscopy (SEM) Analysis

SEM analysis **(**FEI-Philips XL30 Environmental Scanning Electron Microscope with Field Emission Gun (Equipped with EDAX-Energy Dispersive X-ray Analysis Unit)) was

performed for pure HAP, raw materials, treated ceramics and composites to see micromorphology of them in different scales.

3.3.3. Fourier Transform Infrared Spectroscopy (FTIR) Analysis

FTIR spectroscopy (model: Vertex 80v spectrometer with 4 cm^{-1} resolution, brand: Bruker) was done in 400-5000 cm^{-1} spectral region to detect vibrations. ATR mode of FTIR was used. FTIR analysis was done for raw materials, treated ceramics and composites.

3.3.4. X-ray Photoelectron Spectroscopy (XPS) Analysis

XPS analysis **(**Thermo Scientific K-Alpha X-ray Photoelectron Spectrometer) was carried out for raw materials, treated ceramics and composites in between 0 and 1350 eV region to detect chemistry of surface.

3.4. Compressive Strength Measurement

Compressive strength measurement (MTS servo-hydraulic testing machine with maximum 100 kN capacity) was done for composites which were molded 1cmx1cmx1.5cm rectangle prism. In measurements, 0.5 mm/min displacement rate with max displacement 9.0 mm was used. Compressive strengths of these materials were calculated with load until height was less than 30 % of initial length of composites as in similar studies [55], [74]. Compressive strength was calculated by dividing maximum load to initial compressed surface area of sample. Measurements were repeated twice for each composition.

3.5. Degradation Measurement

Degradation study was done by following similar studies in literature [2], [57], [58], [63], [64]. Composites were molded in Teflon mold with 9 mm diameter and 3 mm length for degradation study. Weight of these samples was between 40-170 mg. These samples put in 30 ml of Hanks' Balanced Salt Solution (HBSS). HBSS is a solution without organic species with

7.4 pH. HBSS is an alternative for simulated body fluid (SBF) which is nearly same of human blood surface. The HBSS contains different types of electrolytes; mainly Na^{+} and Cl^{-2} following with Ca^{+2}, K^{+}, HCO_3^{-}, Mg^{+2}, SO_4^{-2} and HPO_4^{-2}. It enables the apatite formation and observation of it [75].

In order to immerse sample in HBSS, a needle was dipped in the samples. Samples were placed in heating oven (brand: Binder) at constant 37 ºC after recording the sample weight. Samples were taken from heating oven in some determined time points during 7 days. Samples were washed to remove HBSS after taking from heating oven and they were weighted again to see swelling capacity of composites. Then, they were dried at 37 ºC until dry weight became constant. Samples were weighted in the first week, on days 1, 3, and 7.

4. RESULTS AND DISCUSSION

4.1. Characterization Results

4.1.1. X-Ray Diffraction (XRD) Analysis

XRD analysis was applied to pure HAP, β-TCP ceramics and PLA powders, modified ceramics and produced composites. Raw powder materials also analyzed to ensure existence of their characteristic peaks and absence of impurities.

4.1.1.1. XRD Analysis of Raw Materials and Treated Ceramics. Figure 4.1 shows that the HAP phase is perfectly crystalline. XRD pattern has good agreement with reference models HAP (PDF 00-001-1008) and calcium phosphate (PDF 00-011-0232) peaks. Existence of calcium phosphate shows that there are some impurities in HAP phase [76]. The result was compared with previous study that is used same brand HAP and it was observed that result peaks after 2θ =40.1° are not matched [77]. This probably caused that search program did not show agreement with HAP-standard pattern (PDF 09-0432). However, other peaks show high similarity with HAP-standard pattern that was referred in literature [78].

XRD result of β-TCP is demonstrated in Figure 4.2. Peaks match with reference of whitlockite (PDF 00-003-0713). In literature survey, β-TCP shows two different reference models, these are whitlockite (PDF 00-003-0713) and pure β-TCP (PDF 00-09-0169) [79]–[81]. Whitlockite name is used for crystallographic form of β-TCP [82]. Used β-TCP (Sigma Aldrich) is a sintered powder. Absence of amorphous structure may be result of sintering of β-TCP.

XRD pattern of PLA is illustrated in Figure 4.3. It shows characteristic peaks of pure PLA positioned at 2θ=17° and 2θ=19.31°. Also, in 2θ region of 10-30° there is an amorphous characteristic shape. Location of characteristic peaks and amorphous structure shows similarity with previous studies [48], [55], [61], [83].

(a)

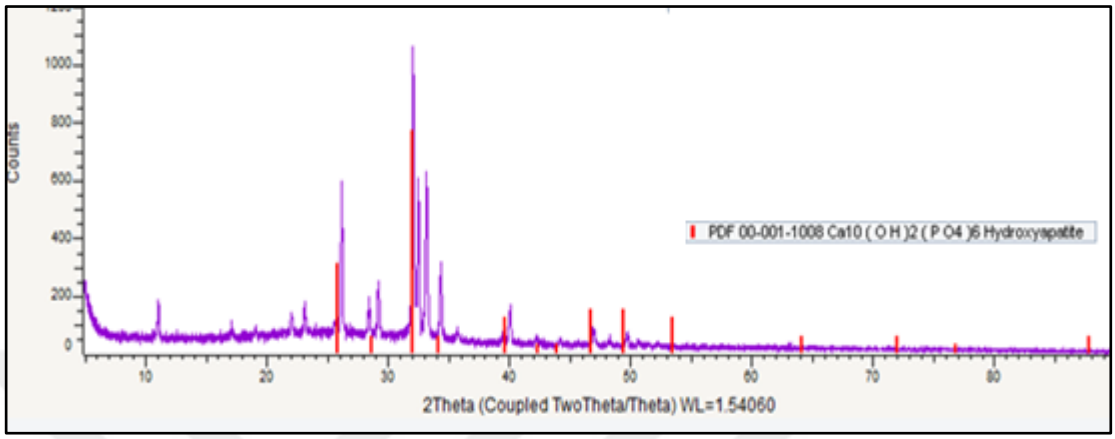

(b)

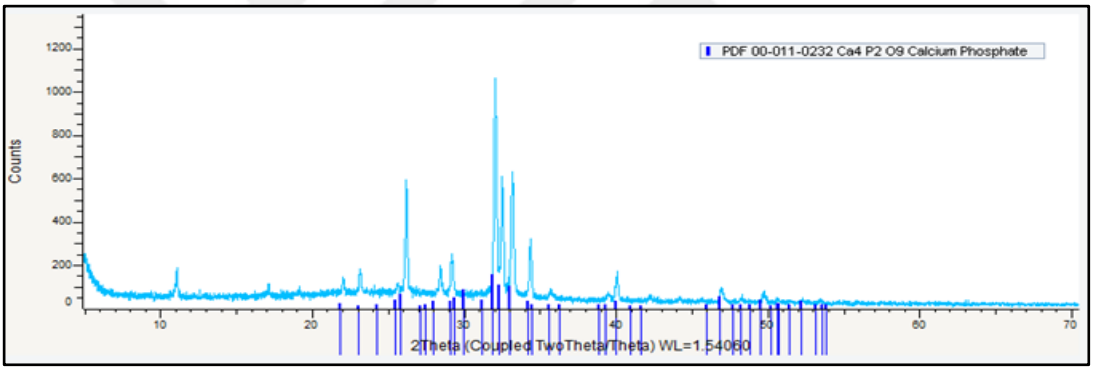

Figure 4.1. XRD pattern of pure HAP and comparison with: (a) HAP (PDF 00-001-1008) and (b) calcium phosphate (PDF 00-011-0232).

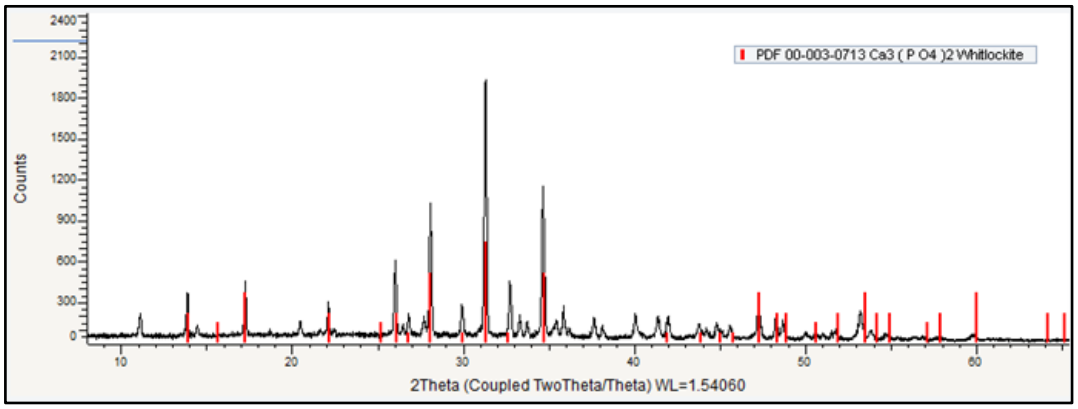

Figure 4.2. XRD pattern of pure β-TCP and comparison with whitlockite (PDF 00-003-0713).

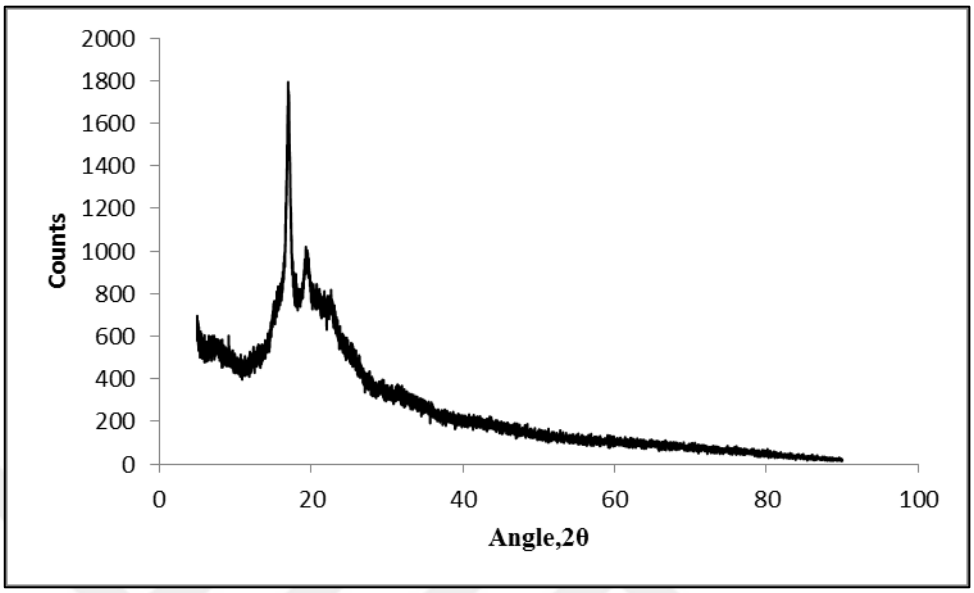

Figure 4.3. XRD pattern of powder PLA.

In this study HAP was treated with silane coupling agent with 1 wt.% and 3 wt.% percentage (Silane A-174). Figure 4.4 reveals the XRD analysis of these intermediate steps before composite production. Figure 4.4.b shows that peaks of pure HAP do not change after silane treatment. However, there are some new intense peaks. These peaks may come from silane A-174 or more possibly from H_2SO_4. Because, pH adjustment of 1 wt.% silane A-174 treatment required more acid addition during production.

All intermediate treatments of β-TCP before composite productions are represented in Figure 4.5. When Figure 4.5.a is compared with pure β-TCP result, it is observed main peaks of β-TCP are present after protonation with phosphoric acid. New peaks after 2θ=30° are related to phosphoric acid. Increase in double peaks of pure β-TCP around 2θ=27° with phosphoric acid treatment may indicate phosphoric acid treatment is achieved. Also, after protonation with phosphoric acid an amorphous structure is observed at region 2θ=25-40°. The same structure keeps itself after different ratio silane treatments (Figures 4.5.b and 4.5.c). Figure 4.5.b shows one percentage of silane does not change the pattern in Figure 4.5.a. It can be explained on basis of silane A174 percentage being too small. When Figures 4.5.a and 4.5.c are compared, it is

observed that intensities of ceramic peaks decrease. This is related with change of Ca/P ratio because of replacement of calcium atoms with silica atoms [65].

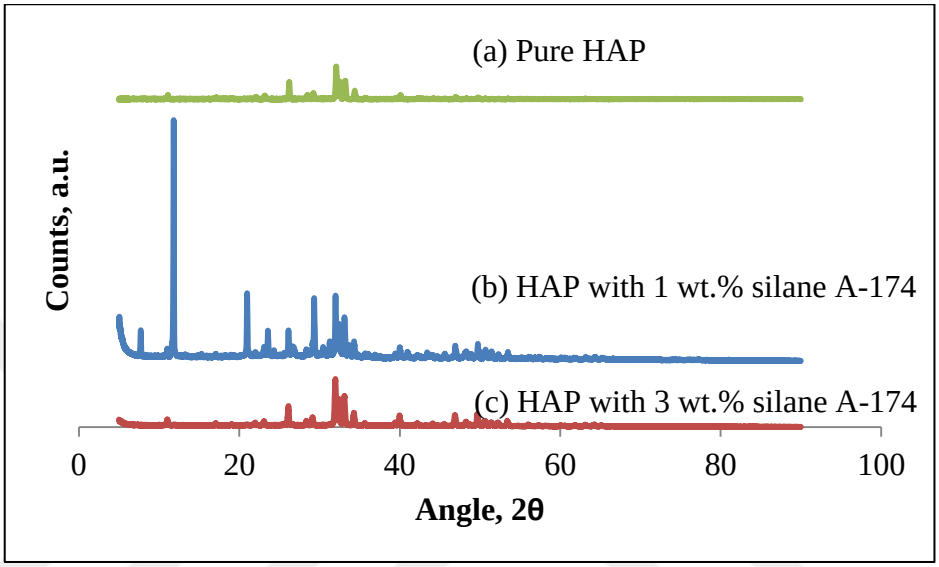

Figure 4.4. XRD patterns of treated HAPs.

4.1.1.2.XRD Analysis of Composites. XRD results of the two composites without treatment that have different polymer/ceramic ratios are displayed in Figure 4.6 and Figure 4.7. Figure 4.6 and Figure 4.7 also include the corresponding raw materials to see differences clearly. It is observed that peaks of pure PLA are located in the same positions in these two composites. However, intensity of these peaks at composites is lower. Moreover, composites have amorphous features at 2θ region of 10-30° that come from pure PLA. When composites without treatment are compared with pure HAP it is observed peak intensities reduced. Also, when insets of Figures 4.6 and 4.7 are investigated, it is observed that location of HAP peaks shifted to left in the composites. This shift is more observable in composite that contains more HAP, PLA40H60. Decrease of peak intensities, amorphous structure observation and shift of HAP peaks indicate interaction of HAP and PLA in composites [55] [10].

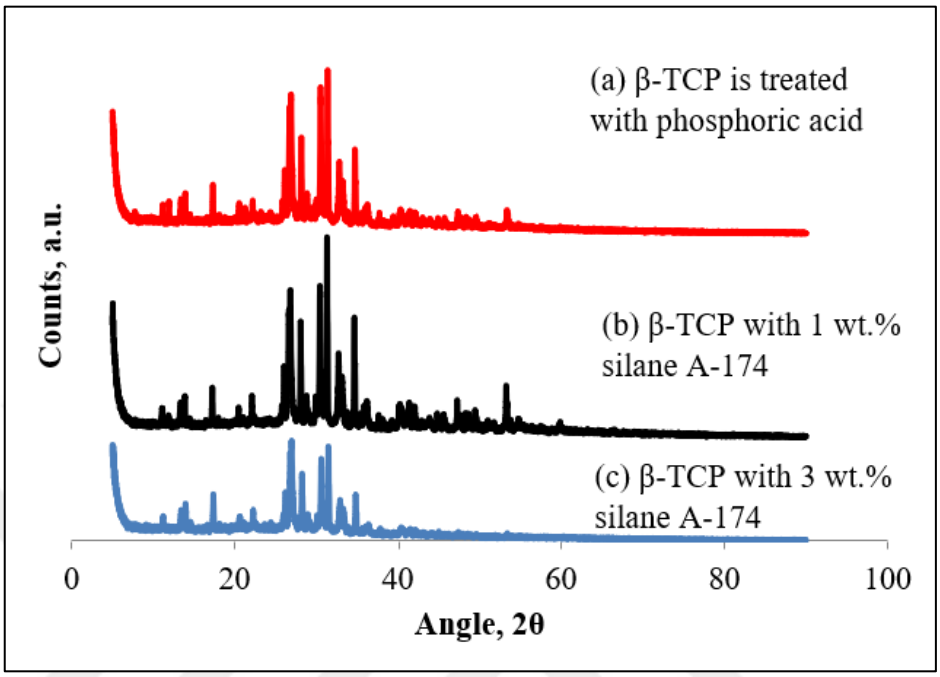

Figure 4.5. XRD patterns of treated β-TCPs.

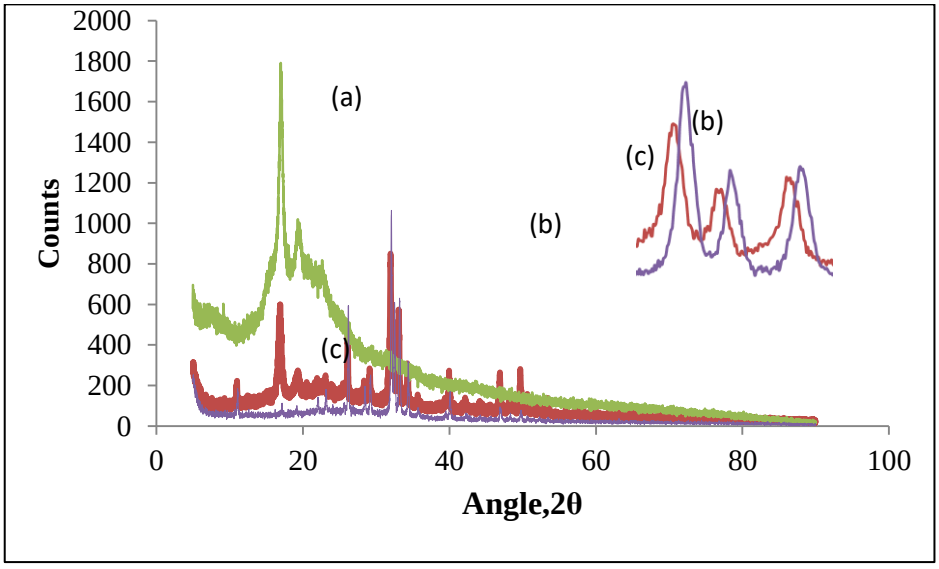

Figure 4.6. XRD patterns of (a) PLA (b) pure HAP (c) PLA40H60.

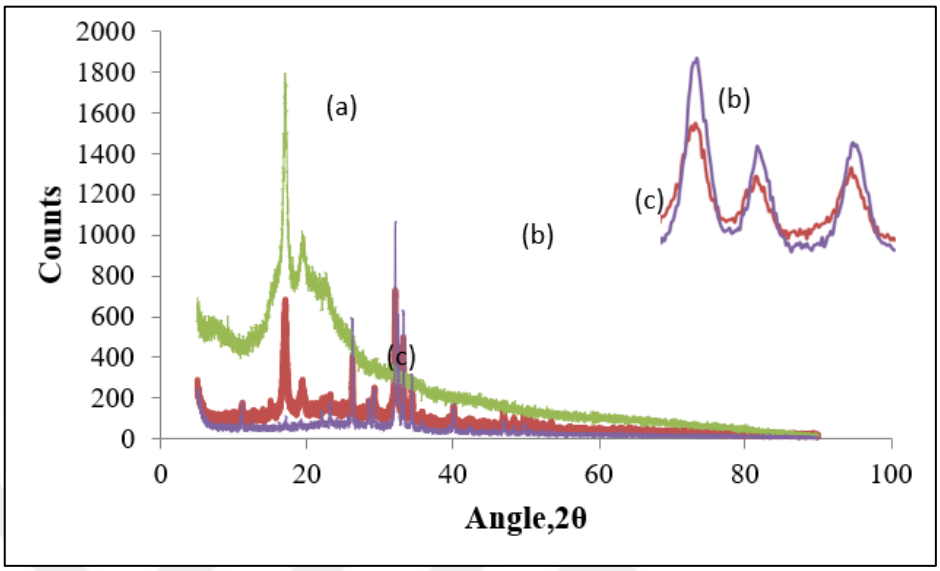

Figure 4.7. XRD patterns of (a) PLA (b) pure HAP (c) PLA50H50 composite.

Figure 4.8 and 4.9 show the XRD results of silane treated HAP including composites. Both composites display peaks of their modified raw ceramics and pure PLA at similar locations. Also, amorphous structure of pure PLA at region 2θ=10-30° is observed in these composites. Peak intensities of composites decrease compared to silane treated HAP and pure PLA. Observation of amorphous structure and intensity reduction can establish interaction between polymer and ceramic with silane.

XRD patterns of pure β-TCP and PLA composites are shown in Figure 4.10 and Figure 4.1. Star sign indicates peaks come from pure β-TCP. PLA40T60 composite contains all peaks of pure β-TCP with similar intensity. Also, the composite includes two characteristic peaks of pure PLA. However, the amorphous structure of PLA disappears in composite. Interfacial interaction between ceramic and polymer may cause the phase change of PLA [55].

PLA50T50 composite includes most intense peaks of pure β-TCP. However, intensities of these peaks decrease extremely in the composite. Also, peaks of pure β-TCP after 2θ=34° are absent in the composite. Study performed by Lin *et al.* [61] indicated that the presence of the XRD peak of β-TCP at 2θ=32° and amorphous structure of PLA proves the entrapping β-TCP

inside of PLA. Difference of two composites shown in Figure 4.10 and Figure 4.11 may be a sign of importance of ceramic/polymer ratio for composite properties.

XRD results of silane treated β-TCP including composites (PLA40T60PASi1 and PLA50T50PASi3) are displayed in Figure 4.12 and Figure 4.13. The results of these composites show peaks related to their raw materials at the corresponding locations. Also, the amorphous structure originating from pure PLA is observed in both composites.

Both composites do not show new peaks due to possibility of too small amount of silane coupling agent (1 wt.%). Peaks of PLA40T60PASi1 composite decreases with respect to both its polymer and ceramic ingredients. This may be related to new bond formation in composite. However, composite PLA50T50PASi3 do not show reducing in peak intensities as it is seen in Figure 4.13.

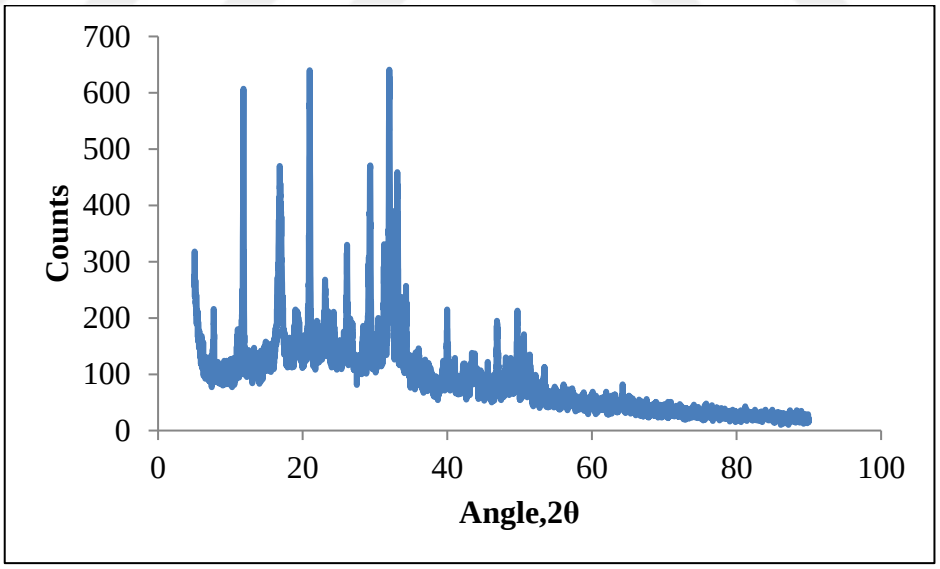

Figure 4.8. XRD pattern of PLA40H60Si1.

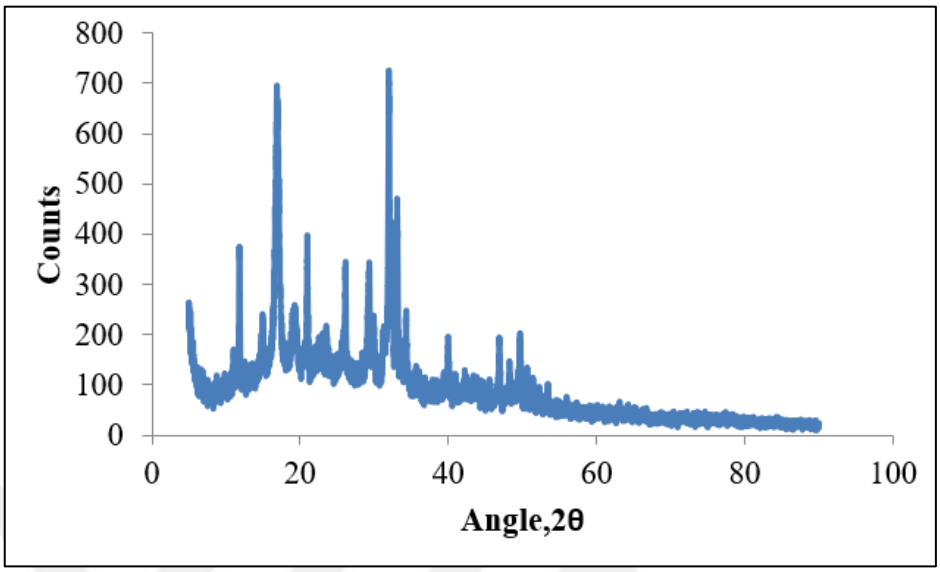

Figure 4.9. XRD pattern of PLA50H50Si3.

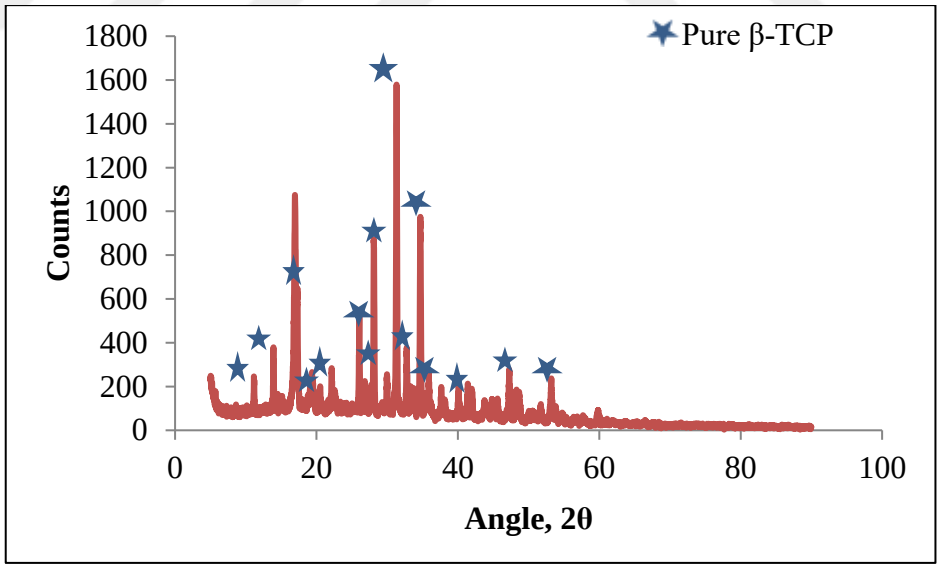

Figure 4.10. XRD pattern of PLA40T60.

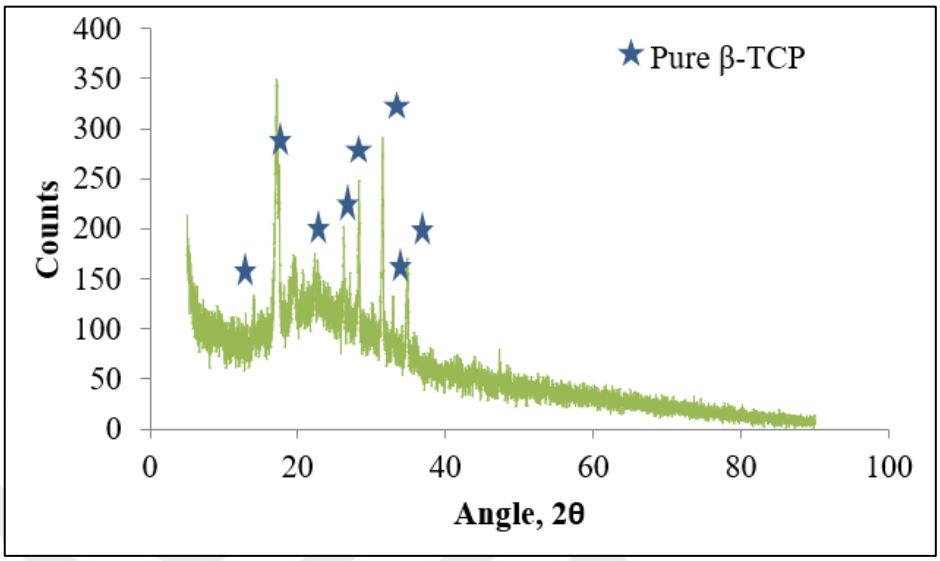

Figure 4.11. XRD pattern of PLA50T50.

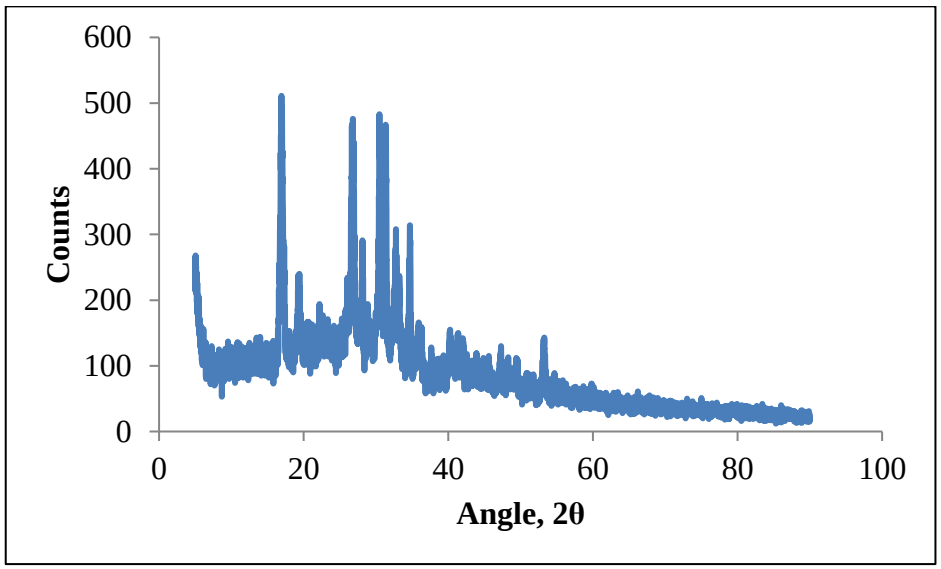

Figure 4.12. XRD pattern of PLA40T60PASi1.

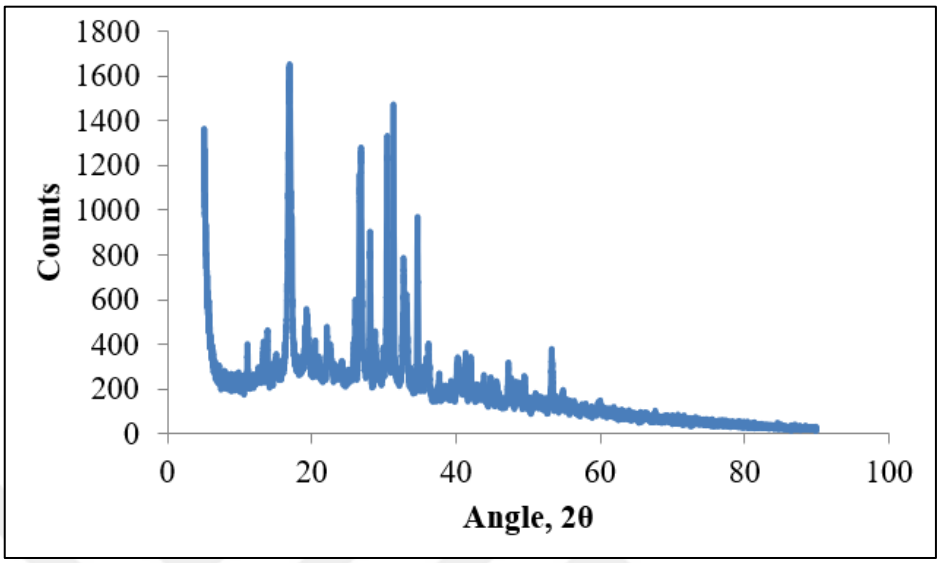

Figure 4.13. XRD pattern of PLA50T50PASi3.

4.1.2. Scanning Electron Microscopy (SEM) Analysis

4.1.2.1.SEM Analysis of Raw Materials and Treated Ceramics. SEM images of raw materials, namely PLA, HAP and β-TCP, in two different scales are represented in Figure 4.14. Images of PLA in Figure 4.14.a and Figure 4.14.b are consistent with previous images [84]. Figure 4.14.c and Figure 4.14.d show the pure HAP powder result. This result is similar to previous images in literature [29]. Crystal structure of pure HAP is seen in Figure 4.14.d. This verifies the observed crystal structure in XRD analysis of pure HAP. SEM images of β-TCP are displayed in Figure 4.14.e and Figure 4.14.f. SEM images of β-TCP crystal are not present at 500 nm scales like PLA and HAP since β-TCP consists of bigger particles as it is seen images. Surface morphology of β-TCP is found compatible with β-TCP image in literature [85] and also with the images of HAP that was sintered at 700 °C [86]. Figure 4.15 reveals the HAP images before and after silane A-174 modifications in 10 μm and 200 nm scales. After silane A-174 modifications filamentous structure on HAP surface is observed.

SEM images of pure β-TCP, protonated β-TCP with phosphoric acid and modified β-TCP with silane A-174 are presented in Figure 4.16.a, b, c, respectively. Covering of β-TCP surface

with phosphate crystal after phosphoric acid treatment is seen in Figure 4.16.b. It is seen that smooth surface structure evolved into a flaky morphology upon treatment with phosphoric acid. However, when Figure 4.16.b and Figure 4.16.c are compared, it is observed that silane treatment addition to phosphoric acid treatment do not change surface.

In previous study of hemp pulp, hemp was modified with sodium hydroxide solution and after 4-6% percent of silane, and it was found that silane treatment after solution treatment did not change surface morphology of hemp pulp [87]. Current result is compatible with this study.

4.1.2.2.SEM Analysis of Composites. Figure 4.17 shows the four produced composites in 1µm scale. These images display a bridge between polymer and ceramic and this situation is similar to images regarding PLA/HA composites in literature [50]. Physical interaction is observed for pure HAP and PLA composite in Figure 4.17.a. Similar interaction is seen in silane treated composites in Figure 4.17.b and Figure 4.17.d. However, pure β-TCP and PLA composite in Figure 4.17.b is different from other composites.

There is accumulation of polymer on the pure β-TCP and there is no interaction in composite in Figure 4.17.c. This result is coherent with a previous study that shows the adhesion between β-TCP- PLA composites is lower than HAP- PLA composites [53]. As a conclusion β-TCP- PLA composites show lower interaction with respect to HAP- PLA composites produced with same ratio.

When the silane treated composites in Figure 4.17.b and Figure 4.17.d are compared with the untreated composites in Figure 4.17.a and Figure 4.17.c, respectively, it is viewed that spread of polymer on ceramic surface improves with silane addition. Morphology changes with respect to the untreated counterparts indicate that silane A-174 treatment on ceramic parts enhances the interaction between the polymer and ceramic parts for both HAP-PLA and PLA-β-TCP composites.

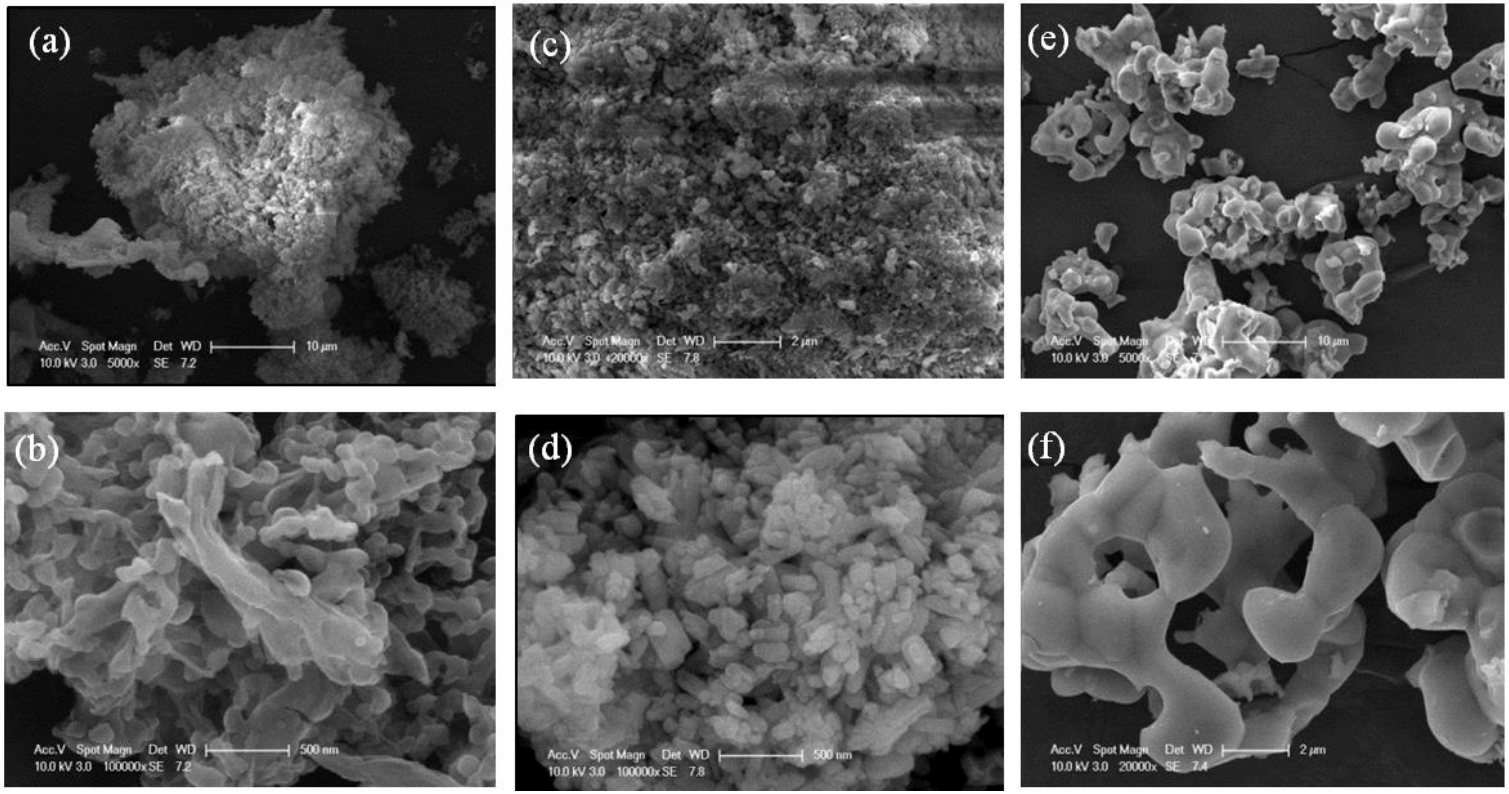

Figure 4.14. SEM of (a) PLA -10 µm, (b) PLA -500 nm, (c) HAP-10 µm, (d) HAP-500 nm, (e) β-TCP-10 µm, (f) β-TCP-2 µm.

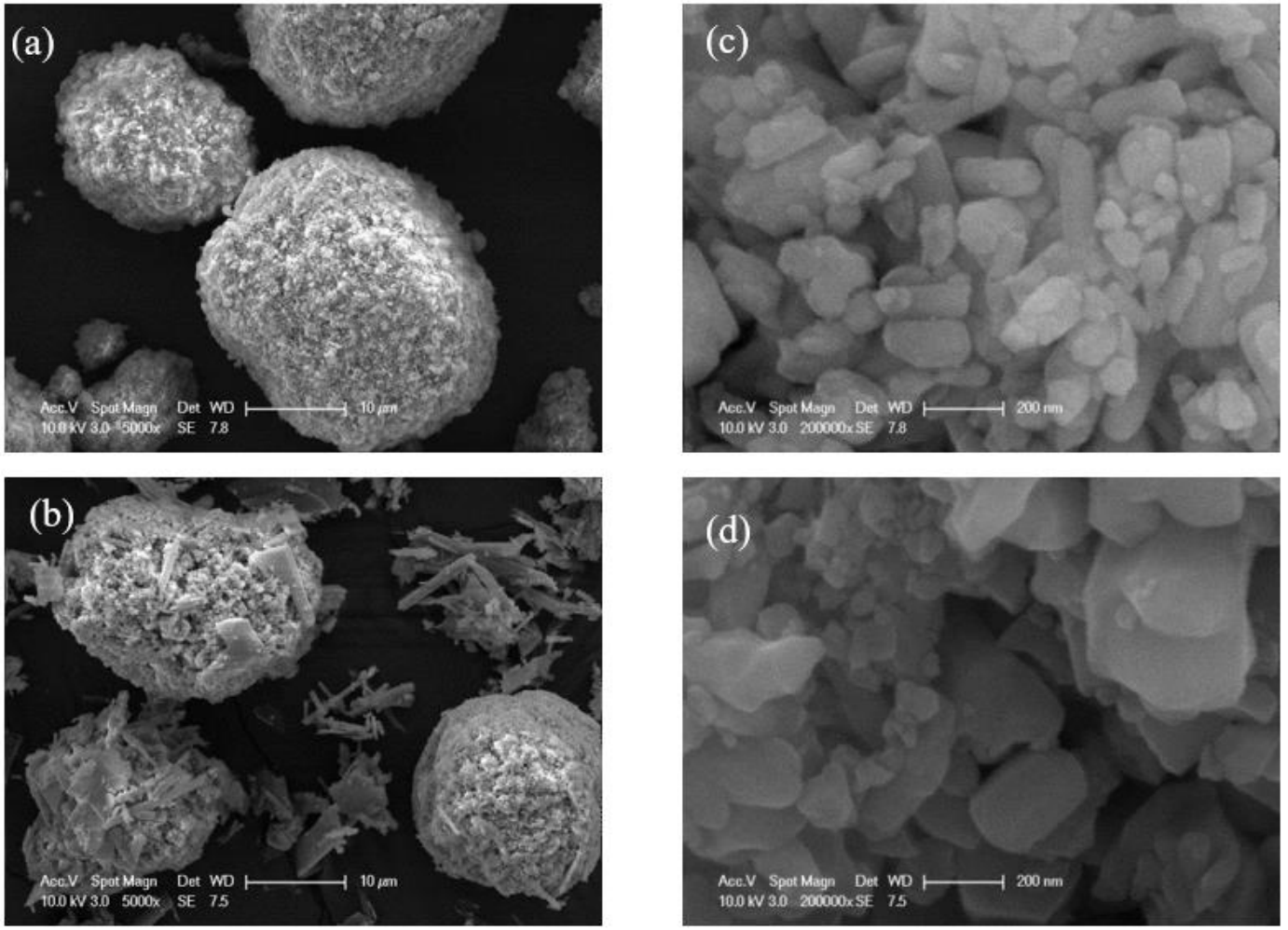

Figure 4.15. SEM of (a) HAP-10 µm, (b) silane A-174 treated HAP-10 µm, (c) HAP-200 nm, (d) silane A-174 treated HAP-200 nm.

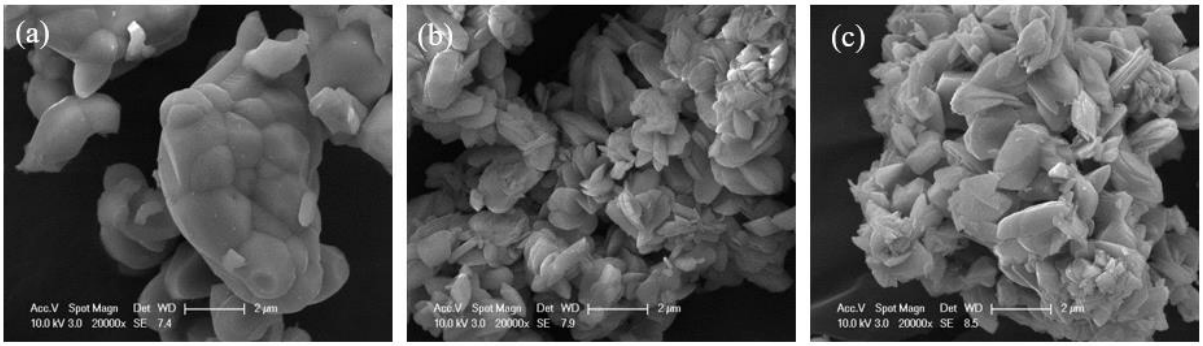

Figure 4.16. SEM of (a) β-TCP -2 µm, (b) phosphoric acid treated β-TCP -2 µm, (c) after silane A-174 treated β-TCP in (b) -2 µm.

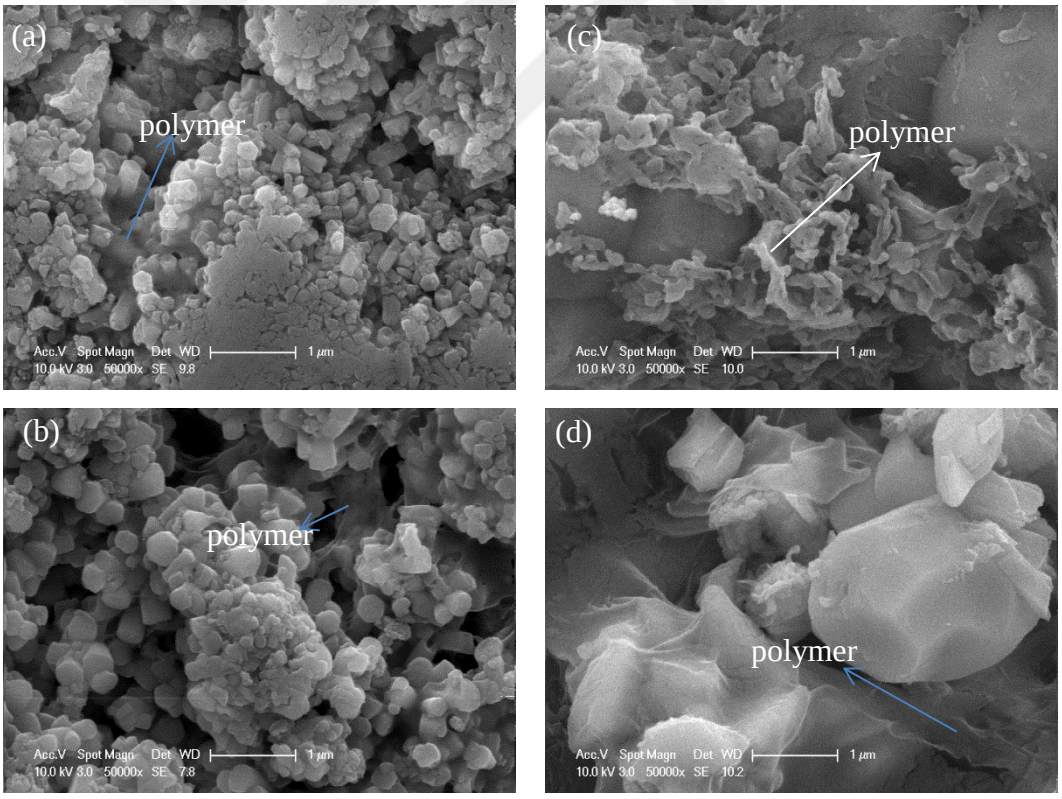

Figure 4.17. SEM of (a) PLA50H50 -1µm, (b) PLA50H50Si3 -1µm, (c) PLA50T50-1µm, (d) 3 PLA50T50PASi3-1µm.

4.1.3. Fourier Transform Infrared Spectroscopy (FTIR) Analysis

FTIR analysis was done for pure HAP, β-TCP, PLA and modified β-TCP and HAP ceramics. Also, analysis was made for all eight produced composites. ATR mode was used to compare results with conclusions of previous studies.

4.1.3.1. FTIR Spectroscopy Analysis of Raw Materials and Treated Ceramics. Figure 4.18 demonstrates the FTIR results of PLA in 400-5000 cm^{-1} wavenumber range. Presence of sharp features in the FTIR patterns of PLA that can be related to its XRD result showing partly crystalline character.

Bands at 668, 757 and 872 cm^{-1} belong to C-O-C vibration, C=O group and C-C stretching, respectively [88], [89]. Band at 1044 cm^{-1} corresponds to CH_3 group [88]. 1085 cm^{-1} and 1182 cm^{-1} bands represent C-O-C symmetric and asymmetric stretching, respectively. Also, band at 1754 cm-1 is related to C=O stretching [2], [55], [58].

Bands of 1456 and 1384 cm^{-1} indicate bending vibration of CH_3 in PLA. Weak bands which are observed at 2896 cm^{-1}, 2947 cm^{-1}, and 2998 cm^{-1} corresponding to C-H stretching are observed with similar shape and band positions in literature [55]. Bands with low absorbance values at 3565 cm^{-1} and beyond values show the existence of -OH groups in the molecular structure.

The band at 1212 cm^{-1} is related to asymmetric C-CO-O vibration and asymmetric CH_3 rotation. Moreover, band at 1130 cm^{-1} indicates the symmetric CH_3 rotation [90]. Presence of 1130 and 1212 cm^{-1} bands indicates amorphous poly-lactic acid. This is in accordance with the observed amorphous structure found in XRD result belonging to poly-lactic acid at 2θ=10-30° region.

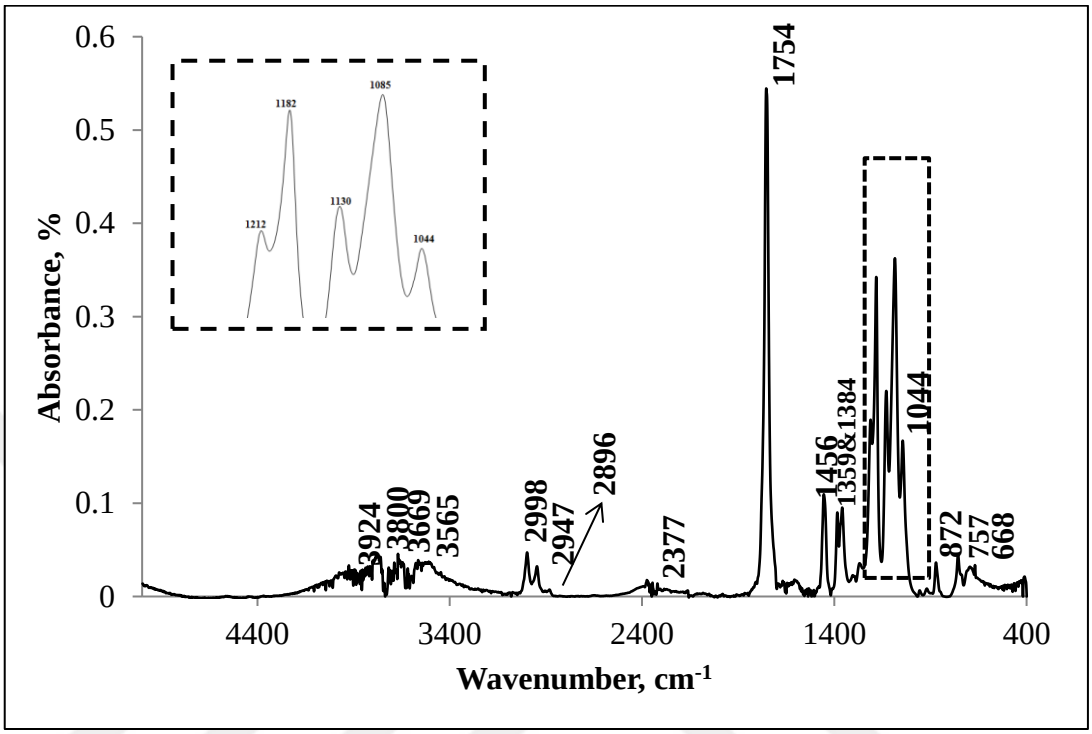

Figure 4.18. FTIR spectrum of powder PLA.

FTIR spectrum of HAP is revealed in Figure 4.19. Crystal structure of HAP which was previously seen in XRD analysis is observed by FTIR analysis, too. FTIR analysis of HAP in Figure 4.19 includes characteristic bands of HAP [91].

Bands at 561, 600, 961, 1024 and 1086 cm^{-1} belong to ν4, ν1, ν3 and ν2 vibrational frequencies of $PO4^{-3}$ group [55], [91], [92].

Vibration and stretching bands of -OH group are observed at 630 and 3571 cm^{-1} wavelengths [55]. In literature bands around 870 and 2000 cm^{-1} are attributed absorbed CO_3^{-2}impurity [91]. This result matches with the observed impurity in XRD analysis results of HAP.

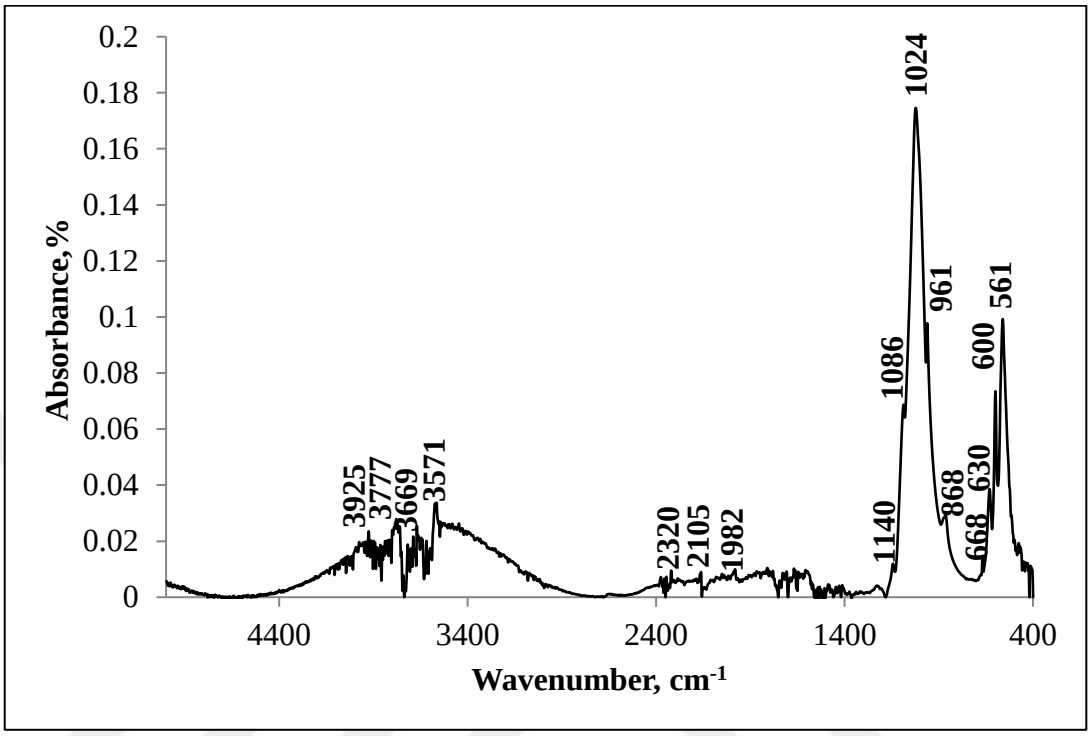

Figure 4.19. FTIR spectrum of HAP.

FTIR spectrum of pure β-TCP is in Figure 4.20. Characteristic bands of β-TCP are seen in FTIR spectrum [85]. Bands at 415 and 439 cm^{-1} indicate the ν2 vibration mode of PO_4^{-3}. Bands in the zoomed section (inset of Figure 4.20) show the ν4 type of PO_4^{-3} vibration. Also, bands at 942, 971 cm^{-1} and 1015, 1035, 1075, 1116 cm^{-1} bands represent the ν1 and ν3 type of PO_4^{-3} vibration, respectively [85], [93], [94].

Band positioned at 727 cm^{-1} belongs to the $P_2O_7^{-3}$ group which comes from calcium pyrophosphate group. According to the previous studies in the literature, this group emerges during transformation to β-TCP phase in production [91], [95]. Band at 3561, 3754 cm^{-1} and around them show the existence of H_2O group [91]. Absorbance values of these bands are weaker than bands of HAP in similar wavenumber, since β-TCP does not contain -OH groups its molecular structure.

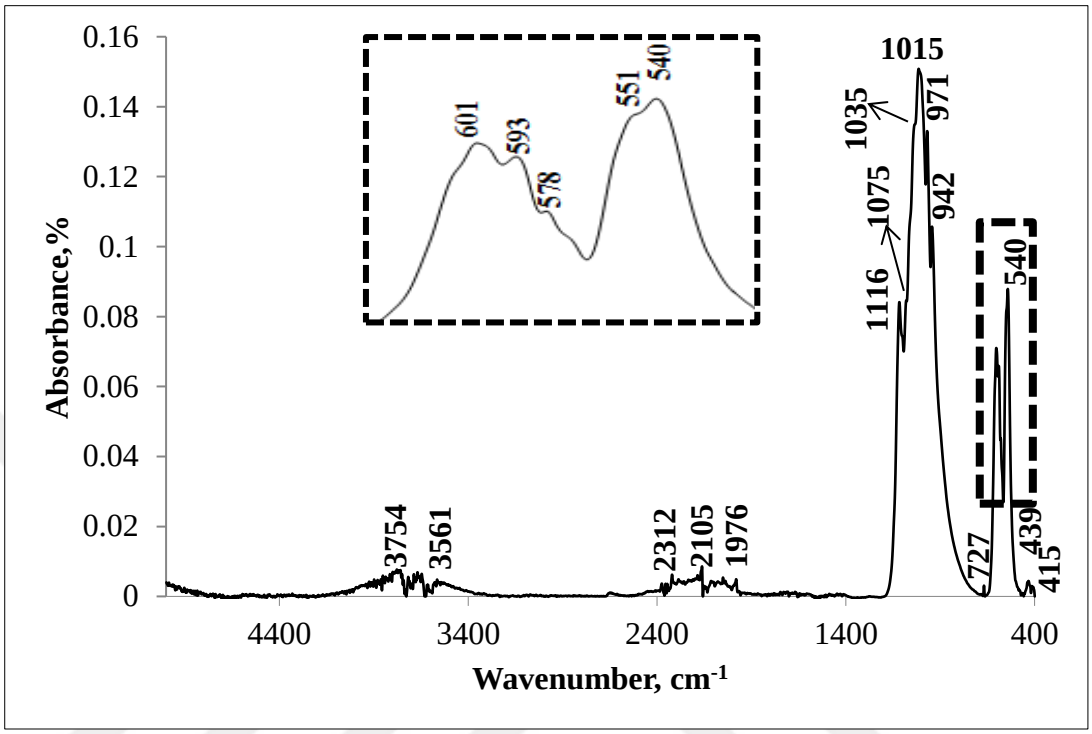

Figure 4.20. FTIR spectrum of β-TCP.

Figure 4.21 and Figure 4.22 show the FTIR results of treated HAP powders. Crystal structure of pure HAP is observed in both silane treated HAP, also. Characteristic bands of pure HAP at 561, 600, 961, 1024 and 1086 cm^{-1} wave numbers are placed in similar locations with low intensities after silane treatment.

The intensity of the band positioned at 630 cm^{-1} related to -OH bonds decreases obviously after silane treatment. Decreasing intensity of -OH bands after silane treatment proves the interaction of silicon and HAP [96]. Most intensive band of HAP at 1024 cm^{-1} shifts slightly to higher wavenumber of 1027 cm^{-1} with silane treatment.

Silane treated samples show difference bands of HAP after 1900 cm^{-1}. New band 1718 cm^{-1} is observed. This band is attributed to C=O bond in literature [97]. This band possibly correspond to C=O bond in structure of silane A-174.

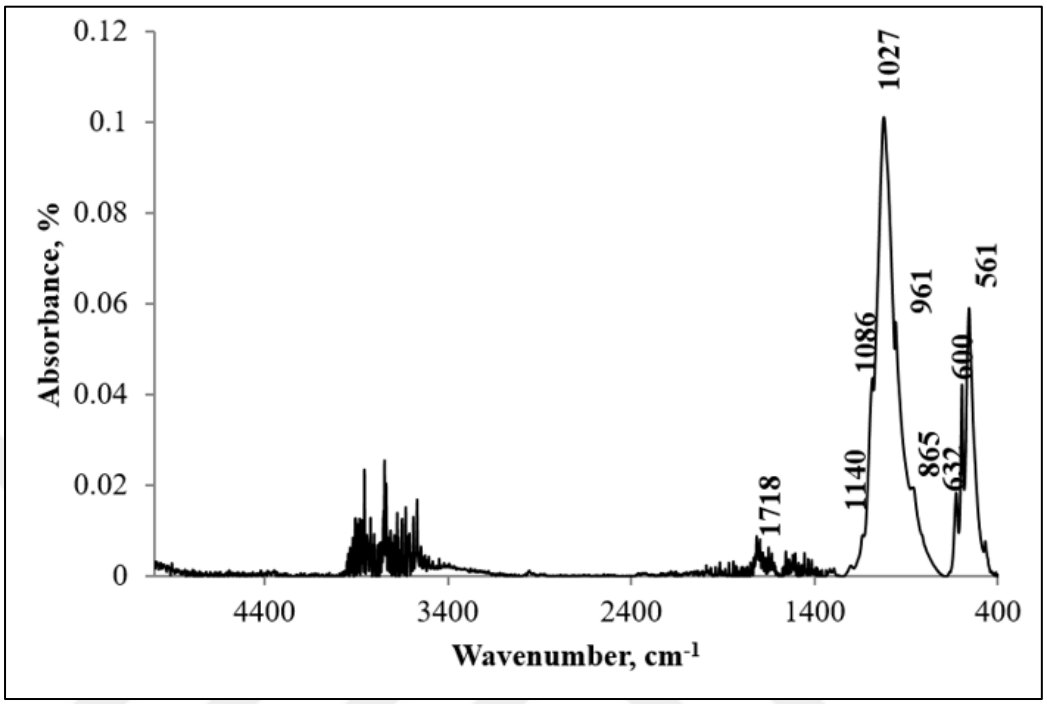

Figure 4.21. FTIR spectrum of HAP with 1 wt.% silane A-174.

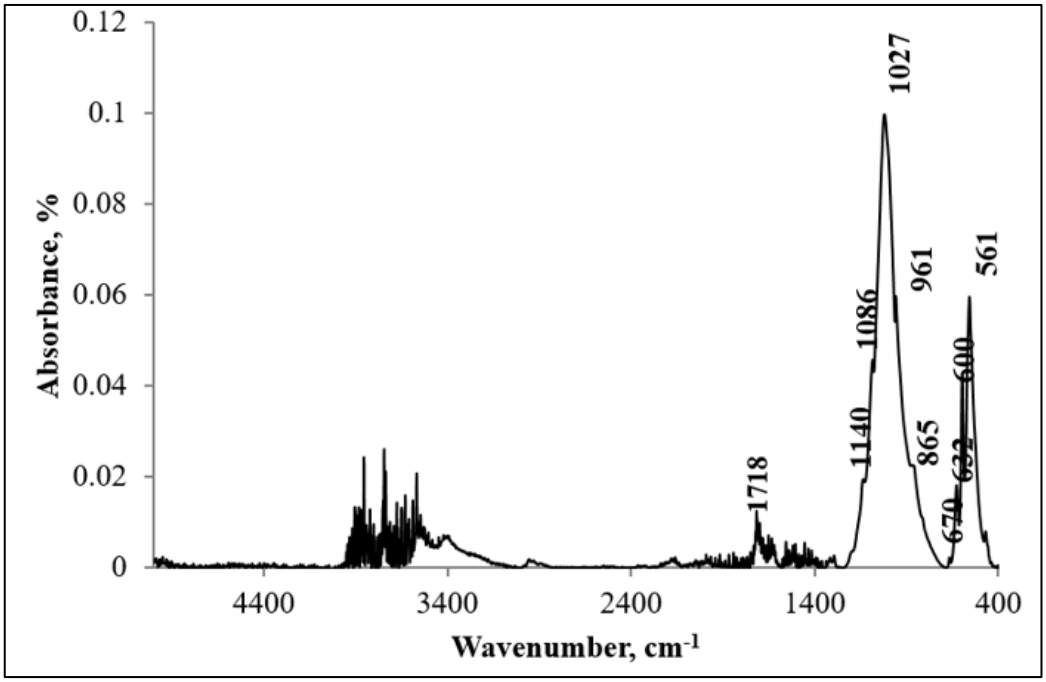

Figure 4.22. FTIR spectrum of HAP with 3 wt.% silane A-174.

Figure 4.23 exhibits the FTIR result of modified β-TCP powder with phosphoric acid. When it is compared with FTIR analysis of pure β-TCP powder (in Figure 4.20) two band structure in zoomed part and bands at 593 and 601 cm^{-1} wave numbers disappears. Also, bands at 942 and 971 cm^{-1} shifts to 954 and 970 cm^{-1} and they loss their intensities. On the other hand, two new and intensive bands arise at 889 and 991 cm^{-1}. Band at 889 cm^{-1} belongs to P-O-P vibration which comes from phosphoric acid [98]. Strongest band of pure β-TCP at 1015 cm^{-1} moves to 1063 cm^{-1} after phosphoric acid treatment. Moreover, bands of pure β-TCP at 1035, 1075 and 1116 cm^{-1} possibly stays under more distinct band at 1126 cm^{-1} after phosphoric acid addition. Besides, band at 727 cm^{-1} which indicates $P_2O_7^{-3}$ group shifts to lower wave number. New bands at 1348, 1403, 1646 and 2862 cm^{-1} display $CaHPO_4$ molecule as pointed out in a previous study [99]. Past studies state that new band formation of $CaHPO_4$ molecule proves the interaction between phosphoric acid and β-TCP [62], [73]. Shift, new formation and disappear of bands indicate the success of phosphoric acid modification.

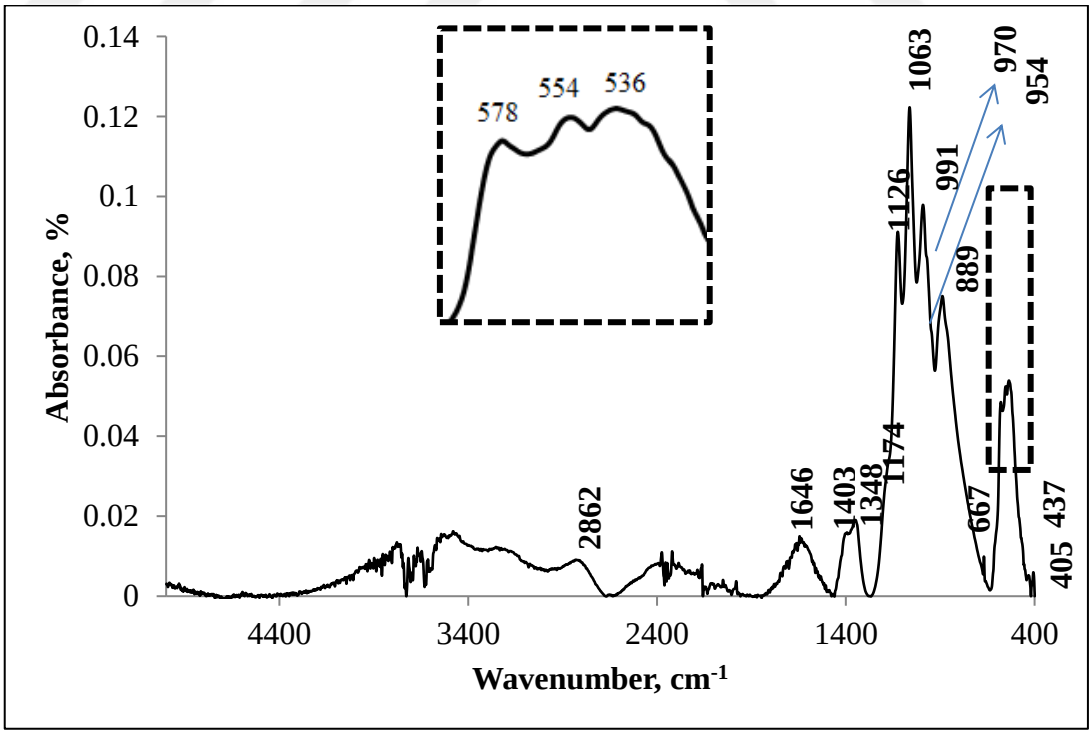

Figure 4.23. FTIR spectrum of phosphoric acid treated β-TCP.

Figure 4.24 and Figure 4.25 show the FTIR spectra of modified β-TCP with 1 wt.% and 3 wt.% of silane A-174 (following phosphoric acid modification procedure), respectively. Both spectra are quite similar. When silane modified β-TCP in Figure 4.24 and Figure 4.25 are compared with modified β-TCP only by phosphoric acid (Figure 4.23), it is observed that spectra are quite similar after silane modification. Table 4.1 shows the FTIR bands of silane A-174.

It should be noted that the these band positions are very close to the positions of characteristic bands of β-TCP [100] and used silane amount is too small, i.e. 1 and 3 wt%. Therefore, band of silane A-174 may not be obvious due to β-TCP bands. However, weakening bands after phosphoric acid modification at 954 cm^{-1} and 970 cm^{-1} become more intensive at 954 cm^{-1} and 978 cm^{-1} wavelength after silane addition. Previous studies states that band positioned at 978 cm^{-1} reveals the P-O-Si bond [60], [72], [101].

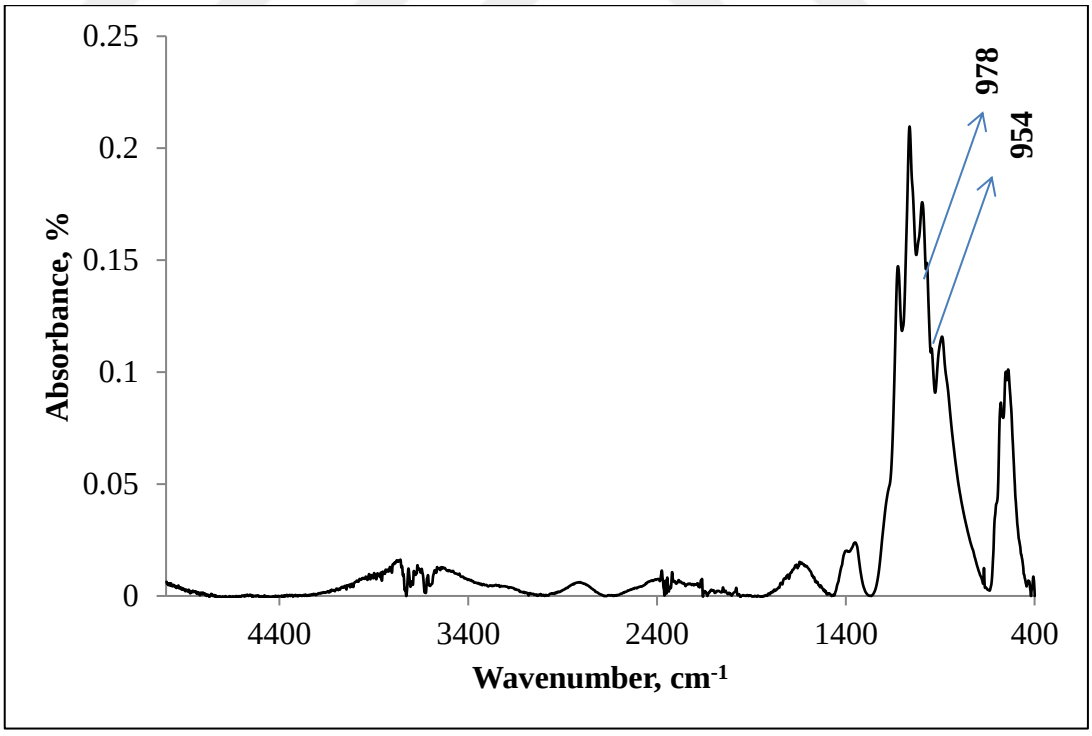

Figure 4.24. FTIR spectrum of β-TCP with 1 wt.% silane A-174.

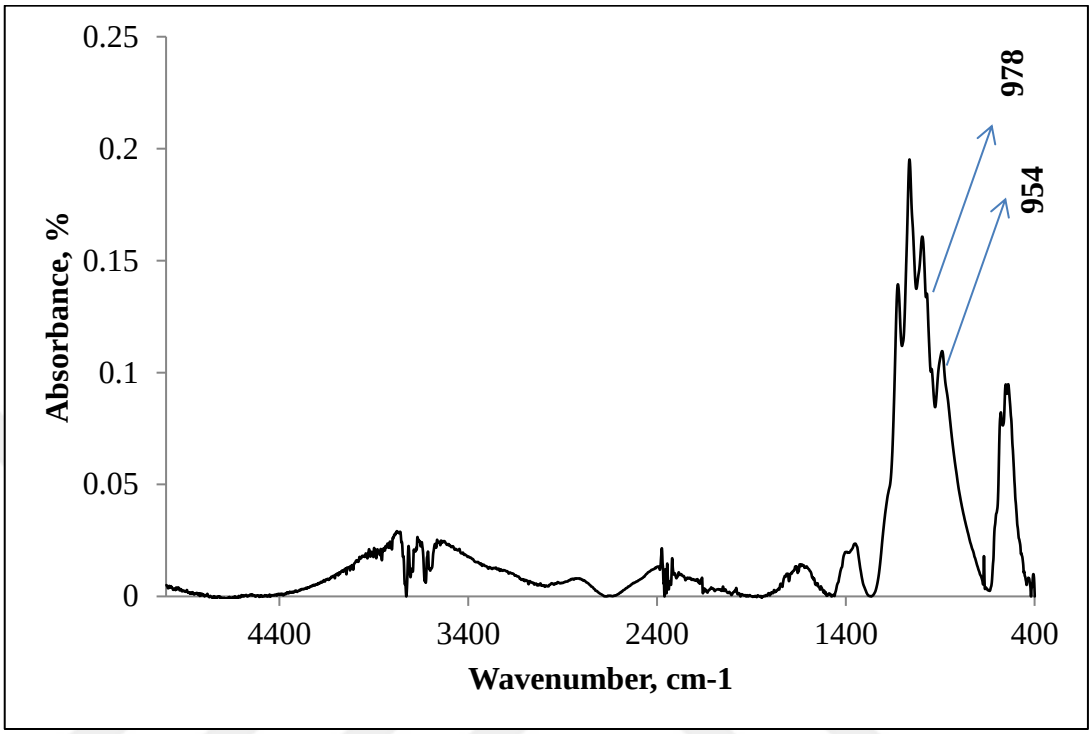

Figure 4.25. FTIR spectrum of β-TCP with 3 wt.% silane A-174.

Table 4.1. Theoretical FTIR Peaks of Silane A-174 in 700-1900 cm^{-1} Region [100].

3- (Trimethoxy silyl) propyl methacrylate (Silane A-174)	
Theoretical Result by Hyper-Chem 7.0	**Vibrational Mode**
838.99	Si-CH_2 (asymmetric stretch)
1076.54	C-O-C (symmetric stretch)
1207.02	Si-O-CH_3 (Si-O bending)
1641.23	C=C (stretch)
1866.92	C=O (C=O asymmetric stretch)

4.1.3.2. FTIR Spectroscopy Analysis of Composites. Figure 4.26 exhibits the FTIR spectra of PLA40H60 and PLA50H50 composites. These results regarding ceramics which have different polymer/ceramic ratios are similar to each other as expected. Composites involve all bands of pure HAP and PLA, i.e. their raw materials. New band formation in FTIR spectra of composite is not seen. Bands located at 564, 601 and 630 cm^{-1} come from phosphate and -OH groups of HAP. Existence of these bands reveals the interaction between HAP and PLA [59]. FTIR spectra of composites exhibit the most intensive band of the HAP at 1024 cm^{-1} that overlaps with 1044 cm^{-1} band of polymer and they are observed together in 1040 cm^{-1} band. This situation is similar to what is reported in literature [58]. Similarly, FTIR band corresponding to polymer at 1085 cm^{-1} overlaps with the characteristic band regarding HAP that is positioned at 1108 cm^{-1}. Also, bands located at 1130, 1212 and 1182 cm^{-1} (signifying polymer content) shift slightly in composites.

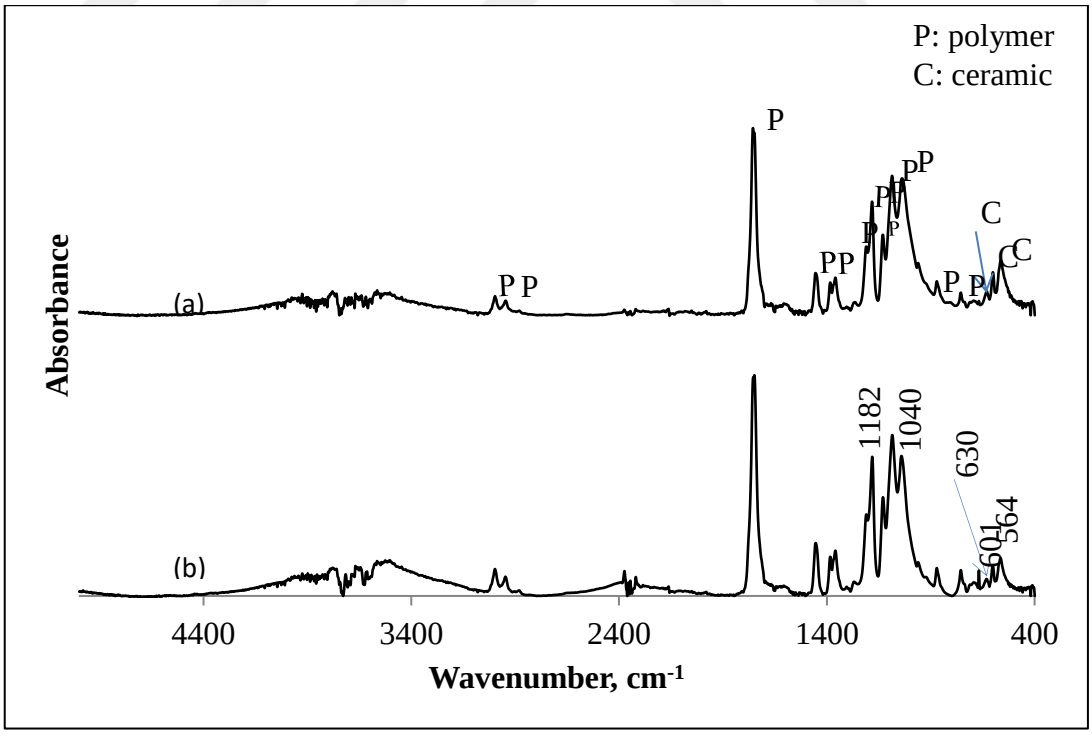

Figure 4.26. FTIR spectra of (a) PLA40H60 (b) PLA50H50.

FTIR results of pure β-TCP and PLA composites are viewed in Figure 4.27. Two composites have different polymer/ceramic ratio and they show similar bands in same band position. PLA50T50 composite in Figure 4.27.b has higher absorbance of bands arising from PLA. Both composites contain all bands of pure β-TCP, as seen in zoomed section of Figure 4.20. Also, the position of the bands of pure β-TCP at 942 cm^{-1} and 971 cm^{-1} shifts to 944 and 968 cm^{-1} in composites.

The FTIR bands related to pure β-TCP (located at 1035, 1075 and 1116 cm^{-1}) and bands indicating PLA (positioned at 1044, 1087 and 1130 cm^{-1}) overlaps in composites. However, band that is present at 1015 cm^{-1} belongs to ν1 vibration of PO_4^{-3} and it is not obvious in the composites.

Weak band positioned at 668 cm^{-1} in the FTIR spectrum of polymer indicating C-O-C vibrations is not present in composites. Although intensities of polymer bands at 757, 1044, 1085, 1130, 1182, 1212, 1359, 1384, 1456, 1754 and 2947, 2988 cm^{-1} decrease, intensity of the band at 872 cm^{-1} wavenumber which indicates that the C-C stretching seems to stay constant in composites.

Bands indicating -OH groups around 3500 cm^{-1} are absent in composites. This may be related with interaction between ceramic and C=O vibration band of pure polymer at 1754 cm^{-1} splits into two as seen at top left side of Figure 4.27.a. One of these bands is located at 1755 cm^{-1} and other one is positioned at a lower frequency (at 1748 cm^{-1}).

In previous study on Poly(d, l-Lactide)/hydroxyapatite nanocomposites it is indicated that the band positioned at 1755 cm^{-1}shows the C=O bond which does not bind the ceramic whereas band present in lower frequency indicates the interaction between polymer and ceramic [52].

According to the results, it is observed that 1748 cm^{-1} band is more pronounced in PLA40T60 ceramic (Figure 4.27. a) and this is compatible with the literature [52].

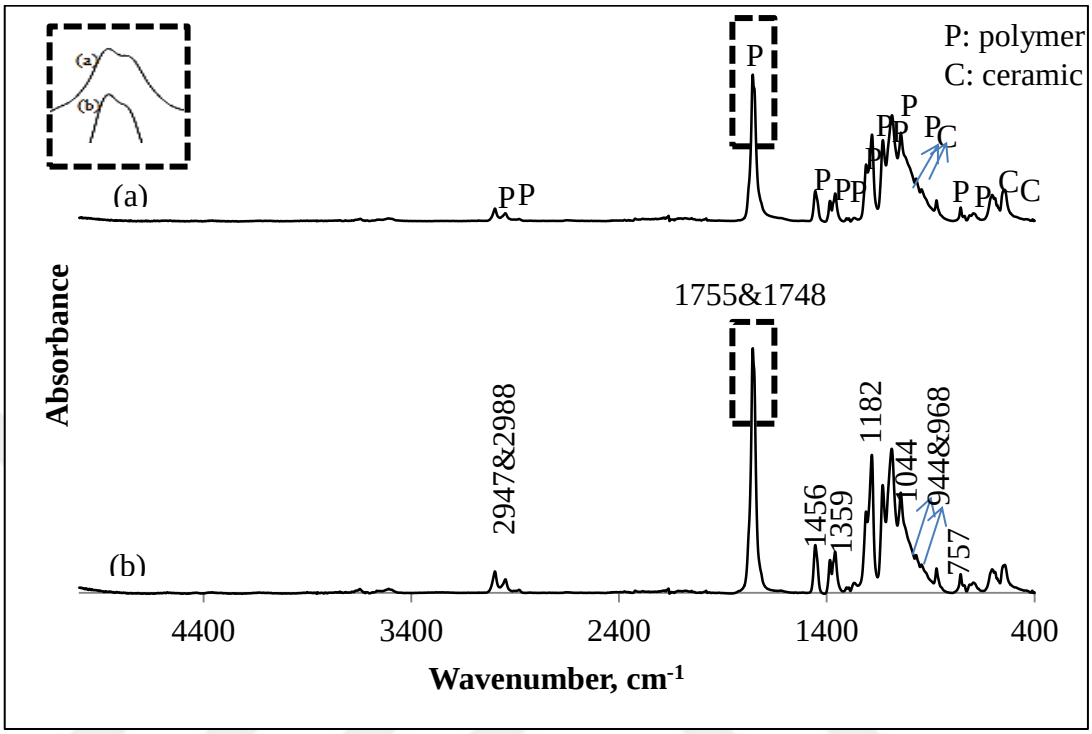

Figure 4.27. FTIR spectra of (a) PLA40T60 (b) PLA50T50.

Figure 4.28 shows the FTIR spectra of silane A-174 modified HAP and PLA composites (PLA40H60Si1 and PLA50H50Si3). Results of PLA40H60Si1 and PLA50H50Si3 composites are compared with unmodified PLA40H60, PLA50H50 composites and modified HAP and pure PLA. The position of the phosphate vibration band at 561 cm^{-1} in the FTIR spectrum of silane modified HAP shifts to 575 cm^{-1} (Figure 4.28.a) and 566 cm^{-1} (Figure 4.28.b) in composites. The position of the band located at 601 cm^{-1} in the FTIR spectrum of HAP does not seem to change in the composite. The position of the characteristic band of HAP located at 961 cm^{-1} moves to 945 cm^{-1} (Figure 4.28.a) and 955 cm^{-1} (Figure 4.28.b) in composites with reduced intensities. It is observed that bands positioned at 869, 1086 cm^{-1} indicating HAP overlap with bands located at 872 and 1085 cm^{-1} that are related to PLA. Also, the feature at 1024 cm^{-1} originating from HAP overlaps with the band at 1044 cm^{-1} coming from PLA as reported in a previous study [58]; and two bands seem as combined at 1047 cm^{-1}. The bands indicating PLA that are positioned at 668, 757, 1182, 1212, 1359, 1384, 1456, 2947 and 2998 cm^{-1} are also seen in composites at the positions. Moreover, new bands at 1622, 3406 and 3533 cm^{-1} (which are

not seen obviously in ceramic and polymer) are formed in composites. These bands have higher intensities in composite that has high HAP percent. Also, band at 1683 cm^{-1} wavelength is observed in PLA40H60Si1 composite. 1622 cm^{-1} and 1683 cm^{-1} bands are assigned to C=O or C=C groups of silane A-174 [56], [102], [103]. However, these bands are not present in FTIR spectrum of treated HAP. Therefore, these bands may be related to interaction in composites.

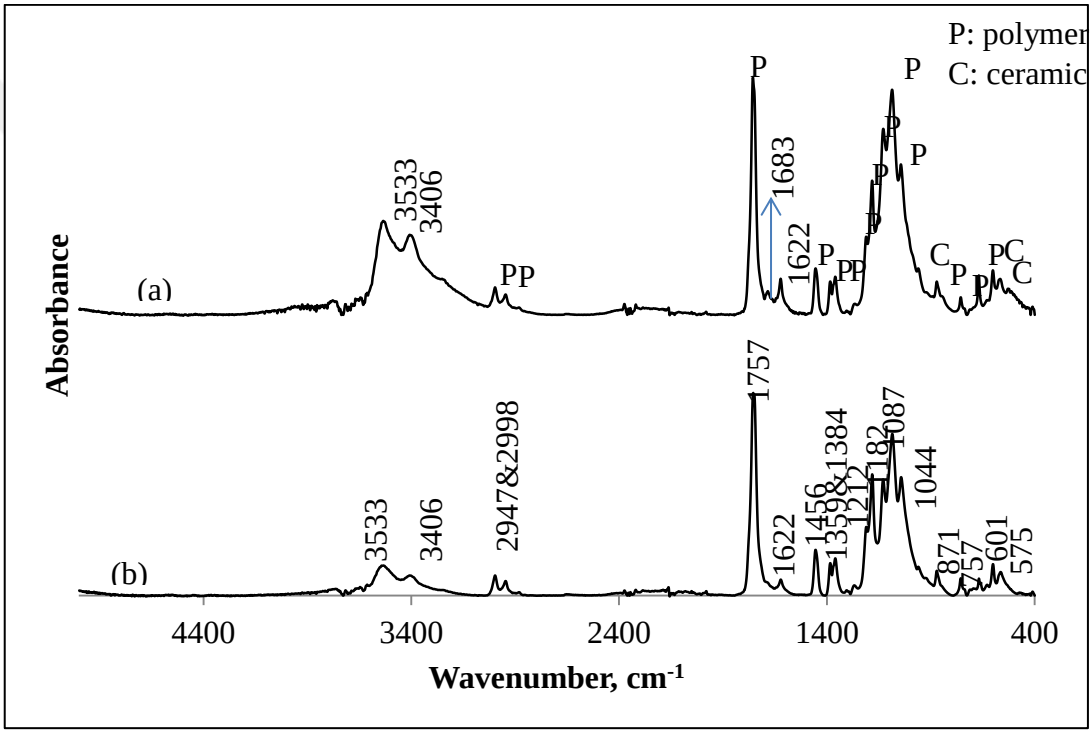

Figure 4.28. FTIR spectra of (a) PLA40H60Si1 (b) PLA50H50Si3.

Figure 4.29 shows the FTIR results of silane A-174 modified β-TCP and PLA composites (PLA40T60PASi1 and PLA50T50PASi3.). Two composites reveal bands at same wave number with different intensities. Results of these modified PLA40T60PASi1 and PLA50T50PASi3 composites are compared with their raw materials, i.e. modified β-TCP and pure PLA powders. The positions of the bands of modified β-TCP that are at 536, 554, 578 cm^{-1} slightly shift to 544, 555 and 580 cm^{-1} in the composites. Also, bands related to modified β-TCP (954, 978 cm^{-1}) stay intact. The position of the band at 889 cm^{-1} in the FTIR spectrum of the modified β-TCP shifts to 916 cm^{-1} and 909 cm^{-1} in PLA40T60PASi1 and PLA50T50PASi3, respectively. The

band located at 991 cm^{-1} regarding β-TCP moves to lower wave numbers in two composites. Changes in these bands, as described above, may sign the interaction between silane A-174 modified β-TCP and PLA. It is thought that FTIR band regarding silane A-174 modified β-TCP (1126 cm^{-1}) and polymer (1130 cm^{-1}) overlap in composites. The positions of the bands originating from polymer at 757 and 872 cm^{-1} do not seem to change in composites. However, band at 668 cm^{-1} disappears in composites like pure β-TCP and PLA composites seen in Figure 4.27. Strongest band of pure β-TCP positioned at 1015 cm^{-1} is not obvious in pure β-TCP and PLA composites as seen in Figure 4.27. Similarly, strongest band of silane modified β-TCP positioned at 1063 cm^{-1} is not seen in silane A-174 modified β-TCP and PLA composites as shown in Figure 4.29. The position of the polymer (at 1044 cm^{-1}) moves to 1048 cm^{-1} (Figure 4.29.a) and 1049 cm^{-1} (Figure 4.29.b) in composites PLA40T60PASi1 and PLA50T50PASi3, respectively. Moreover, position of another feature related to PLA (band at 1085 cm^{-1}) shifts to lower frequency in composites.

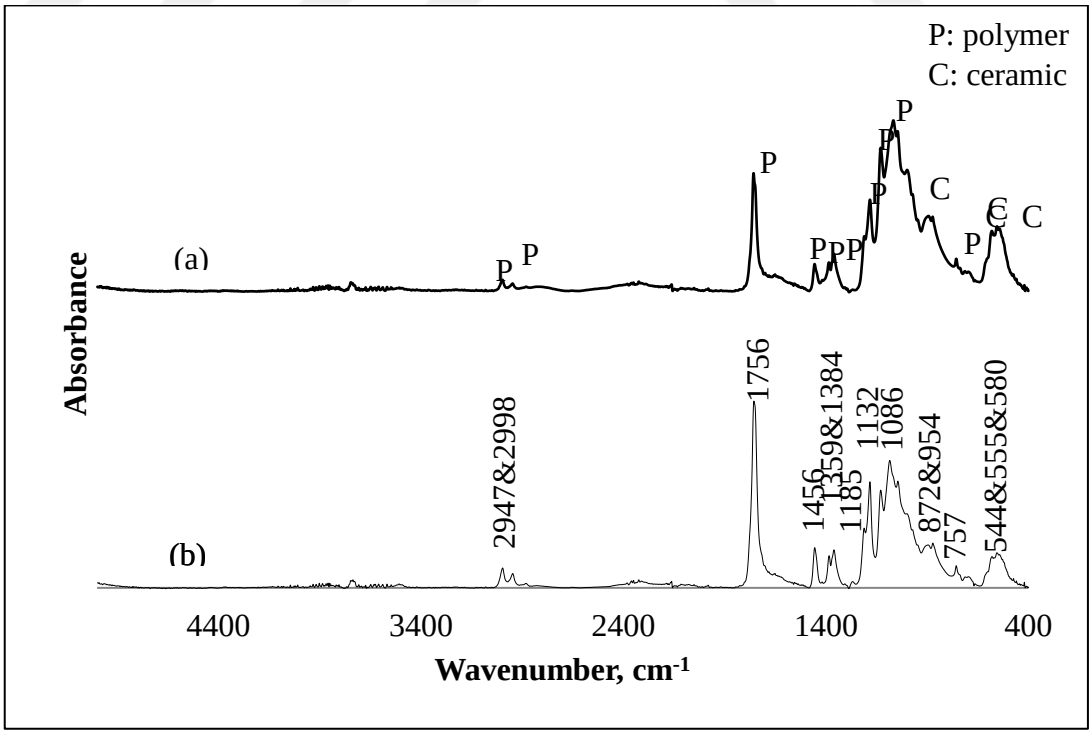

Figure 4.29. FTIR spectra of (a) PLA40T60PASi1 (b) PLA50T50PASi.

4.1.4. X-ray Photoelectron Spectroscopy (XPS) Analysis

XPS analysis was performed on poly-lactic acid, HAP and β-TCP, all in the purchased form, intermediate steps (treated with 3 wt.% silane A-174) of composite production and PLA50H50, PLA50H50Si3, PLA50T50 and PLA50T50PASi3 composites. XPS analysis of composites was done between 0 and 1350 eV region.

4.1.4.1. XPS Analysis of Raw Materials and Treated Ceramics. Figure 4.30 reveals the C 1s, O 1s and overall XPS spectra of pure PLA. Figure 4.30.a shows that PLA has three carbon peaks at 285.18, 286.98 and 289.08 eV. In the literature these peaks correspond to -CH_3 side chain, -CH and C=O in stem chain, respectively [52]. These peaks are also reported to be related to C-C/C-H, C-O/C=O, O-C=O bonds, respectively [104], [105].

O 1s XPS spectrum of poly-lactic acid with a peak at 533.18 eV resembles the related spectra in the literature [52]. This feature should be related to C-O and C=O units in the polymer structure.

Ca 2p, O 1s, P 2p and overall XPS spectra of pure HAP are shown in Figure 4.31. Doublet peaks in Figure 4.31.a correspond to $2p_{3/2}$ and $2p_{3/2}$ of Ca 2p orbit [52]. Binding energies at 530.48 and 133.08 eV observed in Figure 4.31.b and Figure 4.31.c indicate the existence of phosphate oxide and $PO4^{-3}$ in HAP [52].

It is observed that Figure 4.31.d includes additional peaks which are different from peaks in Figure 4.31.a, b, c. It is interesting that carbon peak at 283 eV is observed in the XPS spectrum of HAP. This shows HAP might include some impurities. This observation in the XPS result of HAP confirms the XRD result shown in Figure 4.1. Peaks around 1000 eV may come from oxygen and calcium [57] or carbon residues [106].

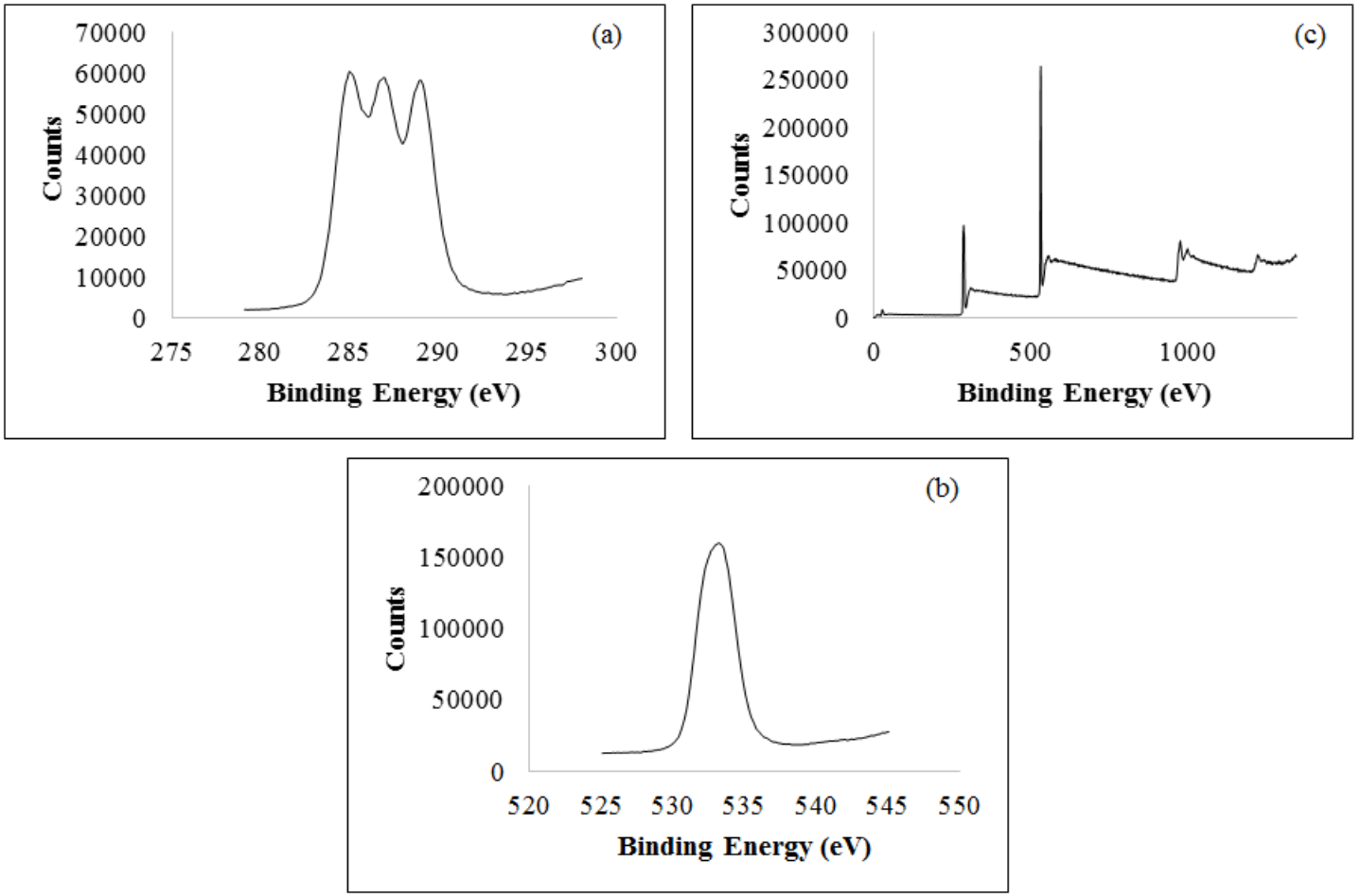

Figure 4.30. (a) C 1s (b) O 1s (c) overall XPS spectra of pure PLA.

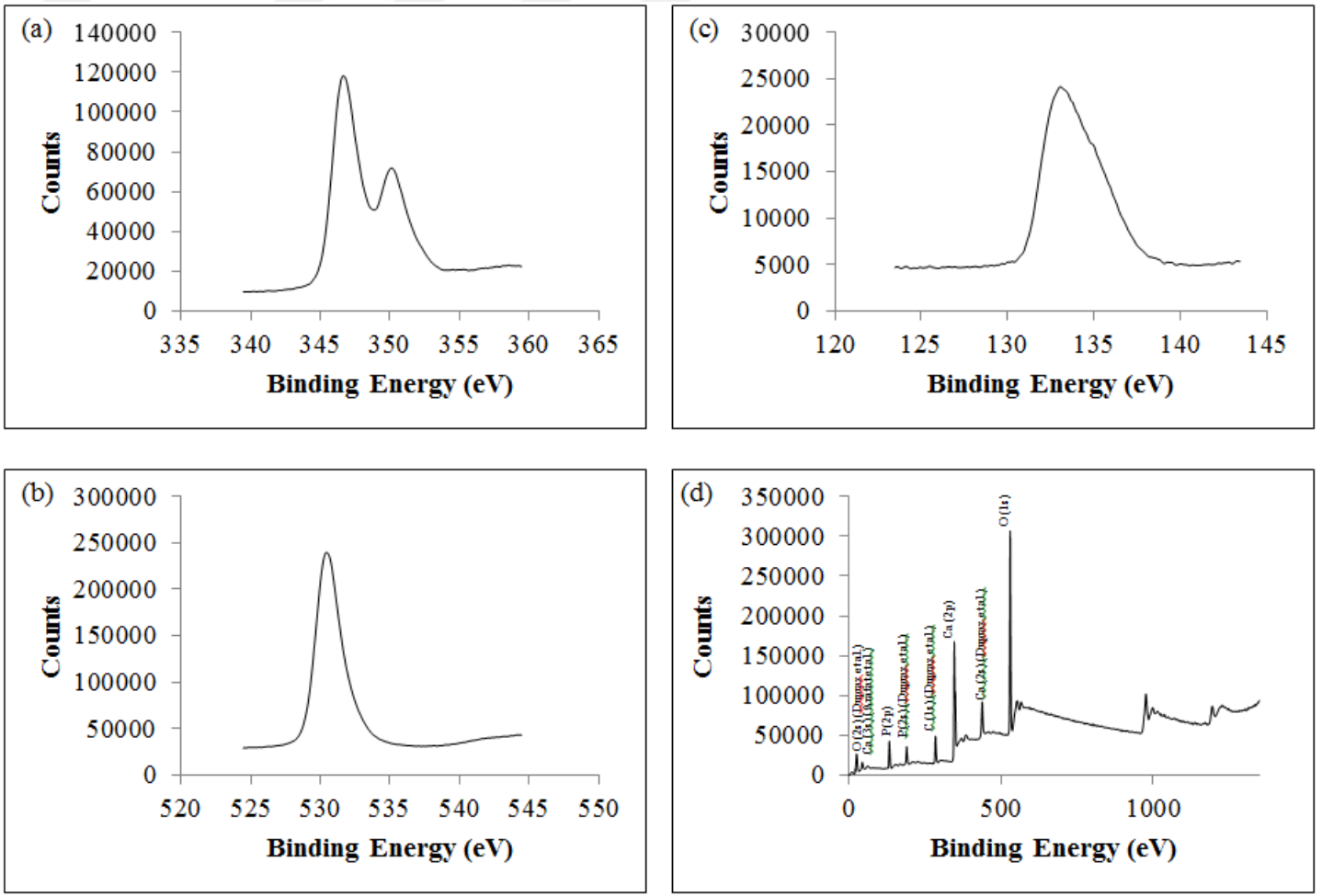

Figure 4.31. (a) Ca 2p (b) O 1s (c) P 2p (d) overall XPS spectra of pure HAP.

Figure 4.32 shows the XPS spectra of HAP treated with 3 wt.% of silane A-174. Ca 2p, P 2p and O 1s binding energies of treated HAP are illustrated in Figure 4.32.a, b and c, respectively. These binding energies are similar to pure HAP. However, intensities of P and Ca peaks decreased.

Si 2p peak is detected in Figure 4.32.e at a binding energy of 101.88 eV, consistent with the literature [31], [57], [96]. Presence of Si peak and reducing intensities of Ca and P peaks show the success of silanization process [57], [62].

In addition to Si peak two new peaks are seen at binding energies 168 and 232 eV in the overall XPS spectrum. Peak at 168 eV comes from sulfuric acid that is used for pH adjustment during silanization process[107], [108].

Figure 4.33 demonstrates the Ca 2p, O 1s, P 2p and overall XPS spectra of pure β-TCP. Pure β-TCP includes calcium, phosphor and oxygen peaks. Overall spectrum of pure β-TCP resembles the spectrum of pure HAP in Figure 4.32.d. However, Ca 2p spectrum of pure β-TCP includes three peaks in 345-360 eV regions (Figure 4.33.a).

P 2p XPS spectrum exhibits a double peak in 130-138 eV regions as shown in Figure 4.33.c. The differences between the XPS spectra of HAP and β-TCP are related with the differences in their formulation and structures.

When overall spectrum of pure β-TCP is closely inspected, unexpected carbon peaks at 286 and 289 eV are observed. Peak at 286 eV is similar to impurity peak (C 1s) of pure HAP. It is named as adventitious carbon [109], [110].

The peak at 289 eV indicates the carbonate peaks. Observation of carbonate peaks in synthetic calcium phosphate is common and it comes from CO_2 in air during synthesis [109], [110].

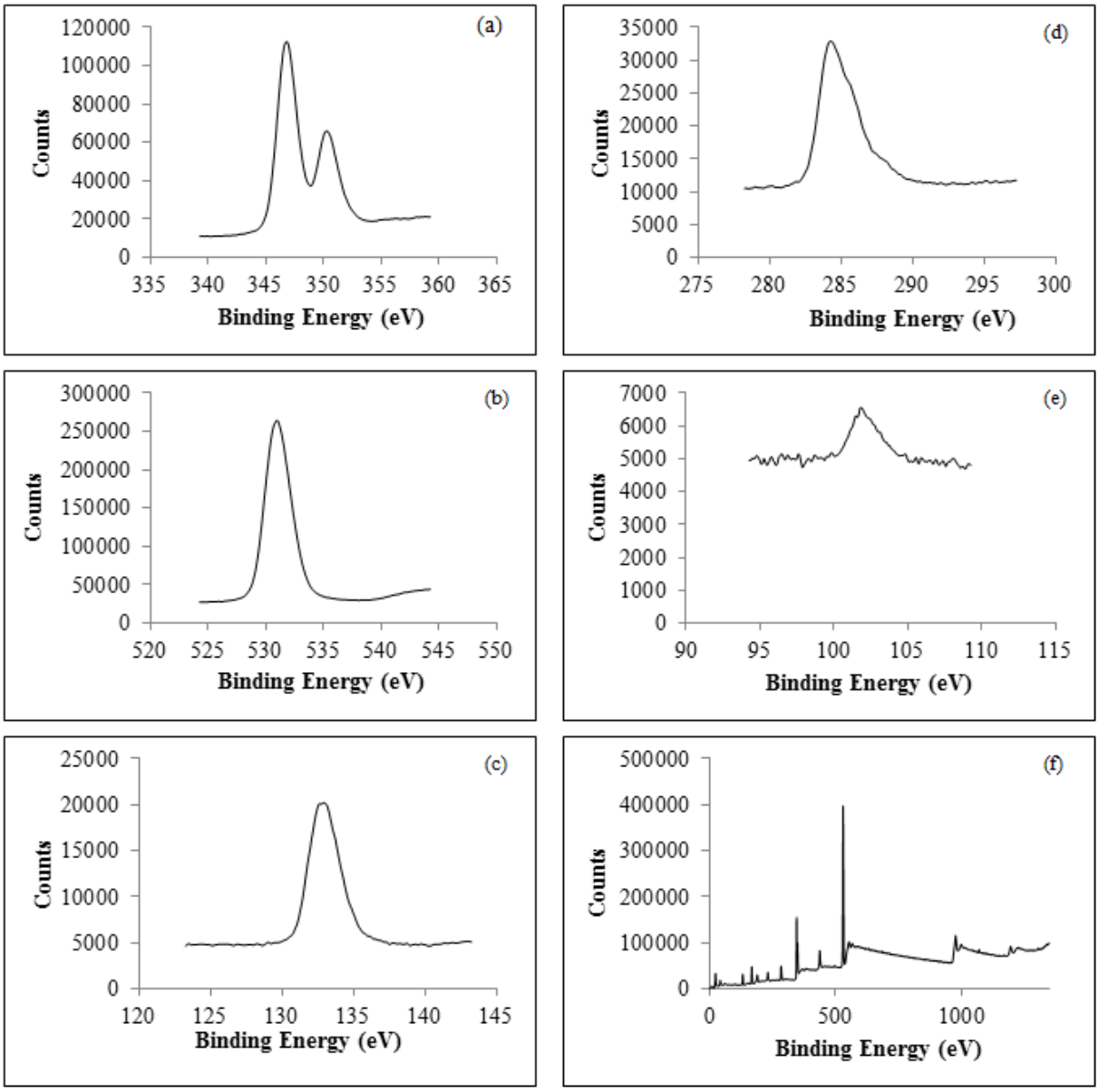

Figure 4.32. (a) Ca 2p (b) O 1s (c) P 2p (d) C 1s (e) Si 2p (f) overall XPS spectra of 3 wt.% silane- A174 treated HAP.

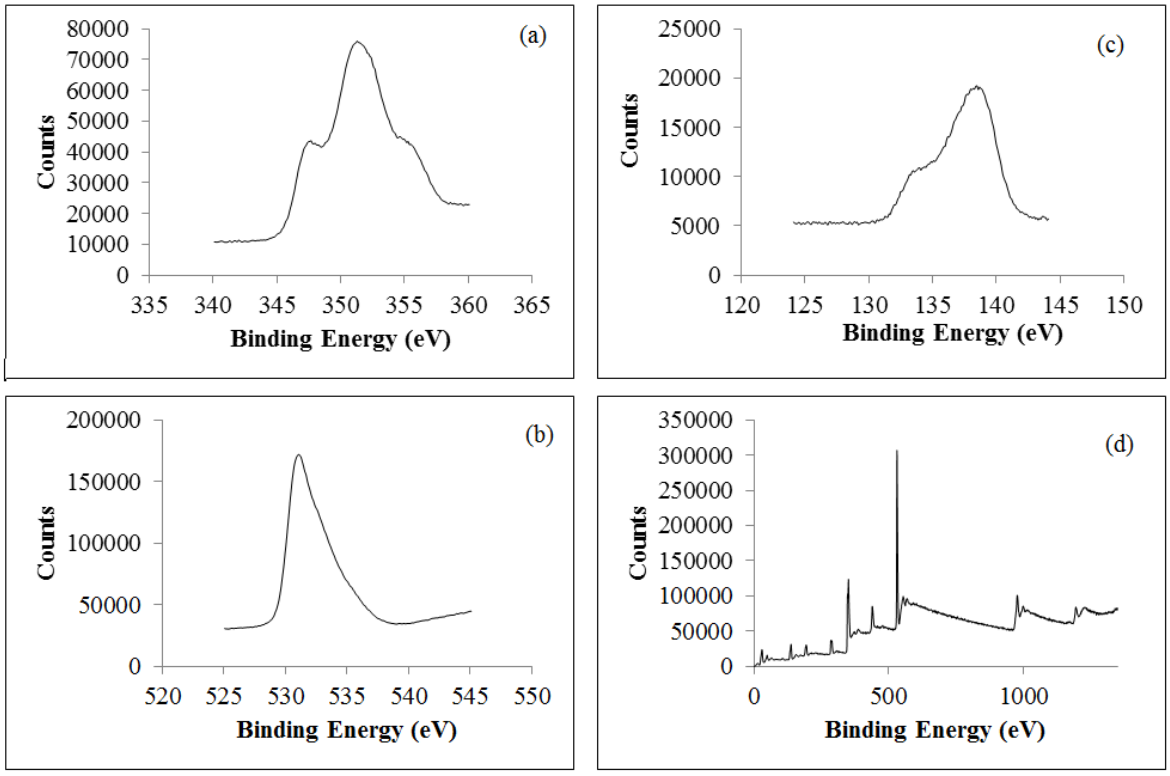

Figure 4.33. (a) Ca 2p (b) O 1s (c) P 2p (d) overall XPS spectra of pure β-TCP.

Figure 4.34 shows Ca 2p, O 1s, P 2p and overall XPS spectra of β-TCP after phosphoric acid addition. O 1s spectrum is similar to the corresponding spectrum in pure β-TCP. Ca peaks of pure β-TCP are positioned at 347, 351 and 355 eV whereas Ca peaks in phosphoric acid treated β-TCP are located at 347 and 351 eV. In addition, P 2p spectrum changes upon treatment (Figure 4.34c).

Aim of phosphoric acid treatment is to increase the OH groups on the surface of β-TCP and to create a surface like HAP. It should be noted that Ca 2p and P 2p spectra in Figure 4.34 resemble the corresponding spectra for pure HAP as seen in Figure 4.31. This shows that the surface of β-TCP is covered with hydroxyl groups after phosphoric acid treatment and surface treatment is achieved.

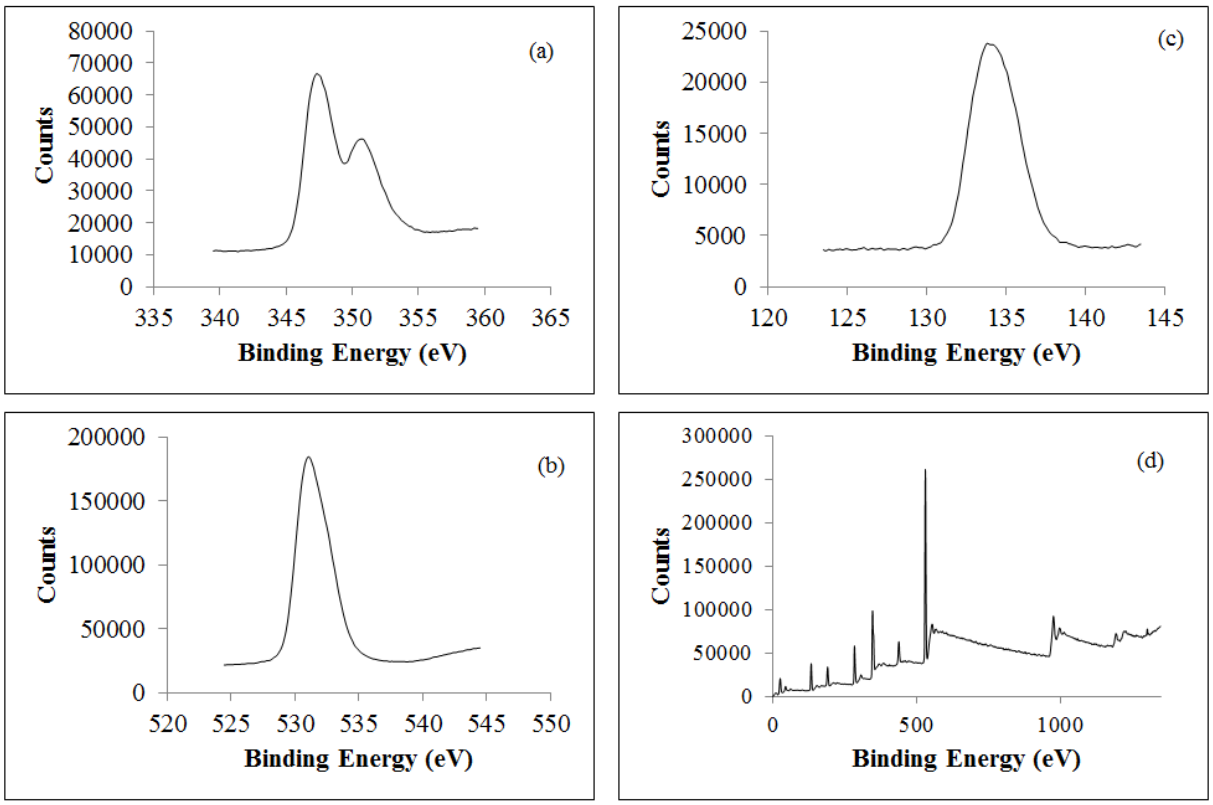

Figure 4.34. (a) Ca 2p (b) O 1s (c) P 2p (d) overall XPS spectra of β-TCP after phosphoric acid treatment.

Ca 2p, O 1s, P 2p, C 1s, Si 2p and overall XPS spectra of phosphoric acid treated β-TCP following silane A-174 treatment is demonstrated in Figure 4.35.

Figure 4.35 shows that silane treatment does not change the shape and locations of Ca, O and P peaks. However, when the overall spectrum of pure β-TCP, β-TCP after phosphoric acid addition and β-TCP after silane treatment is investigated, after silane addition a new C peak at 288 eV with low intensity is observed. This may be related with the carbon atom present in the silane A-174 structure. Si peak which appears in 102.28 eV is consistent with the literature [57], [96].

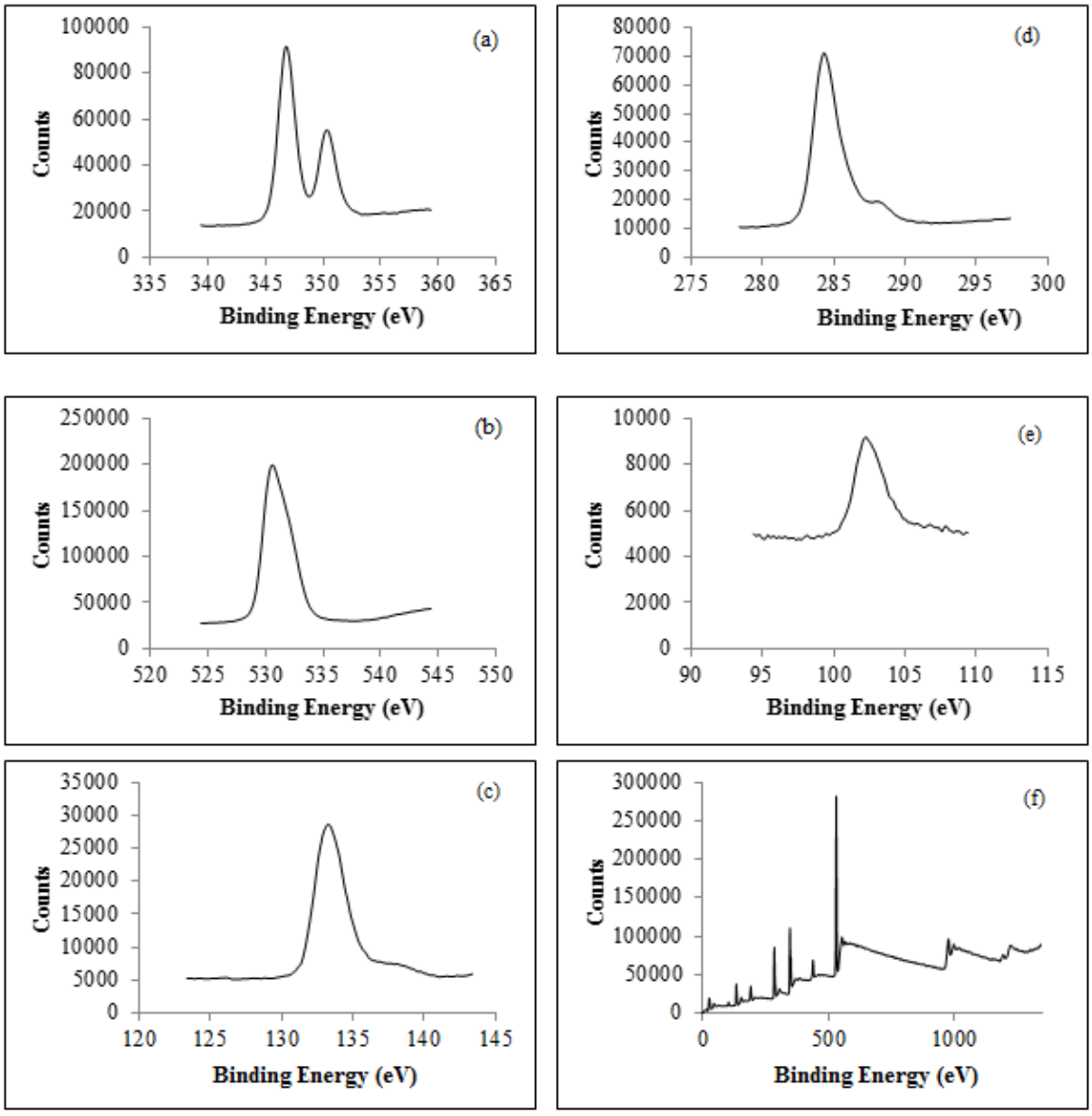

Figure 4.35. (a) Ca 2p (b) O 1s (c) P 2p (d) C 1s (e) Si 2p (f) overall XPS spectra of 3 wt.% silane- A174 treated β-TCP.

4.1.4.2. XPS Analysis of Composites. Figure 4.36 shows the Ca 2p, O 1s, P 2p, C 1s, Si 2p and overall XPS spectra of PLA50H50 composite. Ca 2p spectrum has new multiple features in binding energy range of 345-360 eV. Ca binding energy in PLA50H50 composite seems to be slightly shifted compared to pure HAP. The intensities of the features in Ca 2p, O 1s, P 2p, and C 1s spectra of PLA50H50 composite decrease dramatically compared to features in pure HAP and PLA. It is seen that O 1s spectra of pure HAP and PLA display peaks at 530.48 eV and 533.18 eV, respectively. The feature in O 1s spectrum of PLA50H50 composite is positioned at a higher binding energy, 533.58 eV. Figure 4.37 shows Ca 2p, O 1s, P 2p, C 1s, Si 2p and overall XPS spectra of PLA50H50Si3 composite. Figure 4.37.a reveals that the Ca 2p peaks, similar to PLA50H50, has new multiple features in binding energy range of 345-360 eV. Additionally, the intensities of the features in Ca 2p, O 1s, P 2p, and C 1s spectra of PLA50H50Si3 composite decrease notebly compared to XPS spectra of treated HAP and PLA. It is observed that C 1s peak which belongs to C=O group in PLA shifts to a higher value 289.28 eV for PLA50H50Si3 composite, possibly indicating more interaction, i.e. more electron shift [52]. It is interesting to note that Si 2p spectrum indicates no Si presence on the surface, although PLA50H50Si3 composite includes 3 wt.% silane content. This may be related with the ceramic surface is considerably covered with PLA [31].

Ca 2p, O 1s, P 2p, C 1s, Si 2p, and overall XPS spectra of PLA50T50 composite is displayed in Figure 4.38. It is interesting to note that the composite surface does not contain Ca and P elements whereas the intensity of peak in C1s spectrum is very high. This result could be indicative of the fact that polymer is dominating the composite surface. This may be related with physical accumulation of polymer on ceramic surface which was shown in the corresponding SEM image (Figure 4.17.c).

Figure 4.39 exhibits the Ca 2p, O 1s, P 2p, C 1s, Si 2p, and overall XPS spectra of PLA50T50PASi3 composite. The presence of Ca, P, C, and Si atoms are obvious although their intensities considerably decrease compared to silane treated β-TCP and PLA, possibly indicating their interactions. It should be noted that Si 2p spectrum of PLA50H50Si3 composite does not show any feature contrary to what is observed in PLA50T50PASi3 composite. This

result could indicate more interaction of the polymer with the modified surface in HAP containing composites.

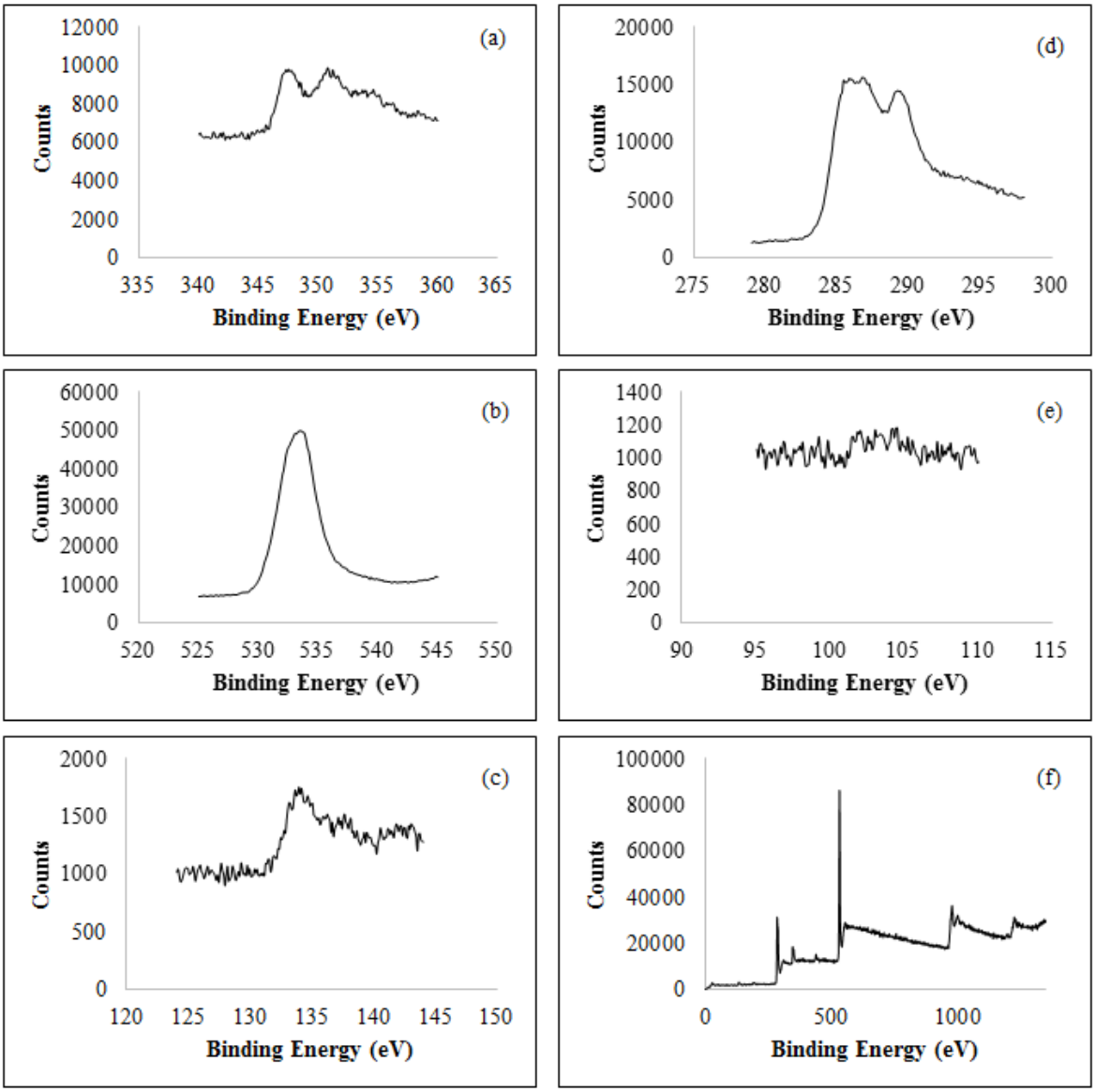

Figure 4.36. (a) Ca 2p (b) O 1s (c) P 2p (d) C 1s (e) Si 2p (f) overall XPS spectra of PLA50H50.

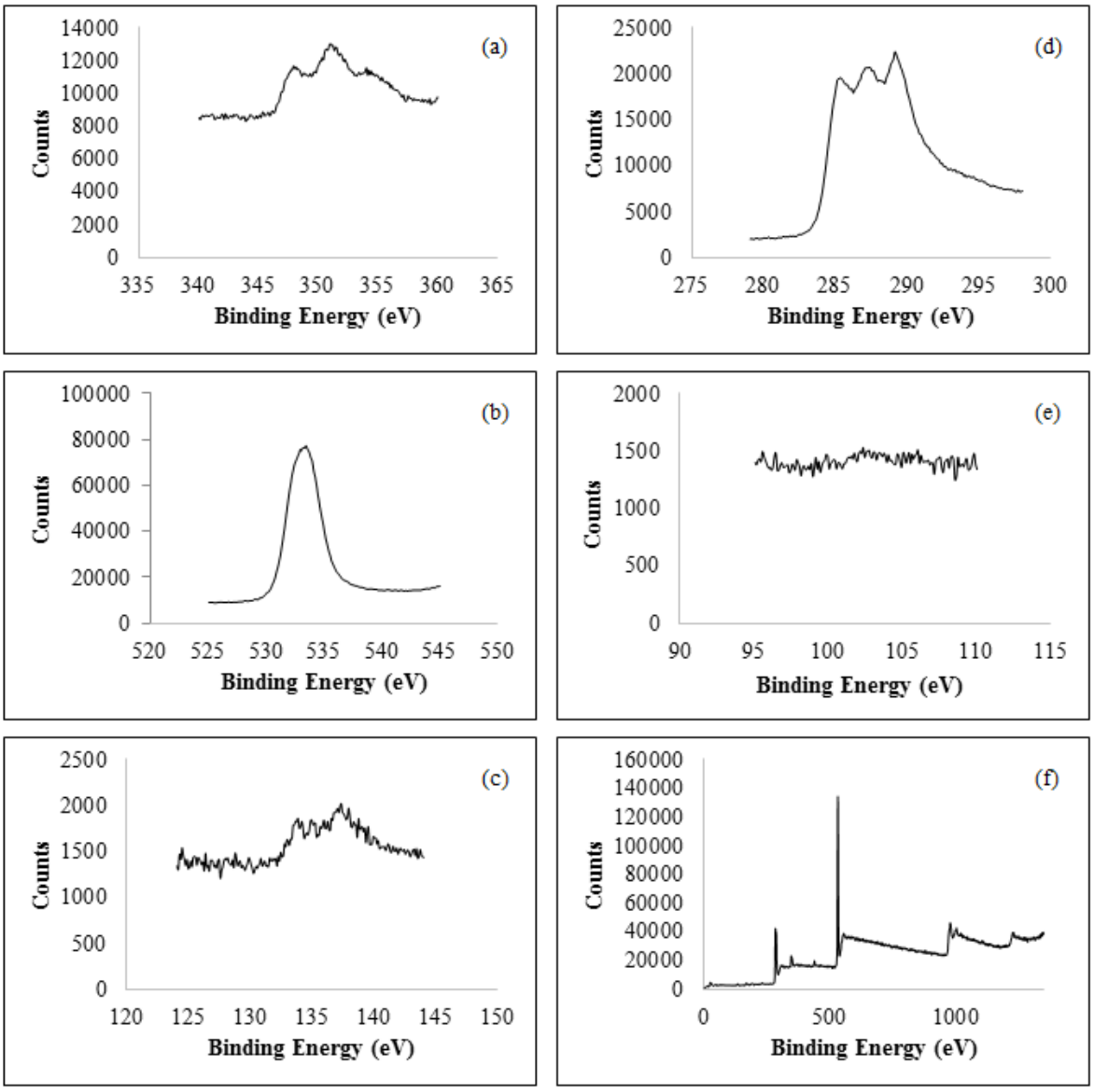

Figure 4.37. (a) Ca 2p (b) O 1s (c) P 2p (d) C 1s (e) Si 2p (f) overall XPS spectra of PLA50H50Si3.

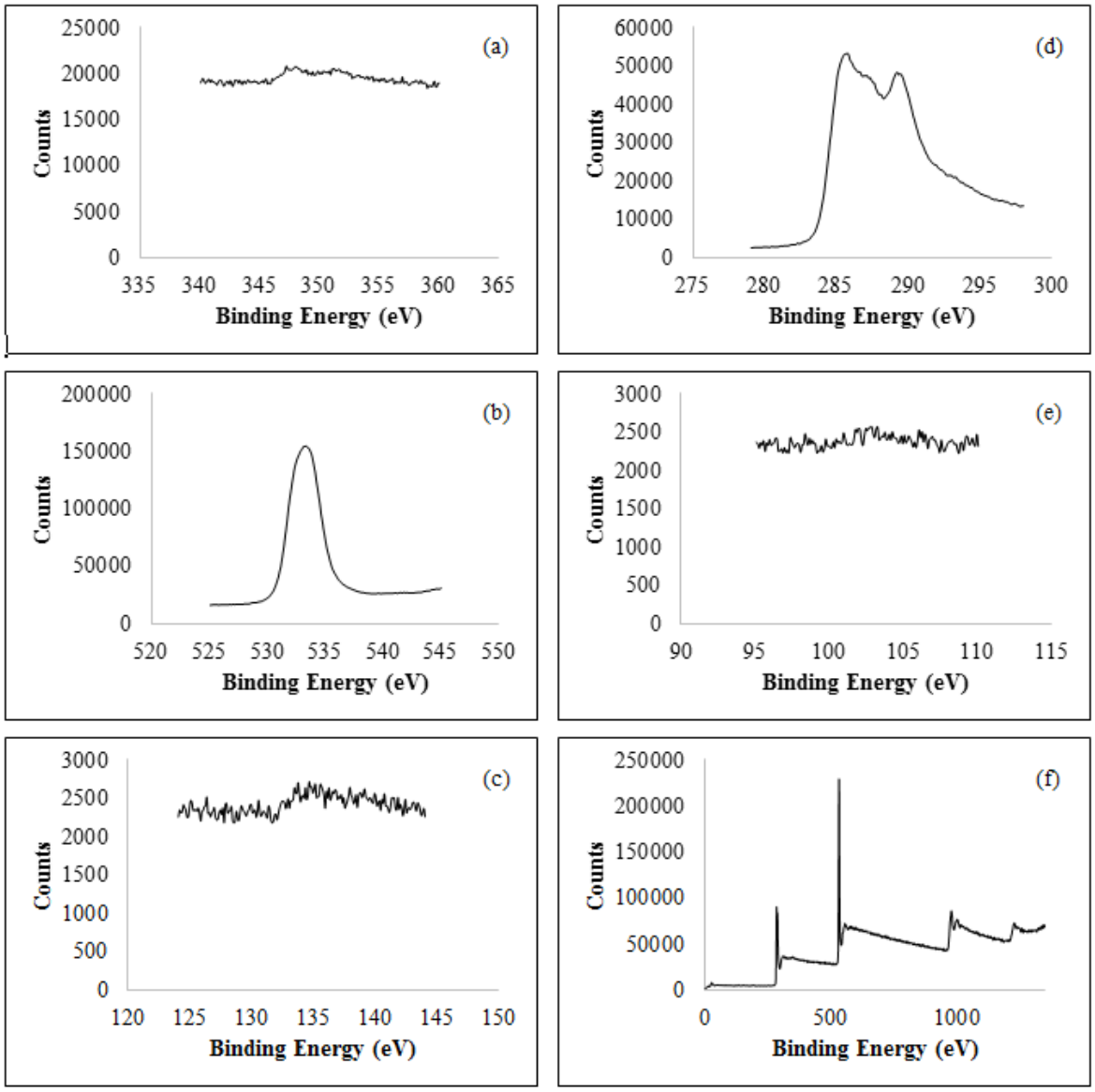

Figure 4.38. (a) Ca 2p (b) O 1s (c) P 2p (d) C 1s (e) Si 2p (f) overall XPS spectra of PLA50T50.

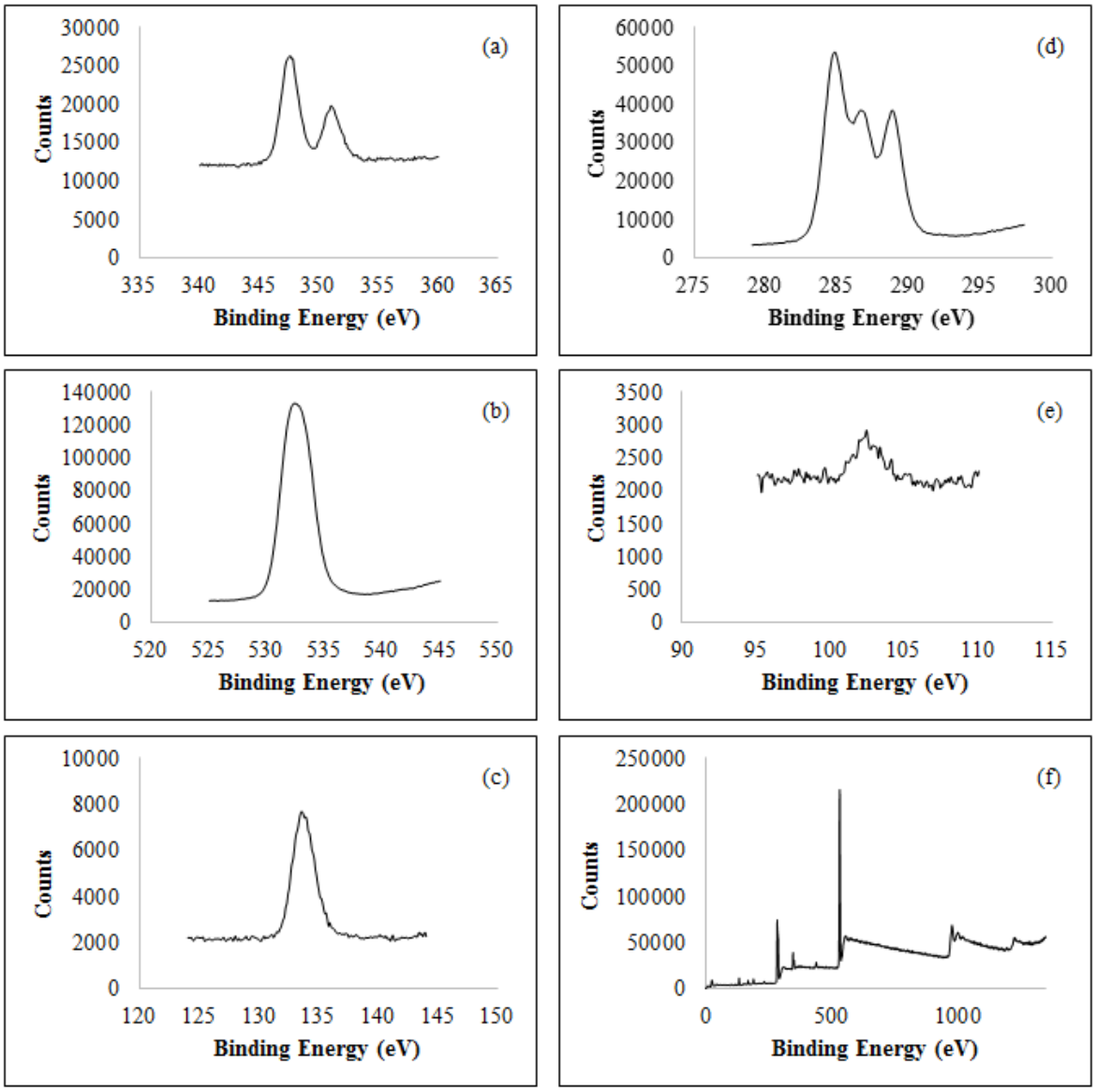

Figure 4.39. (a) Ca 2p (b) O 1s (c) P 2p (d) C 1s (e) Si 2p (f) overall XPS spectra of PLA50T50PASi3.

4.2. Mechanical Measurement Results

Mechanical durability of composites is one of the most important parameters in the tissue engineering applications, especially for healing of hard tissues [111]. According to reached mechanical values, materials are chosen for appropriate tissue. For example, materials which show the compressive strength above from 88 MPa can be us in cortical bone trauma. Materials which have from 3 MPa to 12 MPa can be chosen for cancellous bone treatments [2], [26], [30], [31].

Compressive load and displacement curves of each composite with same composition are obtained and represented in same figure. Also, strain and stress curve of all materials are presented in small figures as insets in compressive load and displacement graphs. Figures B.1-9 İnclude the compressive load and displacement curves, and strain and stress curves of PLA cement, and the composites studied in this thesis. Average ultimate compressive strength values of pure PLA and composites duplicates are listed in Table 4.2.

Table 4.2. Compressive Strength of Composites.

Materials	**Compressive Strength (MPa)**	**Stress Strain Curve Structure**
Pure Polymer	14	Ductile Polymer
PLA50H50	94	Ductile Polymer
PLA40H60	19	Catastrophic Failure
PLA50H50Si3	364	Ductile Polymer
PLA40H60Si1	15	Catastrophic Failure
PLA50T50	1.5	Catastrophic Failure
PLA40T60	7.9	Ductile Polymer
PLA50T50PASi3	14	Ductile Polymer
PLA40T60PASi1	4.3	Ductile Polymer

Two different structures are observed in compressive load and displacement of composites. First one is referred as ductile polymer characteristic which shows bone unique property [112]. Ductile polymer structure possesses three sections. First section is initial response which stress increases with strain quasi-elastic linearly. Second section is plateau response which has negligible slope and third section is densification part which shows the rapid increase [113], [114]. Densification section is transforming from porous material to solid structure [113]. Second structure is catastrophic failure of composites [115] which means decrease after reaching a maximum value. It relates with the low mechanical durability and low dispersion between polymer and ceramic [49].

Silane treatment of ceramics can have huge effect in enhancing mechanical properties of polymer-ceramic composites. For example, β-TCP-polymer composite (PLA50T50) displays a compressive strength value of 1.5 MPa while PLA50T50PASi3 specimen formed by 3 wt.% silane treated β-TCP resulted in a compressive strength value of 14 MPa.

It is seen that silane treatment of HAP results in obtaining composites with superior mechanical performance values. It is seen in Table 4.2 that PLA50H50 that was formed without silane modification of HAP has a compressive value of 90 MPa. The silane treatment results in obtaining PLA50H50Si3 composite with a compressive strength of 364 MPa. It should be noted that this value is much higher compared to what is reported in the literature as summarized in Table 2.2. The values reported previously vary between 14.9-212 MPa.

It should be noted that the percentages of the coupling agents should be carefully determined. For instance, PLA40T60 composite that does not involve any ceramic treatment had a compressive strength of 7.9 MPa while the composite based on 1 wt.% silane treated β-TCP (PLA40T60PASi1) resulted in a comparable compressive strength value of 4.3 MPa indicating no progress. Similar result is observed compressive strength values of PLA40H60 and PLA40H60Si1. These results confirm the amount of silane is important parameter for bone regeneration materials [31], [65] and interfacial interaction of PLA and ceramics increases with 3 wt.% of silane treatment [70].

Compressive strengths of β-TCP and PLA composites even after phosphoric acid and 3 wt.% silane A-174 treatment of β-TCP , are still lower than compressive strength of both cancellous bone and cortical bone [2], [26], [30]. Compressive strength of PLA50H50 composites is found in compressive strength region of cortical bone. Compressive strength of PLA50H50Si3 composite exceed the maximum compressive strength value of cortical bone (i.e. 193 MPa [26]) . In literature it is stated that mechanical strength of scaffolds should be in the compressive strength range of host tissue for successful bearing application [70]. However, compressive strength of bone replacement materials decreases in short time after placing in body fluid [50]. Therefore, producing composite, which has slightly higher strength than bone, may be necessary to prevent low bearing.

4.3. *in Vitro* Degradation Analysis Results

For applications in bone tissue engineering it is important for biocomposites to exhibit controlled biodegradation in addition to showing good mechanical performance. In this context, *in vitro* degradation of pure PLA cement which was obtained by chloroform addition and composites are studied. Specimens were synthesized using molds with dimensions 9 mmx3 mm and their weights were recorded. The specimens were then immersed in HBSS fluids and kept in simulated-body conditions for 7 days. Composite PLA40T60 cannot be poured in molds due to its crumbled structure. With 1 wt.% silane addition PLA40T60PASi1 was molded but it cracks during measurements. Therefore, data for PLA40T60 and PLA40T60PASi1 could not be taken. Mass loss percentages after 7 days being exposed to HBSS fluid are presented in Table 4.3.

Table 4.3. Mass Loss Percentage of Samples in First 7 Days.

Material	**Mass loss (wt.%) in 7 days**
Pure PLA	6.2
PLA50H50	1.0
PLA40H60	0.9

Table 4.3. Mass Loss Percentage of Samples in First 7 Days. (cont.)

Material	Mass loss (wt.%) in 7 days
PLA50H50Si3	1.1
PLA40H60Si1	0.9
PLA50T50	25.3
PLA40T60	Not moldable
PLA50T50PASi3	7.9
PLA40T60PASi1	Cracking

The maximum amount of mass loss is observed for PLA50T50 (25.3 wt.%) obtained. β-TCP is known with its high biodegradation ability. This is consistent with the observed high mass loss in PLA50T50 [39]. The composite synthesized based on β-TCP, modified by phosphoric acid followed by (3 wt.%) silane treatment, seems to result in more controlled biodegradation as PLA50T50PASi3 loses 7.9 % of its initial mass after exposure to HBSS for 7 days.

Stable nature of HAP seems to reduce the mass loss of composites that are synthesized based on it [39], [2]. PLA50H50 and PLA40H60 seem to be quite stable in HBSS conditions as these materials lose about ~1 wt.% of their initial masses as it is seen in Table 4.3. PLA50H50Si3 and PLA40H60Si1 lose ~1 wt.% of their initial masses as well. Therefore, it is concluded that employing silane A-174 treated hydroxyapatite in the synthesis of composite does not seem to influence the biodegradation, at least within the limited timeframe of the experiments.

It should be noted that the formation of apatite crystal may begin after 3-7 weeks in simulated body fluid and degradation profiles can change significantly in this period [2], [116]. Therefore, long term measurements need to be made to support these findings.

5. CONCLUSIONS AND RECOMMENDATIONS

5.1. Conclusions

In this study, HAP-PLA and β-TCP-PLA composites were produced at ambient conditions using two different polymer/ceramic ratios. The effect of surface treatment of ceramics was also investigated. For surface modification of HAP, silane A-174 with 1 wt.% and 3 wt.% were used. For β-TCP ceramic treatment, protonation was done with phosphoric acid solution before the addition of 1 wt.% and 3 wt.% of silane A-174 to enhance hydroxyl groups on the surface of β-TCP. XRD, FTIR, SEM and XPS analyses were carried out to characterize raw materials, treated ceramics and manufactured composites. Compressive strength measurements and degradation studies in HBSS were also performed pure PLA and composites.

XRD pattern of HAP was in agreement with the reference models of HAP (PDF 00-001-1008) and calcium phosphate (PDF 00-011-0232). The agreement with calcium phosphate model indicated the existence of some impurities. XRD peaks of β-TCP matched with the reference model of whitlockite (PDF 00-003-0713), which is the crystallographic form of β-TCP. Characteristic peaks of pure PLA positioned at 2θ=17° and 2θ=19.31°, and an amorphous characteristic located in the region 2θ=10-30° were observed from XRD analysis. Increase in the intensities of double peaks of pure β-TCP (around 2θ=27°) was observed after phosphoric acid treatment. These results were attributed the achievement of protonation. Silane A-174 addition did not change the XRD pattern of β-TCP. However, decrease in the intensity of some peaks was observed, which was ascribed to the change of Ca/P ratio because of the replacement of calcium atoms with silica atoms. Amorphous structure of pure PLA was observed in both HAP and β-TCP including composites and the reduction in the intensities and the shifts in the peaks indicated the PLA and ceramic interactions. However, the effect of silane treatment on the composites was not clear according to the XRD results, which can be explained by the usage of rather small amount of coupling agent.

SEM images of raw materials in the present study were found in agreement with the literature results. Silane treatment resulted in filamentous HAP surface structure. Phosphate crystals on β-TCP surface were observed after protonation. SEM results did not show clear interaction between the PLA and untreated β-TCP. Morphology of the composites with modified ceramics showed signs of interaction with improved dispersion of polymer on ceramic surface.

Characteristic peaks of raw materials were seen in their FTIR spectra. After phosphoric acid treatment, bands regarding pure β-TCP located at 593 and 601 cm^{-1} disappeared. Strongest band of pure β-TCP at 1015 cm^{-1} moved to 1063 cm^{-1} after phosphoric acid treatment. New bands at 1348, 1403, 1646 and 2862 cm^{-1} related to $CaHPO_4$ formation. $CaHPO_4$ peaks and other changes were interpreted as the successful interaction between phosphoric acid and β-TCP. After 1 wt.% and 3 wt.% silane A-174 addition, the modification of β-TCP peak at 978 cm^{-1} was attributed to the formation of P-O-Si bond, hence achievement of silane A-174 treatment was obtained. New peak formation in FTIR results of unmodified ceramic containing composites was not seen; however, overlap, shift and totally disappearance of some peaks in composites indicated the polymer and ceramic interaction. Formations of new peaks located at 622, 3406 and 3533 cm^{-1} were observed in the modified HAP including composites.

XPS results of pure materials were compatible with the literature. Moreover, carbon peak at 283 eV in C 1s spectrum of HAP confirmed the existence of impurities. Si peaks were seen after silane treatment of in both ceramics according to the XPS results. Also, an interesting result was obtained after phosphoric acid treatment; Ca 2p and P 2p spectra of modified β-TCP changed into a form resembling the XPS spectra of HAP. This change possibly contributed to improvement of the compressive strength. In treated and untreated HAP including composites, Ca peaks shifted to higher binding energies with lower intensity. Silane terated HAP including composite did not show any Si peak at the surface. This was attributed to the coverage of ceramic surface by PLA considerably. XPS peaks of Ca and P were not seen on the surface of PLA50T50 composite whereas C peak of PLA was found with quite high intensity. Reason behind was physical accumulation of polymer on ceramic surface which was shown in also the corresponding SEM image. Similar to HAP including composites, XPS peaks of Ca 2p, P 2p and C 1s decreased in PLA50T50PASi3. However, percent decrease in PLA50T50PASi3 was

lower than hydroxyapatite containing composites. Also, Si 2p spectrum of PLA50H50Si3 composite did not show any feature contrary to what is observed in PLA50T50PASi3 composite. Low reduce in Ca 2p, P 2p and C 1s and unchanged Si feature in PLA50T50PASi3 could indicate more interaction of the polymer with the surface in HAP containing composites.

Compressive strength measurements indicated that performance of β-TCP including composites was lower than that of HAP containing composites. 1 wt.% of silane treatment was found insufficient for HAP and β-TCP including composites when compared with their untreated counterparts. However, 3 wt.% of silane treatment enhanced the strength of both HAP (from 94 MPa to 364 MPa) and β-TCP including (from 1.5 MPa to 14 MPa) composites. Compressive strength of PLA50T50PASi3 (14 MPa) was still lower than the minimum required compressive strength value of cortical bone. Compressive strength values of PLA50H50 and PLA50H50Si3 matched with the performance of human cortical bone. This was an important improvement that was achieved at room conditions and signifies the achievement of our process and manufacturing parameters for high mechanical performance.

Degradation studies showed that β-TCP including composites are more degradable than HAP including composites. Silane modification decreased the mass loss affinity of β-TCP including composites whereas silane treatment did not cause a meaningful change in HAP including composites.

5.2. Recommendations

For future studies different polymer and ceramic ratios may be investigated to further see the effect of composition on mechanical and degradation behavior of composites. Biphasic calcium phosphate (BCP) may be used in the future experiments to improve the properties of composites aiming to control of bioactivity and biodegradation properties [117].

In this study, the effect of silane A-174 treatment was investigated; however, it would be interesting to use different coupling agents with different functionalities. In literature, silane agents with different functionalities were studied, however after silane treatment composite

production was not performed. Therefore, a comprehensive study investigating different silane agents together with composite production would be beneficial. In addition, other coupling agents like etidronic acid and hexa-methylene diisocyanate in phosphate glass-polymer systems [63] can be employed in calcium phosphate and polymer systems to improve dispersion performance between polymer and ceramic.

Tensile strength is another important parameter for high performance cortical bone [2]. Analyzing bending, tensile strengths and their modulus for produced composites might be complementary to these results.

Degradation study of the composites was performed using a limited time frame (one week). Long term investigation of composite degradations would be necessary to predict real performance of these materials. Also, SEM, FTIR and mechanical analyses in some time points of degradation could give more information to see surface, performance and characteristic changes in composites after degradation. In addition to degradation, bioactivity can be investigated by measuring the released calcium and phosphorous ions in simulated body fluid similar to previous studies [61], [64].

REFERENCES

1. S. Ramakrishna, J. Mayer, E. Wintermantel, and K. W. Leong, “Biomedical applications of polymer-composite materials: a review”, *Compos. Sci. Technol.*, vol. 61, no. 9, pp. 1189–1224, 2001.

2. N. Gültekin, “Preparation and Characterization of Hydroxyapatite and Polymer Composite Biomaterials”, İzmir Institute of Technology, 2002.

3. A. R. Amini, C. T. Laurencin, and S. P. Nukavarapu, “Bone tissue engineering: recent advances and challenges”, *Crit. Rev. Biomed. Eng.*, vol. 40, no. 5, pp. 363–408, 2012.

4. A. K Nair, A. Gautieri, S.-W. Chang, and M. J Buehler, “Molecular Mechanics of Mineralized Collagen Fibrils in Bone”, *Nat. Commun.*, vol. 4, p. 1724, Apr. 2013.

5. A. Szcześ, L. Hołysz, and E. Chibowski, “Synthesis of hydroxyapatite for biomedical applications”, *Adv. Colloid Interface Sci.*, vol. 249, pp. 321–330, 2017.

6. H. Zhang *et al.*, “Molecular dynamics simulations on the interaction between polymers and hydroxyapatite with and without coupling agents”, *Acta Biomater.*, vol. 5, no. 4, pp. 1169–1181, 2009.

7. I. Armentano, M. Dottori, E. Fortunati, S. Mattioli, and J. M. Kenny, “Biodegradable polymer matrix nanocomposites for tissue engineering: A review”, *Polym. Degrad. Stab.*, vol. 95, no. 11, pp. 2126–2146, 2010.

8. L. L. Hench, “Biomaterials: A Forecast for the Future”, *Biomaterials*, vol. 19, pp. 1419–1423, Sep. 1998.

9. M. N. Helmus, “Overview of Biomedical Materials”, *MRS Bull.*, vol. 16, no. 9, pp. 33–38, 1991.

10. R. Jain and D. Kapoor, “The dynamic interface: A review”, *J. Int. Soc. Prev. Community Dent.*, vol. 5, no. 5, pp. 354–358, 2015.

11. G. Heness and B. Ben-Nissan, “Innovative Bioceramics”, *Mater Forum*, vol. 27, Nov. 2003.

12. Y. Liu, Y. Zheng, and B. Hayes, “Degradable, absorbable or resorbable—what is the best grammatical modifier for an implant that is eventually absorbed by the body?”, *Sci. China Mater.*, vol. 60, no. 5, pp. 377–391, 2017.

13. D. Debarun *et al.*, “Bioresorption and Degradation of Biomaterials”, *Adv. Biochem. Eng. Biotechnol*, vol. 126, Oct. 2011.

14. Z. Sheikh, M.-N. Abdallah, A. A. Hanafi, S. Misbahuddin, H. Rashid, and M. Glogauer, “Mechanisms of in Vivo Degradation and Resorption of Calcium Phosphate Based Biomaterials”, *Materials (Basel).*, vol. 8, no. 11, pp. 7913–7925, Jun. 2015.

15. R. Z. LeGeros, “Biodegradation and bioresorption of calcium phosphate ceramics”, *Clin. Mater.*, vol. 14, no. 1, pp. 65–88, 1993.

16. P. M. Galletti, “Biomaterials: Facts and Fiction BT - Heart Replacement”, 1998, pp. 103–109.

17. A. V Krasnikov, V. V Annikov, Y. A. Vatnikov, E. Sotnikova, E. Kulikov, and V. I. Parshina, “Analysis of dental implants’ biointegration in animals”, *Biol. Med.*, vol. 8, May 2016.

18. F. J. O’Brien, “Biomaterials & scaffolds for tissue engineering”, *Mater. Today*, vol. 14,

no. 3, pp. 88–95, 2011.

19. K. Samarawickrama, “A Review on Bone Grafting, Bone Substitutes and Bone Tissue Engineering”, in *Proceedings of the 2nd International Conference on Medical and Health Informatics*, 2018.

20. A. Odén, E. Mccloskey, J. A. Kanis, N. C. Harvey, and H. Johansson, “Burden of high fracture probability worldwide: secular increases 2010–2040”, *Osteoporos. Int.*, vol. 26, May 2015.

21. M. Swetha, K. Sahithi, A. Moorthi, N. Srinivasan, K. Ramasamy, and N. Selvamurugan, “Biocomposites containing natural polymers and hydroxyapatite for bone tissue engineering”, *Int. J. Biol. Macromol.*, vol. 47, no. 1, pp. 1–4, 2010.

22. M. M. Stevens, “Biomaterials for bone tissue engineering”, *Mater. Today*, vol. 11, no. 5, pp. 18–25, 2008.

23. D. Zhang, X. Wu, J. Chen, and K. Lin, “The development of collagen based composite scaffolds for bone regeneration”, *Bioact. Mater.*, vol. 3, no. 1, pp. 129–138, 2018.

24. S. Saravanan, R. S. Leena, and N. Selvamurugan, “Chitosan based biocomposite scaffolds for bone tissue engineering”, *Int. J. Biol. Macromol.*, vol. 93, pp. 1354–1365, 2016.

25. W. Wang and K. W. K. Yeung, “Bone grafts and biomaterials substitutes for bone defect repair: A review”, *Bioact. Mater.*, vol. 2, no. 4, pp. 224–247, 2017.

26. V. P. Orlovskii, V. S. Komlev, and S. M. Barinov, “Hydroxyapatite and Hydroxyapatite-Based Ceramics”, *Inorg. Mater.*, vol. 38, no. 10, pp. 973–984, 2002.

27. D. Burr, “Bone material properties and mineral matrix contributions to fracture risk or

age in women and men", *J. Musculoskelet. Neuronal Interact.*, vol. 2, pp. 201–204, Apr. 2002.

28. E. Şahin, "Synthesis and characterization of calcium phosphate cement based macroporous scaffolds", Graduate School of Engineering and Sciences of İzmir Institute of Technology, 2012.

29. E. Hasret, "Synthesis And Characterization Of Hydroxyapatite And Investigation Of Its Adsorbent Properties", İstanbul Technical University, Institute of Science and Technology, 2010.

30. M. Rehman, M. A. Madni, and T. Webster, "The era of biofunctional biomaterials in orthopedics: what does the future hold?", *Expert Rev. Med. Devices*, vol. 15, Jan. 2018.

31. M. Tarik Arafat *et al.*, "High performance additive manufactured scaffolds for bone tissue engineering application", *Soft Matter*, vol. 7, no. 18, pp. 8013–8022, 2011.

32. H. Zhang, *Ice Templating and Freeze-Drying for Porous Materials and Their Applications*. 2018.

33. R. Florencio-Silva, G. R. da S. Sasso, E. Sasso-Cerri, M. J. Simões, and P. S. Cerri, "Biology of Bone Tissue: Structure, Function, and Factors That Influence Bone Cells", *Biomed Res. Int.*, vol. 2015, p. 421746, 2015.

34. Y.-Q. Yang, Y.-Y. Tan, R. Wong, A. Wenden, L.-K. Zhang, and A. B. M. Rabie, "The role of vascular endothelial growth factor in ossification," *Int. J. Oral Sci.*, vol. 4, no. 2, pp. 64–68, Jun. 2012.

35. A. Grosso, M. Burger, A. Lunger, D. Schaefer, A. Banfi, and N. Di Maggio, "It Takes Two to Tango: Coupling of Angiogenesis and Osteogenesis for Bone Regeneration", *Front. Bioeng. Biotechnol.*, vol. 5, p. 68, Nov. 2017.

36. R. Setiawati and P. Rahardjo, “Bone Development and Growth”, in *Osteogenesis and Bone Regeneration*, 2018.

37. K. D. Hankenson, M. Dishowitz, C. Gray, and M. Schenker, “Angiogenesis in bone regeneration”, *Injury*, vol. 42, no. 6, pp. 556–561, Jun. 2011.

38. L. L. Hench and J. M. Polak, “Third-Generation Biomedical Materials”, *Science (80-.).*, vol. 295, no. 5557, pp. 1014 LP – 1017, Feb. 2002.

39. J. Jeong, J. H. Kim, J. H. Shim, N. S. Hwang, and C. Y. Heo, “Bioactive calcium phosphate materials and applications in bone regeneration”, *Biomater. Res.*, vol. 23, p. 4, Jan. 2019.

40. D. Arcos, “Silicon substituted hydroxyapatites. A method to upgrade calcium phosphate based implants”, *J. Mater. Chem.*, vol. 15, Apr. 2005.

41. F. Matassi, L. Nistri, D. Chicon Paez, and M. Innocenti, “New biomaterials for bone regeneration”, *Clin. Cases Miner. Bone Metab.*, vol. 8, no. 1, pp. 21–24, 2011.

42. C. Shi, Z. Yuan, F. Han, C. Zhu, and B. Li, *Polymeric biomaterials for bone regeneration*, vol. 1. 2016.

43. M. Alizadeh-Osgouei, Y. Li, and C. Wen, “A comprehensive review of biodegradable synthetic polymer-ceramic composites and their manufacture for biomedical applications”, *Bioact. Mater.*, vol. 4, no. 1, pp. 22–36, 2019.

44. K. Hamad, "Properties and Medical Applications of Polylactic Acid: A Review", *eXPRESS Polymer Letters*, vol. 9. 2015.

45. G. Narayanan, V. N. Vernekar, E. L. Kuyinu, and C. T. Laurencin, “Poly (lactic acid)-based biomaterials for orthopaedic regenerative engineering”, *Adv. Drug Deliv. Rev.*, vol.

107, pp. 247–276, Dec. 2016.

46. R. Pawar, S. U. Tekale, S. Shisodia, J. T. Totre, and A. J. Domb, “Biomedical Applications of Poly(Lactic Acid)”, *Rec. Pat. Regen. Med.*, vol. 4, May 2014.

47. S. Venugopalan and T. Rajendran," Role of Polylactic Acid in Bone Regeneration –A Systematic Revie*w*", *Journal of pharmaceutical sciences and researc*h, vol. 7. 2015.

48. S. In Jeong, E. Kyoung Ko, J. Yum, C. Ho Jung, Y. M. Lee, and H. Shin, “Nanofibrous Poly(lactic acid)/Hydroxyapatite Composite Scaffolds for Guided Tissue Regeneration”, *Macromol. Biosci.*, vol. 8, pp. 328–338, Apr. 2008.

49. J. Li, X.L.Lu, and Y. F. Zheng, “Effect of surface modified hydroxyapatite on the tensile property improvement of HA/PLA composite”, *Appl. Surf. Sci.*, vol. 255, no. 2, pp. 494–497, 2008.

50. J. Russias, E. Saiz, R. K. Nalla, K. Gryn, R. O. Ritchie, and A. P. Tomsia, “Fabrication and mechanical properties of PLA/HA composites: A study of in vitro degradation”, *Mater. Sci. Eng. C, Biomim. Supramol. Syst.*, vol. 26, no. 8, pp. 1289–1295, Sep. 2006.

51. N. Gültekin, F. Tihminlioglu, R. Ciftcioglu, M. Çiftçioğlu, and S. Harsa, “Preparation and Characterization of PolyLactide-Hydroxyapatite Biocomposites”, *Key Eng. Mater.*, vol. 264–268, pp. 1953–1956, Jan. 2004.

52. S. Zhou *et al.*, “Hydrogen Bonding Interaction of Poly(d,l-Lactide)/hydroxyapatite Nanocomposites”, *Chem. Mater.*, vol. 19, no. 2, pp. 247–253, Jan. 2007.

53. L. M. Mathieu, P.-E. Bourban, and J.-A. E. Månson, “Processing of homogeneous ceramic/polymer blends for bioresorbable composites”, *Compos. Sci. Technol.*, vol. 66, no. 11, pp. 1606–1614, 2006.

54. S. M. Nainar, S. Begum, M. N. M. Ansari, and H. Anuar, “Tensile Properties and Morphological Studies on HA/PLA Biocomposites for Tissue Engineering Scaffolds”, *Int. J. Eng. Res.*, vol. 3, pp. 186–189, Mar. 2014.

55. E. Nejati, H. Mirzadeh, and M. Zandi, “Synthesis and characterization of nano-hydroxyapatite rods/poly(l-lactide acid) composite scaffolds for bone tissue engineering”, *Compos. Part A Appl. Sci. Manuf.*, vol. 39, no. 10, pp. 1589–1596, 2008.

56. S. Rakmae, Y. Ruksakulpiwat, W. Sutapun, and N. Suppakarn, “Physical properties and cytotoxicity of surface-modified bovine bone-based hydroxyapatite/poly(lactic acid) composites”, *J. Compos. Mater.*, vol. 45, no. 12, pp. 1259–1269, Dec. 2010.

57. A. M. P. Dupraz, J. R. de Wijn, S. A. T. v.d. Meer, and K. de Groot, “Characterization of silane-treated hydroxyapatite powders for use as filler in biodegradable composites”, *J. Biomed. Mater. Res.*, vol. 30, no. 2, pp. 231–238, Feb. 1996.

58. N. Jing, X. Jiang, Q. Wang, Y. Tang, and P. Zhang, “Attenuated total reflectance/Fourier transform infrared (ATR/FTIR) mapping coupled with principal component analysis for the study of in vitro degradation of porous polylactide/hydroxyapatite composite material”, *Anal. Methods*, vol. 6, Jul. 2014.

59. C. B. Danoux, D. Barbieri, H. Yuan, J. D. de Bruijn, C. A. van Blitterswijk, and P. Habibovic, “In vitro and in vivo bioactivity assessment of a polylactic acid/hydroxyapatite composite for bone regeneration”, *Biomatter*, vol. 4, pp. e27664–e27664, Jan. 2014.

60. S. M. Zhang, J. Liu, W. Zhou, L. Cheng, and X. D. Guo, “Interfacial fabrication and property of hydroxyapatite/polylactide resorbable bone fixation composites”, *Curr. Appl. Phys.*, vol. 5, no. 5, pp. 516–518, 2005.

61. L. C. Lin, S. J. Chang, S. M. Kuo, G. C.-C. Niu, H. K. Keng, and P. H. Tsai, “Preparation

and evaluation of β-TCP/polylactide microspheres as osteogenesis materials", *J. Appl. Polym. Sci.*, vol. 108, no. 5, pp. 3210–3217, Jun. 2008.

62. F. Ma and P. Liu, "Surface Modification of β-TCP with Stearic Acid and Its Effects on β-TCP/PLLA Biodegradable Composite Nanofibers", *J. Bone Reports Recomm.*, vol. 02, Jan. 2016.

63. M. S. Hasan, I. Ahmed, A. J. Parsons, C. D. Rudd, G. S. Walker, and C. A. Scotchford, "Investigating the use of coupling agents to improve the interfacial properties between a resorbable phosphate glass and polylactic acid matrix", *J. Biomater. Appl.*, vol. 28, no. 3, pp. 354–366, Jul. 2012.

64. M. Bernstein *et al.*, "Low Temperature Fabrication of β-TCP–PCL Nanocomposites for Bone Implants", *Adv. Eng. Mater.*, vol. 12, no. 8, pp. B341–B347, Aug. 2010.

65. O. Cisneros, W. Herrera, M. I. Loría-Bastarrachea, Y. Veranes-Pantoja, J. Cauich, and M. Cervantes, "Towards optimization of the silanization process of hydroxyapatite for its use in bone cement formulations", *Mater. Sci. Eng. C*, vol. 40, pp. 157–163, Jul. 2014.

66. N. Ignjatovic, K. Delijic, M. Vukcevic, and D. Uskoković, "The Designing of Properties of Hydroxyapatite/poly–L–lactide Composite Materials by Hot Pressing", *Zeitschrift für Met.*, vol. 92, pp. 145–149, Feb. 2001.

67. N. Ignjatovic and D. Uskoković, "Biodegradable composites based on nanocrystalline calcium phosphate and bioresorbable polymers", *Adv. Appl. Ceram.*, vol. 107, pp. 142–147, May 2008.

68. X. Zhang *et al.*, "Mechanical properties and cytocompatibility of carbon fibre reinforced nano-hydroxyapatite/polyamide66 ternary biocomposite", *J. Mech. Behav. Biomed. Mater.*, vol. 42, pp. 267–273, 2015.

69. K. C. Ang, K. F. Leong, C. K. Chua, and C. Margam, “Compressive properties and degradability of poly(ε-caprolatone)/hydroxyapatite composites under accelerated hydrolytic degradation”, *J. Biomed. Mater. Res. A*, vol. 80, pp. 655–660, Mar. 2007.

70. C. Sarkar, S. K. Sahu, A. Sinha, J. Chakraborty, and S. Garai, “Facile synthesis of carbon fiber reinforced polymer-hydroxyapatite ternary composite: A mechanically strong bioactive bone graft”, *Mater. Sci. Eng. C*, vol. 97, pp. 388–396, 2019.

71. C. Bressy, V. Giang Ngo, F. Ziarelli, and A. Margaillan, “New Insights into the Adsorption of 3-(Trimethoxysilyl)propylmethacrylate on Hydroxylated ZnO Nanopowders”, *Langmuir*, vol. 28, pp. 3290–3297, Jan. 2012.

72. Q. Dong *et al.*, “A new bioactive polylactide-based composite with high mechanical strength”, *Colloids Surfaces A Physicochem. Eng. Asp.*, vol. 457, pp. 256–262, 2014.

73. C. Kunze *et al.*, “Surface modification of tricalcium phosphate for improvement of the interfacial compatibility with biodegradable polymers”, *Biomaterials*, vol. 24, no. 6, pp. 967–974, 2003.

74. S.-J. Hong *et al.*, “The biomechanical evaluation of calcium phosphate cements for use in vertebroplasty”, *J. Neurosurg. Spine SPI*, vol. 4, no. 2, pp. 154–159, 2006.

75. H. Suzuki, R. Yagi, T. Waki, T. Wada, C. Ohkubo, and T. Hayakawa, “Study of Apatite Deposition in a Simulated Body Fluid Immersion Experiment”, *J. Oral Tissue Eng.*, pp. 9–14, Oct. 2016.

76. H. EL Boujaady, M. Mourabet, E. R. Abdelhadi, M. Bennani-Ziatni, R. El Hamri, and T. Abderrahim, “Adsorption of a textile dye on synthesized calcium deficient hydroxyapatite (CDHAp): Kinetic and thermodynamic studies”, vol. 7, pp. 4049–4063, Jan. 2016.

77. A. L. Giraldo-Betancur *et al.*, “Comparison of physicochemical properties of bio and commercial hydroxyapatite”, *Curr. Appl. Phys.*, vol. 13, no. 7, pp. 1383–1390, 2013.

78. T. Araujo Batista, Z. S. Macedo, P. Santa-Cruz, and M. Valerio, “Production and characterization of pure and Cr3+-doped hydroxyapatite for biomedical applications as fluorescent probes”, *J. Mater. Sci.*, vol. 42, pp. 2236–2243, Apr. 2007.

79. U. Klammert, A. Ignatius, U. Wolfram, T. Reuther, and U. Gbureck, “In vivo degradation of low temperature calcium and magnesium phosphate ceramics in a heterotopic model”, *Acta Biomater.*, vol. 7, no. 9, pp. 3469–3475, 2011.

80. D. Dos Santos Tavares, L. de Oliveira Castro, G. Soares, G. Alves, and J. Granjeiro, “Synthesis and cytotoxicity evaluation of granular magnesium substituted Î²-tricalcium phosphate”, *J. Appl. Oral Sci.*, vol. 21, pp. 37–42, Feb. 2013.

81. M. Seidenstuecker, Y. Mrestani, R. Neubert, A. Bernstein, and H. Mayr, “Release Kinetics and Antibacterial Efficacy of Microporous -TCP Coatings”, *J. Nanomater.*, vol. 2013, pp. 1–8, Nov. 2013.

82. M. Hafezi, “Preparation and characterization of whitlockite-merwinite nanocomposite”, *J. Ceram. Process. Res.*, Jan. 2013.

83. Y. Lu, Y.-C. Chen, and P.-H. Zhang, “Preparation and Characterisation of Polylactic acid (PLA)/Polycaprolactone (PCL) Composite Microfibre Membranes”, *Fibres Text. East. Eur.*, vol. 24, pp. 17–25, Apr. 2016.

84. J. Yong *et al.*, “Femtosecond Laser Direct Writing of Porous Network Microstructures for Fabricating Super-Slippery Surfaces with Excellent Liquid Repellence and Anti-Cell Proliferation”, *Adv. Mater. Interfaces*, vol. 5, no. 7, p. 1701479, Apr. 2018.

85. C. Ruiz-Aguilar, U. Olivares-Pinto, E. A. Aguilar-Reyes, R. López-Juárez, and I.

Alfonso, “Characterization of β-tricalcium phosphate powders synthesized by sol–gel and mechanosynthesis”, *Boletín la Soc. Española Cerámica y Vidr.*, vol. 57, no. 5, pp. 213–220, 2018.

86. N. K. Nguyen, M. Leoni, D. Maniglio, and C. Migliaresi, “Hydroxyapatite nanorods: Soft-template synthesis, characterization and preliminary in vitro tests”, *J. Biomater. Appl.*, vol. 28, no. 1, pp. 49–61, Apr. 2012.

87. N. Suardana, Y. Piao, J. K. Lim, and B. Indonesia, “Mechanical properties of HEMP fibers and HEMP/PP composites: Effects of chemical surface treatment”, *Mater. Phys. Mech.*, vol. 11, Jan. 2011.

88. M. Arthur Cuiffo, J. Snyder, A. Elliott, N. Romero, S. Kannan, and G. Halada, “Impact of the Fused Deposition (FDM) Printing Process on Polylactic Acid (PLA) Chemistry and Structure”, *Appl. Sci.*, vol. 7, p. 579, Jun. 2017.

89. K. P. Rajan, “Studies on nanocomposites of polypropylene and polylactic acid blends reinforced with halloysite nanotubes”, 2016.

90. E. Meaurio, N. López-Rodríguez, and J.-R. Sarasua, “Infrared Spectrum of Poly(l-lactide): Application to Crystallinity Studies”, *Macromolecules*, vol. 39, pp. 9291–9301, Dec. 2006.

91. L. Berzina-Cimdina and N. Borodajenko, “Research of Calcium Phosphates Using Fourier Transform Infrared Spectroscopy”, *Infrared Spectrosc. - Mater. Sci. Eng. Technol.*, Apr. 2012.

92. I. Mobasherpour, M. S. Heshajin, A. Kazemzadeh, and M. Zakeri, “Synthesis of nanocrystalline hydroxyapatite by using precipitation method”, *J. Alloys Compd.*, vol. 430, no. 1, pp. 330–333, 2007.

93. A. E. Y. Asmae Massit, B. C. El Idrissi, and K. Yamni, “Synthesis and characterization of nano-sized β-Tricalcium phosphate: Effects of the aging time”, *IOSR J. Appl. Chem*, vol. 7, pp. 57–61, Jan. 2014.

94. C. Stähli, J. Thüring, L. Galea, S. Tadier, M. Bohner, and N. Döbelin, “Hydrogen-substituted β-tricalcium phosphate synthesized in organic media”, *Acta Crystallogr. B. Struct. Sci. Cryst. Eng. Mater.*, vol. 72, no. Pt 6, pp. 875–884, Dec. 2016.

95. Y. Wang, J. Gao, J. Hu, and Y. Zhang, “Solid reaction mechanism of CaHPO4·2H2O + CaCO3 with and without yttria”, *Rare Met.*, vol. 28, no. 1, pp. 77–81, 2009.

96. C. Botelho, M. Lopes, I. Gibson, S. Best, and J. D Santos, “Structural analysis of Si-substituted hydroxyapatite: Zeta potential and X-ray photoelectron spectroscopy”, *J. Mater. Sci. Mater. Med.*, vol. 13, pp. 1123–1127, Jan. 2003.

97. M. Kantcheva, “FT-IR spectroscopic investigation of the reactivity of NOx species adsorbed on Cu2+/ZrO2 and CuSO4/ZrO2 catalysts toward decane”, *Appl. Catal. B Environ.*, vol. 42, no. 1, pp. 89–109, 2003.

98. Y. A. Fadeeva, L. I. Demina, Y. G. Gorbunova, L. E. Shmukler, L. P. Safonova, and A. Y. Tsivadze, “Orthophosphoric Acid-;N,N-Dimethylformamide System: IR Study”, *Russ. J. Coord. Chem.*, vol. 29, no. 7, pp. 515–518, 2003.

99. C. Yang, K. Lin, and J. Chang, “A simple way to synthesize 3D hierarchical HAp porous microspheres with sustained drug release”, *Ceram. Int.*, vol. 41, May 2015.

100. R. Salgado-Delgado; A.M. Salgado-Delgado, “Theoretical and experimental spectroscopic analysis by FTIR in the effect of the silanes on the chemical modification of the surface of rice husk”, *Int. J. Eng. Res. Appl.*, vol. 6, pp. 04–07, 2016.

101. K. Sinko, A. Meiszterics, J. Rohonczy, B. Kobzi, and S. Kubuki, “Effect of phosphorus

precursors on the structure of bioactive calcium phosphate silicate systems", *Mater. Sci. Eng. C*, vol. 73, Jan. 2017.

102. L. B. Capeletti, "Fourier Transform Infrared and Raman Characterization of Silica-Based Materials", J. H. Z. E.-M. T. Stauffer, Ed. Rijeka: IntechOpen, 2016, p. Ch. 1.

103. J. P. Matinlinna, M. Özcan, L. V. J. Lassila, and P. K. Vallittu, "The effect of a 3-methacryloxypropyltrimethoxysilane and vinyltriisopropoxysilane blend and tris(3-trimethoxysilylpropyl)isocyanurate on the shear bond strength of composite resin to titanium metal", *Dent. Mater.*, vol. 20, no. 9, pp. 804–813, 2004.

104. P. Stloukal *et al.*, "Effect of plasma treatment on the release kinetics of a chemotherapy drug from biodegradable polyester films and polyester urethane films", *Int. J. Polym. Mater. Polym. Biomater.*, vol. 67, no. 3, pp. 161–173, Feb. 2018.

105. F. Rezaei, T. Planckaert, P. Van Der Voort, "Chemical and morphological characterization of nanofibers produced by plasma-treated electrospinning solutions", *23rd International Symposium on Plasma Chemistry*, 2017, p. 4.

106. B. Zribi *et al.*, "A microfluidic electrochemical biosensor based on multiwall carbon nanotube/ferrocene for genomic DNA detection of Mycobacterium tuberculosis in clinical isolates", *Biomicrofluidics*, vol. 10, p. 14115, Feb. 2016.

107. A. Ghahremaninezhad, D. G. Dixon, and E. Asselin, "Electrochemical and XPS analysis of chalcopyrite (CuFeS2) dissolution in sulfuric acid solution", *Electrochim. Acta*, vol. 87, pp. 97–112, 2013.

108. Y. W. Yang and L. J. Fan, "High-Resolution XPS Study of Decanethiol on Au(111): Single Sulfur−Gold Bonding Interaction", *Langmuir*, vol. 18, no. 4, pp. 1157–1164, Feb. 2002.

109. J. Stoch and J. Gablankowska-Kukucz, “Effect of carbonate contaminations on the XPS O 1s band structure in metal oxides”, *Surf. Interface Anal.*, vol. 17, pp. 165–167, Mar. 1991.

110. H. B. Lu, C. T. Campbell, D. J. Graham, and B. Ratner, “Surface Characterization of Hydroxyapatite and Related Calcium Phosphates by XPS and TOF-SIMS”, *Anal. Chem.*, vol. 72, pp. 2886–2894, Aug. 2000.

111. H. Shi *et al.*, “Poly(glycerol sebacate)-modified polylactic acid scaffolds with improved hydrophilicity, mechanical strength and bioactivity for bone tissue regeneration”, *RSC Adv.*, vol. 5, pp. 79703–79714, Sep. 2015.

112. Y.-P. Guo, J.-J. Guan, J. Yang, Y. Wang, C. Zhang, and Q.-F. Ke, “Hybrid Nanostructured Hydroxyapatite/Chitosan Composite Scaffold: Bioinspired Fabrication, Mechanical Property and Biological Property”, *J. Mater. Chem. B*, vol. 3, May 2015.

113. M. Hrubovčáková, “Biodegradable Polylactic acid and Polylactic acid/Hydroxyapatite Coated Iron Foams for Bone Replacement Materials”, *Int. J. Electrochem. Sci.*, vol. 12, pp. 11122–11136, Dec. 2017.

114. J.-W. Kim, K.-H. Shin, Y.-H. Koh, M. J. Hah, J. Moon, and H.-E. Kim, “Production of Poly(ε-Caprolactone)/Hydroxyapatite Composite Scaffolds with a Tailored Macro/Micro-Porous Structure, High Mechanical Properties, and Excellent Bioactivity”, *Materials (Basel).*, vol. 10, no. 10, p. 1123, Sep. 2017.

115. J. Luo, J. Faivre, H. Engqvist, and C. Persson, “The Addition of Poly(Vinyl Alcohol) Fibers to Apatitic Calcium Phosphate Cement Can Improve Its Toughness”, *Materials (Basel).*, vol. 12, p. 1531, May 2019.

116. H. Li, M. Gong, A. Yang, J. Ma, X. Li, and Y. Yan, “Degradable biocomposite of nano calcium-deficient hydroxyapatite-multi(amino acid) copolymer”, *Int. J. Nanomedicine*,

vol. 7, pp. 1287–1295, Mar. 2012.

117. M. Ebrahimi, M. Botelho, and S. Dorozhkin, “Biphasic calcium phosphates bioceramics (HA/TCP): Concept, physicochemical properties and the impact of standardization of study protocols in biomaterials research”, *Mater. Sci. Eng. C*, vol. 71, pp. 1293–1312, Nov. 2016.

APPENDIX A: CHARACTERIZATION RESULTS OF PELLET PLA

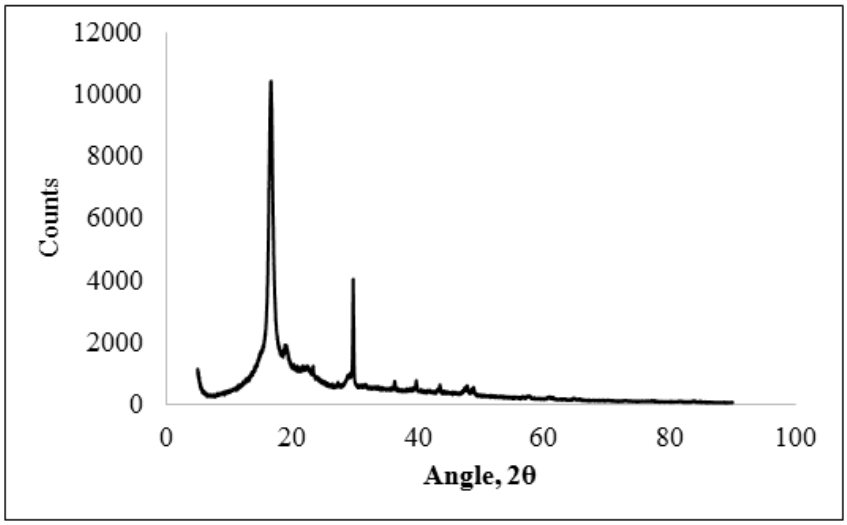

Figure A.1. XRD result of pellet PLA.

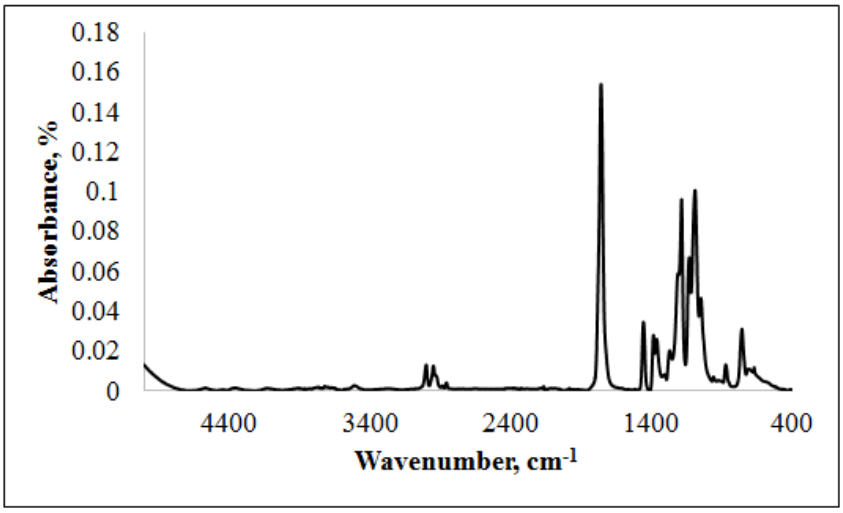

Figure A.2. FTIR result of pellet PLA.

APPENDIX B: MECHANICAL CHARACTERIZATION OF PLA CEMENT AND COMPOSITES

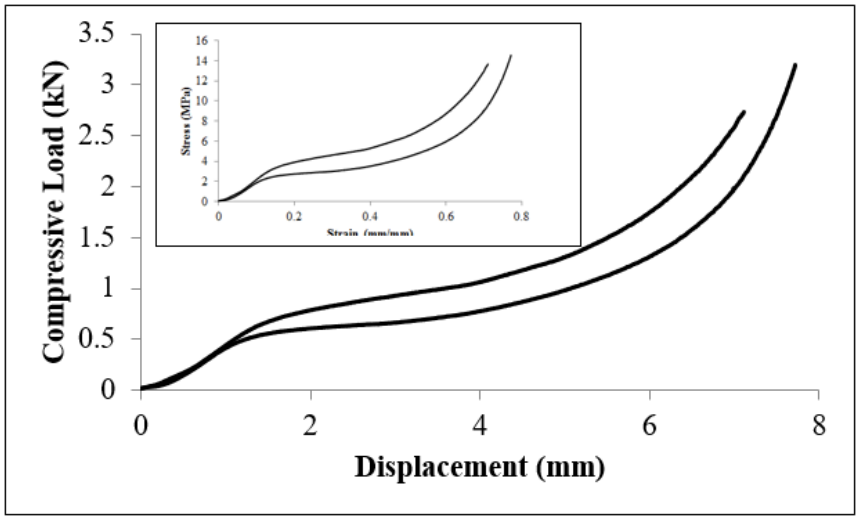

Figure B.1. Compressive load versus displacement curves of pure PLA cement (prepared by chloroform). The inset shows the corresponding stress versus strain curves.

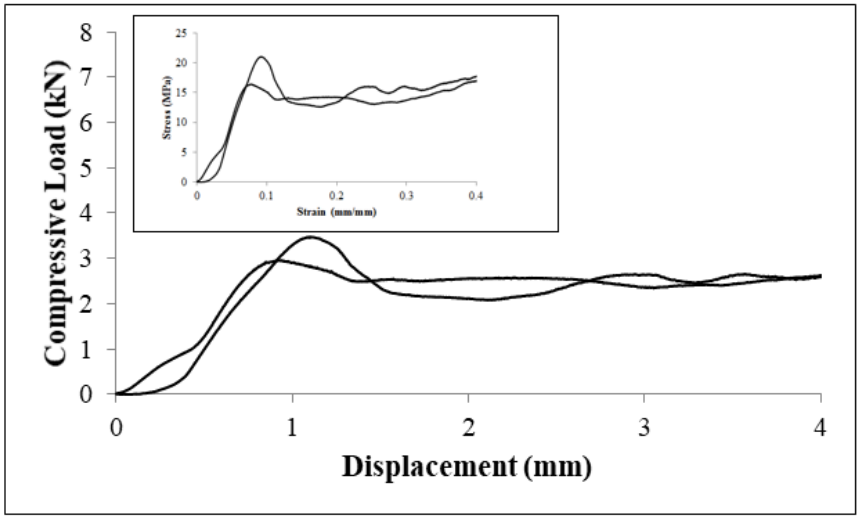

Figure B.2. Compressive load versus displacement curves of PLA40H60 specimens. The inset shows the corresponding stress versus strain curves.

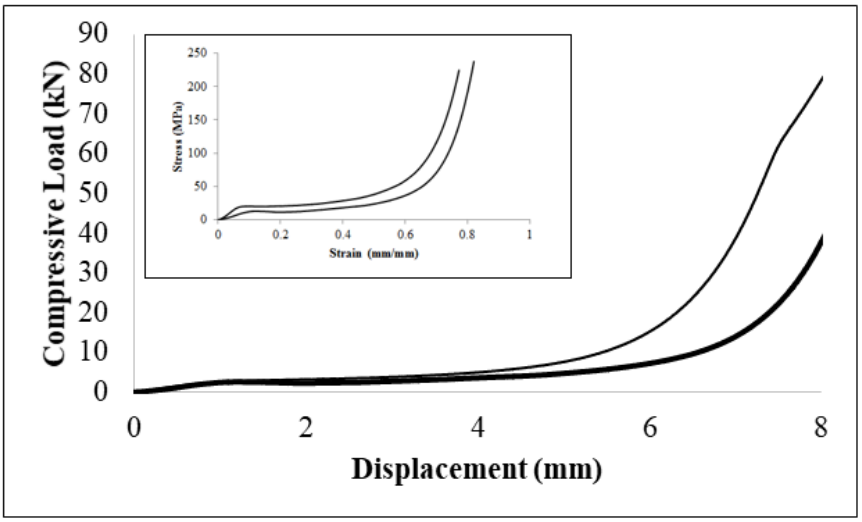

Figure B.3. Compressive load versus displacement curves ofPLA50H50 specimens. The inset shows the corresponding stress versus strain curves.

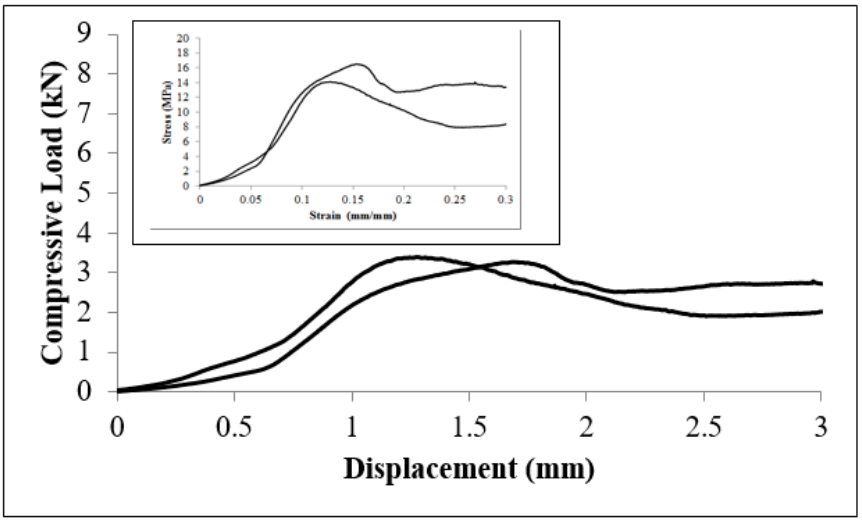

Figure B.4. Compressive load versus displacement curves of PLA40H60Si1 specimens. The inset shows the corresponding stress versus strain curves.

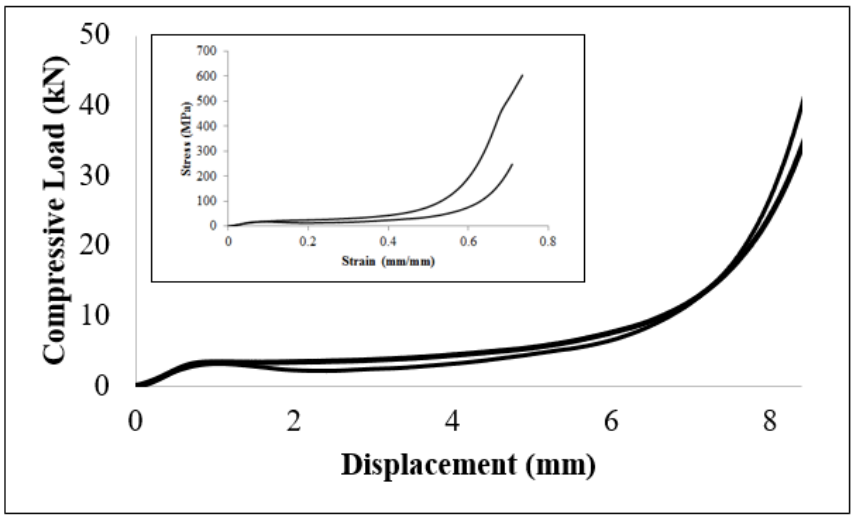

Figure B.5. Compressive load versus displacement curves of PLA50H50Si3 specimens. The inset shows the corresponding stress versus strain curves.

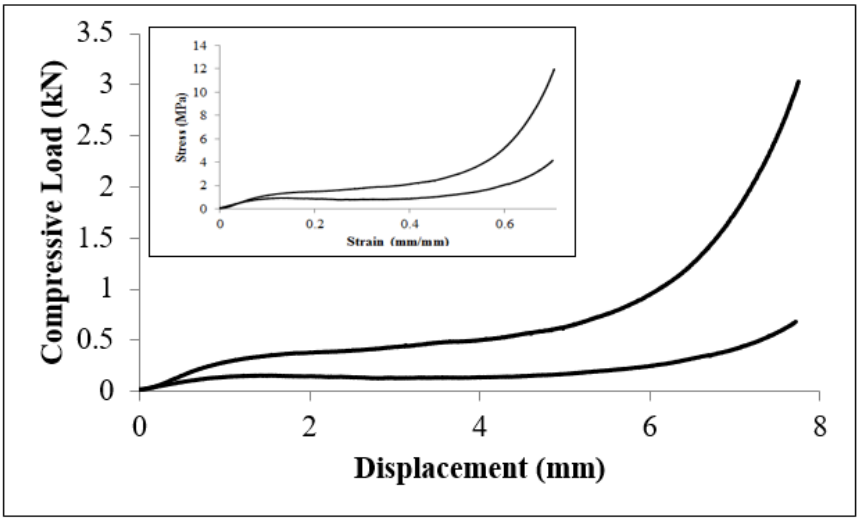

Figure B.6. Compressive load versus displacement curves of PLA40T60 specimens. The inset shows the corresponding stress versus strain curves.

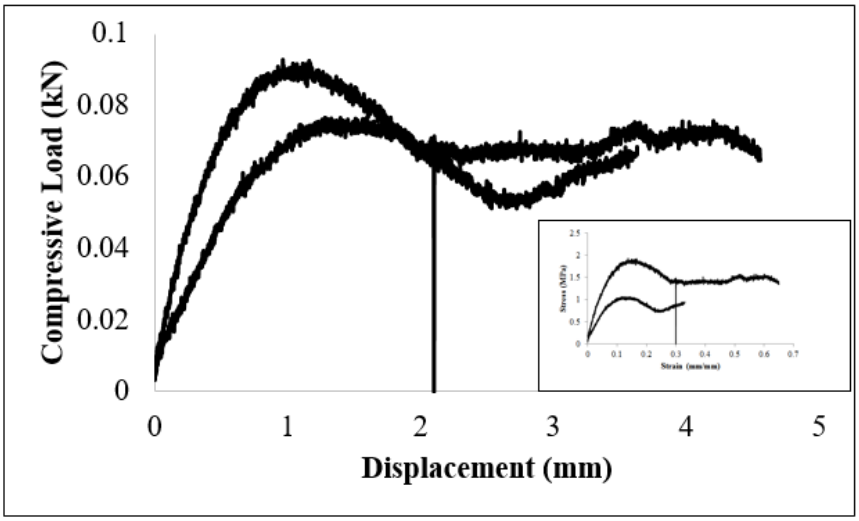

Figure B.7. Compressive load versus displacement curves of PLA50T50 specimens. The inset shows the corresponding stress versus strain curves.

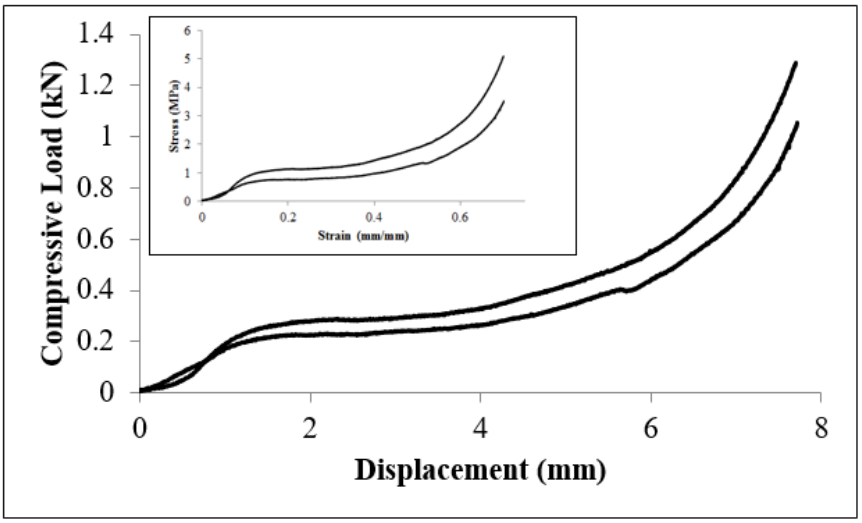

Figure B.8. Compressive load versus displacement curves of PLA40T60Si1 specimens. The inset shows the corresponding stress versus strain curves.

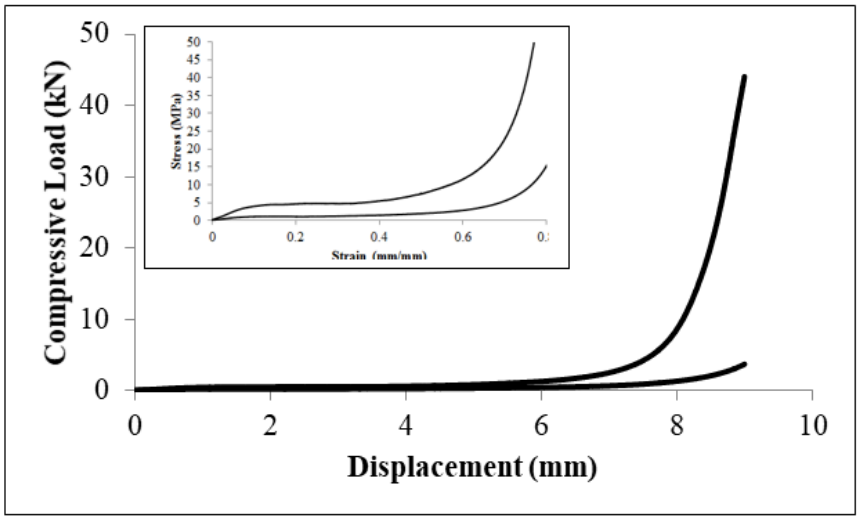

Figure B.9. Compressive load versus displacement curves of PLA50T50PASi3 specimens. The inset shows the corresponding stress versus strain curves.